Geotechnical and Structures Laboratory

**US Army Corps of Engineers**®
Engineer Research and
Development Center

# Field Testing and Load Rating Report, Bridge S-4360, Camp Hovey, South Korea

Brett Commander, Jesse Grimson, Wilmel Varela-Ortiz, Terry R. Stanton, Gerardo I. Velazquez, and Gerald M. Hansler

July 2008

# Field Testing and Load Rating Report, Bridge S-4360, Camp Hovey, South Korea

Brett Commander and Jesse Grimson

*Bridge Diagnostics, Inc.*
*1965 57th Court North, Suite 106*
*Boulder, CO 80301*

Wilmel Varela-Ortiz, Terry R. Stanton, and Gerardo I. Velazquez

*Geotechnical and Structures Laboratory*
*U.S. Army Engineer Research and Development Center*
*3909 Halls Ferry Road*
*Vicksburg, MS 39180-6199*

Gerald M. Hansler

*Eighth U.S. Army*
*Seoul, South Korea*

Final report

Prepared for   Headquarters, Installation Management Command (IMCOM)
          Arlington, VA 22202

**Abstract:** In June 2007, Bridge Diagnostics, Inc. (BDI), was contracted by the U.S. Army Corps of Engineers to perform live-load testing and load rating on Bridge S-4360 at Camp Hovey, South Korea, in conjunction with two other structures, S-1801 and S-1090 at Camp Casey. A primary goal of the live-load testing was to determine the relative effects of different military load configurations. Of particular interest was determining the benefit of using the Heavy Equipment Transporter System (HETS) to transport heavy equipment such as an M1A1 tank. Another goal was to use the measured load responses to verify and calibrate a finite element model of the structure.

The model resulting from the structural identification procedure was then used to generate accurate load ratings for specific AASHTO (American Association of State Highway and Transportation Officials) and military load configurations. Both the direct load test and subsequent load rating results indicated that the MIA1 tank generated greater flexural stresses than did the HETS carrying the M1A1 tank.

The bridge appeared to be in good condition and was apparently designed to carry heavy military loads. Load rating calculations determined that all vehicles considered could cross the bridge within Inventory (normal design) stress limits.

# Contents

**Report Documentation Page**

# Figures and Tables

## Figures

## Tables

# Preface

This report describes the load testing process and analytical results conducted for Bridge S-4360 at Camp Hovey, South Korea. The load test was one of three tests performed in June 2007 to obtain more accurate bridge load ratings with respect to HETS and other heavy military load configurations. This project was arranged and supervised by Terry R. Stanton of the U.S. Army Engineer Research and Development Center (ERDC).

The work was performed by Bridge Diagnostics, Inc. (BDI), under Contract No. W912HZ-07-C-0045, and by personnel of the Structural Engineering Branch (StEB), ERDC Geotechnical and Structures Laboratory (GSL). This report was prepared by Jesse Grimson and Brett Commander of BDI; Wilmel Varela-Ortiz, Terry R. Stanton, and Gerardo I. Velazquez, GSL; and LTC Gerald M. Hansler, Deputy Assistant Chief of Staff, Eighth U.S. Army. Technical review of the document was performed by Carmen Y. Lugo and Sharon B. Garner, StEB.

The Army Bridge Inspection Program is sponsored by the Army Transportation Infrastructure Program (ATIP) of the Headquarters, Installation Management Command (IMCOM), Arlington, VA. The IMCOM provided funding for this investigation. Questions should be directed to Ali A. Achmar, IMCOM ATIP Program Manager (telephone 210-295-2038).

This publication was prepared under the overall project supervision of James S. Shore, Chief, StEB; Dr. Robert L. Hall, Chief, Geosciences and Structures Division; Dr. William P. Grogan, Deputy Director, GSL; and Dr. David W. Pittman, Director, GSL.

COL Richard B. Jenkins was Commander and Executive Director of ERDC. Dr. James R. Houston was Director.

# Unit Conversion Factors

| Multiply | By | To Obtain |
|---|---|---|
| degrees Fahrenheit | (F-32)/1.8 | degrees Celsius |
| feet | 0.3048 | meters |
| foot-pounds force | 1.355818 | joules |
| inches | 0.0254 | meters |
| inch-pounds (force) | 0.1129848 | newton meters |
| kips (force) per square inch | 6.894757 | megapascals |
| miles per hour | 0.44704 | meters per second |
| pounds (force) | 4.448222 | newtons |
| pounds (force) per foot | 14.59390 | newtons per meter |
| pounds (force) per inch | 175.1268 | newtons per meter |
| square feet | 0.09290304 | square meters |
| square inches | 6.4516 E-04 | square meters |
| tons (force) | 8,896.443 | newtons |

# 1    Introduction and Result Summary

The Bridge Diagnostics, Inc. (BDI), Structural Testing System (STS) was used for measuring strains at 64 locations on the superstructure while it was subjected to a variety of vehicle loads. Load configurations included a three-axle dump truck, an empty Heavy Equipment Transporter System (HETS), an M1A1 tank, and a HETS hauling an M1A1 tank. Measurements were examined to determine the relative response magnitudes from the different load configurations. Of particular interest was the difference in load effects between the direct loading with an M1A1 tank and the M1A1 tank transported with a HETS.

Load test results were also used to verify and "calibrate" a finite element model of the superstructure, which was in turn used to develop load ratings using the American Association of State Highway and Transportation Officials (AASHTO) Load and Resistance Factor Design (LRFD) and Load and Resistance Factor Rating (LRFR) procedures.

Load test and load rating results indicated that the M1A1 tank generated greater flexural stresses and that it was preferable to transport the tank with the HETS. It was also determined that this bridge was likely designed for heavy military loads, since load ratings for all vehicles examined were above 1.o at the Inventory limit. Table 1 presents the limiting load rating factors and gross weights for several AASHTO and military load configurations. The component controlling the load ratings for all two-lane load conditions was the midspan moment of the interior beams. The exterior beam moment capacity controlled the load limits for all wide military vehicles where only single-lane loading could be applied.

Table 1. Critical load rating factors (RF) and weights.

| Rating Vehicle | Location | LRFR - Inventory | | LRFR - Operating | |
|---|---|---|---|---|---|
| | | RF | Tonnes | RF | Tonnes |
| HS-20 | Interior end span | 2.70 | 88.2 | 3.50 | 114.3 |
| HS-26 | Interior end span | 2.08 | 114.6 | 2.69 | 148.6 |
| HS-30 | Interior end span | 1.80 | 132.3 | 2.33 | 171.5 |
| Type 3 | Interior end span | 3.47 | 132.2 | 4.50 | 171.4 |
| Type 3-3 | Interior end span | 4.21 | 275.0 | 5.46 | 356.5 |
| Type 3S2 | Interior end span | 3.72 | 270.0 | 4.82 | 349.9 |
| M1A1 tank[1] | Exterior end span | 1.23 | 75.4 | 1.59 | 97.7 |
| Empty HET[1] | Interior end span | 5.15 | 200.9 | 6.68 | 260.4 |
| HET with M1A1 tank[1] | Interior end span | 1.76 | 184.8 | 2.28 | 239.6 |
| Korean HET[1] | Interior end span | 1.69 | 124.9 | 2.19 | 161.9 |
| PLS | Interior end span | 2.23 | 138.5 | 2.89 | 179.6 |
| MLC60 (wheeled)[1] | Interior end span | 1.97 | 107.2 | 2.55 | 139.0 |
| MLC60 (tracked)[1] | Interior end span | 1.46 | 79.5 | 1.89 | 103.0 |
| MLC70 (wheeled)[1] | Exterior end span | 1.73 | 109.9 | 2.24 | 142.4 |
| MLC70 (tracked)[1] | Exterior end span | 1.30 | 82.6 | 1.69 | 107.0 |

[1]  Single-lane loading only.

# 2   Structural Testing Information

Bridge S-4360 is located at Camp Casey in South Korea. It is a two-span, noncontinuous, steel beam bridge. The bridge consists of nine beam-lines and a reinforced concrete deck. The spans are roughly 12 m each, and the abutment and pier supports are aligned perpendicular to the roadway. The steel beams are 600-mm deep rolled sections of varying shape. The bridge was strengthened at some point by the addition/replacement of three interior beam-lines. New beams have different section properties than the original six beam-lines. Shear stud connectors were specified on the design plans, indicating the deck was to be composite with beams for all live-load applications. It was noted during the instrumentation process that the actual span lengths and beam cross-section dimensions varied slightly from those specified in the plans.

The bridge was instrumented with 64 strain transducers, as shown in Figure 1–Figure 4. Controlled load tests were performed with a loaded three-axle dump truck driven slowly across the bridge along three pre-scribed paths. In addition to the dump truck, live-load tests were per-formed with an M1A1 tank, an empty HETS, and a HETS loaded with an M1A1 tank. Strains were measured from all sensors at a rate of 40 Hz dur-ing the entire load cycle. The longitudinal truck position was measured and recorded remotely and stored with the strain data.

Information specific to this load test is summarized in Table 2. Axle con-figurations and weights of the test vehicles used for this bridge are illu-strated in Figure 5 through Figure 8 and summarized in Table 3 through Table 6. Note that only the dump truck was used to calibrate the model.

Additional information is provided in the appendixes as follows: measured and computed strain comparisons (Appendix A); field notes (Appendix B); detailed outline of the field testing procedures (Appendix C); specifications of the BDI strain transducers, Structural Testing System, and AutoClicker (Appendixes D–F); description of the principles guiding the integrated approach applied to modeling and analysis (Appendix G); and a detailed outline of the load rating procedures (Appendix H).
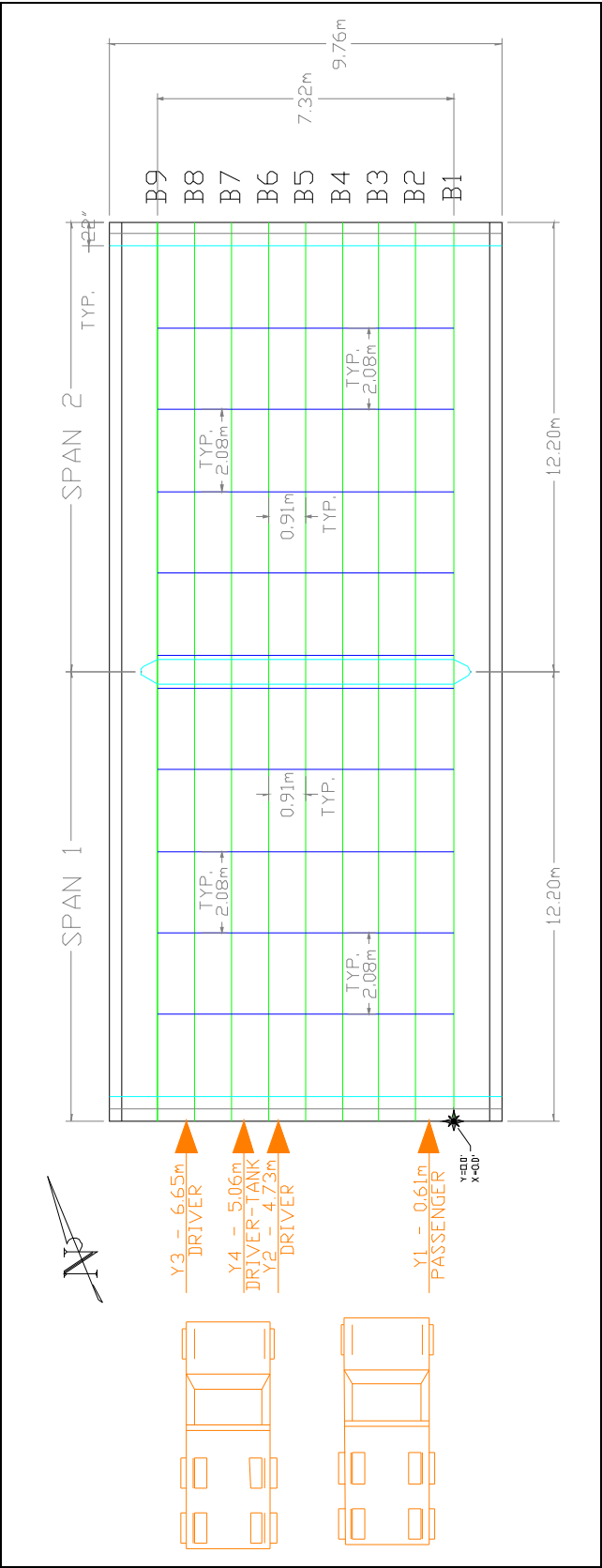
**Figure 1. Overall plan view and dimensions.**
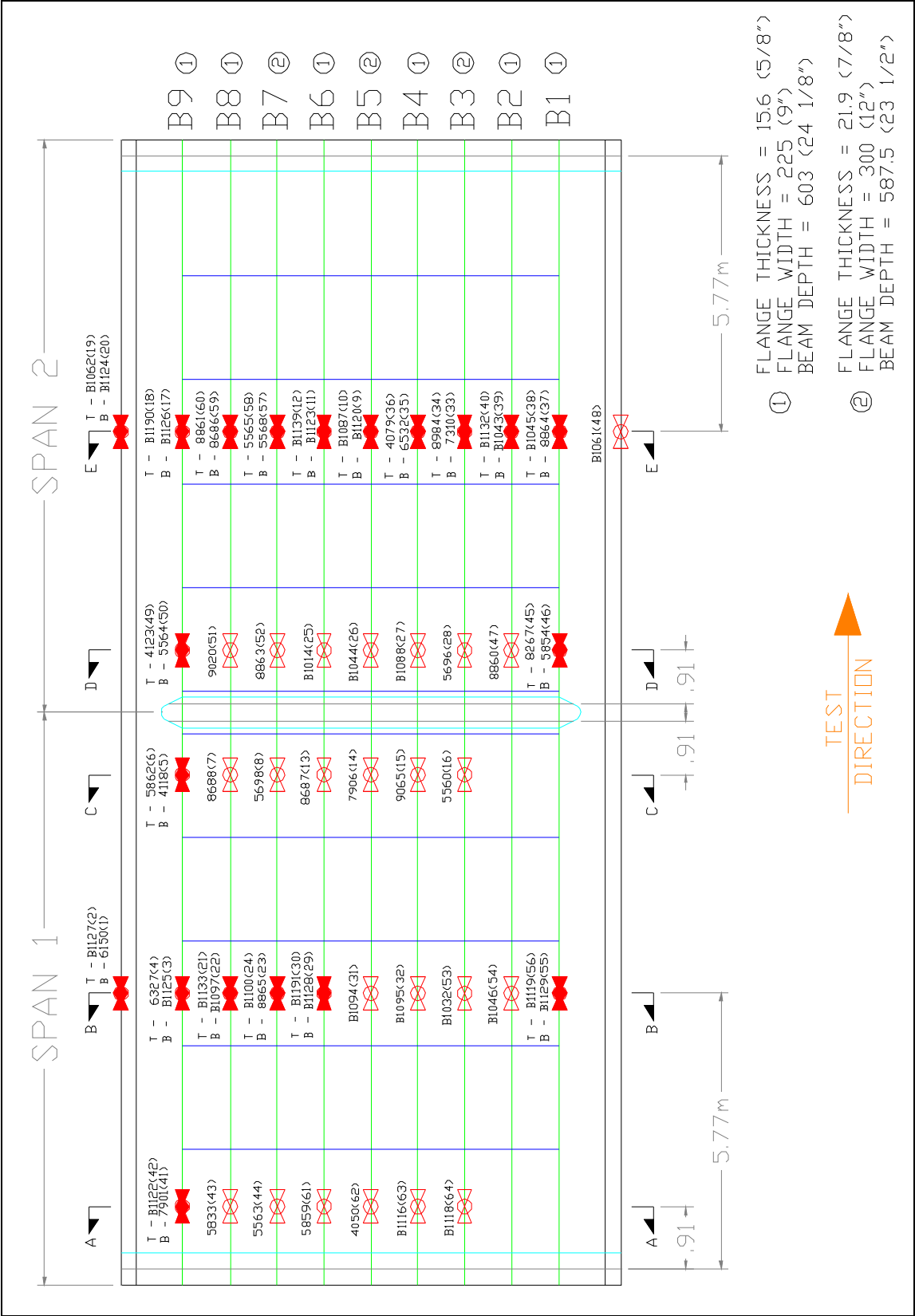
**Figure 2. Instrumentation plan.**

SECTION A-A

B1122(42)
37.5
TYP.
B1118(64)  B1116(65)  4050(62)  5859(61)  5563(44)  5833(43)  7901(41)

B1  B2  B3  B4  B5  B6  B7  B8  B9

SECTION B-B

B1127(2)
6"
TYP.
6150(1)
B1119(56)  B1191(30)  B1100(24)  B1133(21)  6327(4)
37.5
TYP.
3"
TYP.
B1129(55)  B1046(54)  B1032(53)  B1095(32)  B1094(31)  B1128(29)  8865(23)  B1097(22)  B1125(3)

B1  B2  B3  B4  B5  B6  B7  B8  B9

SECTION C-C

5B62(6)
37.5
TYP.
5560(16)  9065(15)  7906(14)  8687(17)  5698(8)  868B(7)  411B(5)

B1  B2  B3  B4  B5  B6  B7  B8  B9

Figure 3. Instrumentation details at cross sections A–C.
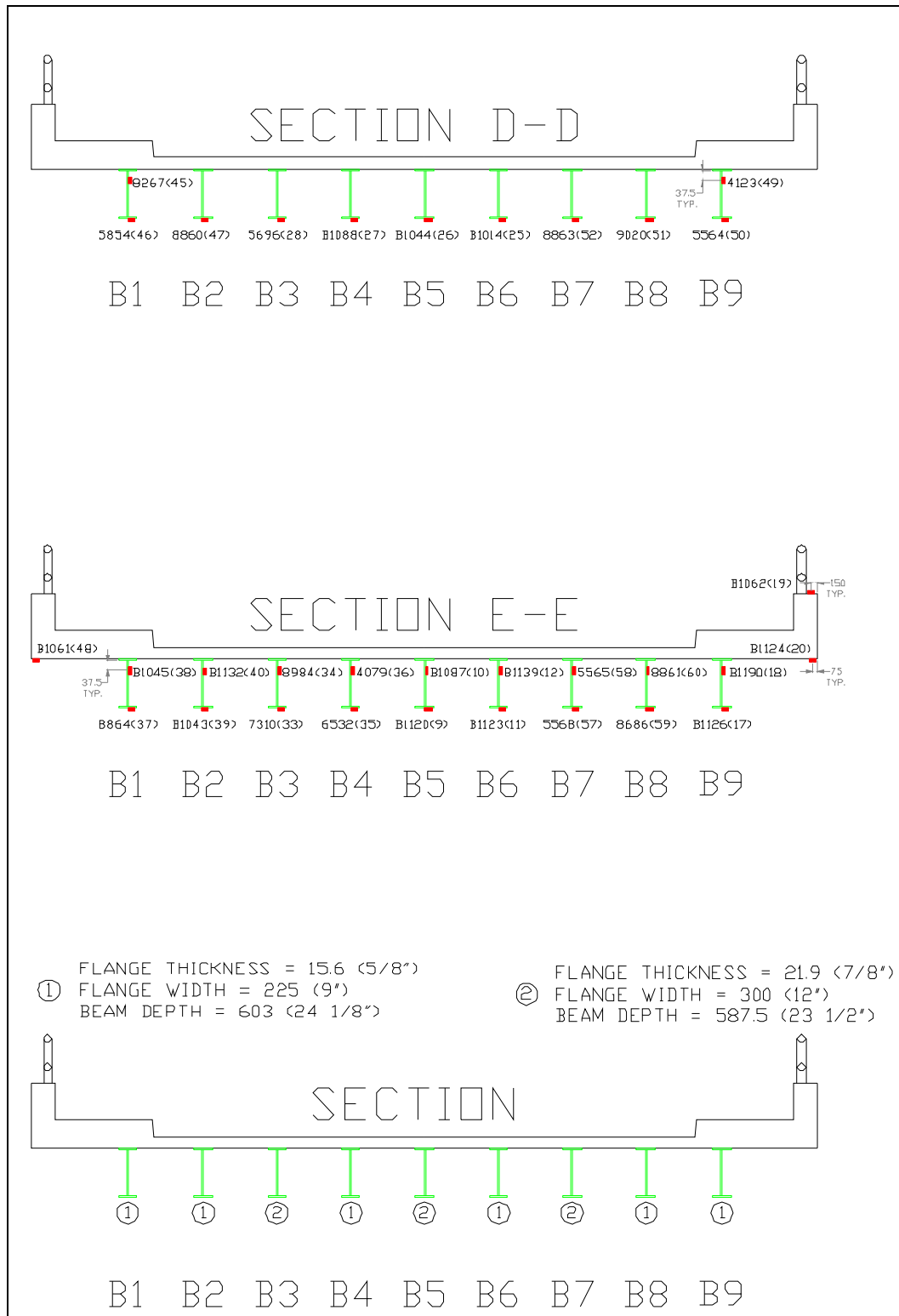
Figure 4. Instrumentation details at cross sections D–E.

Table 2. Structure description and testing notes.

| Item | Description |
|---|---|
| Structure Name | S-4360 |
| Date Built / Renovated | Unknown / 1977<br>A36 steel assumed based on U.S. Army Corps of Engineers (USACE) load rating 2007<br>($Fy$ = 248 MPa) |
| BDI Project Number | 060701-103 |
| Testing Date | June 12, 2007 |
| Client's Structure ID # | S-4360 |
| Location/Route | Camp Hovey, South Korea |
| Structure Type | Steel girder with reinforced concrete deck |
| Total Number of Spans | 2 |
| Span Length(s) | Span 1: 12.20 m; Span 2: 12.20 m |
| Skew | 0 deg |
| Structure/Roadway Width | 9.76 m / 7.32 m |
| Deck Type | Reinforced concrete |
| Other Structure Info | N/A |
| Spans Tested | 2 |
| Test Reference Location (X = 0; Y = 0) | Edge of sidewalk, southeast corner |
| Test Vehicle Direction | North |
| Test Beginning Point | -3 m + ½ wheel revolution from expansion joint |
| Lateral Load Position(s) | 4 |
| Number/Type of Sensors | 64 strain transducers |
| STS Sample Rate | 40 Hz |
| Number of Test Vehicles | 3 |
| Structure Access Type | Flat-bed truck and ladder |
| Structure Access Provided by | USACE |
| Traffic Control Provided by | USACE |
| Total Field Testing Time | 8 hr |
| Field Notes | See Appendix B |
| Additional Nondestructive Testing Info | N/A |
| Visual Condition | Structure in good to fair condition |
| Data Files<br>    4360DT-1.dat<br>    4360DT-2.dat<br>    4360DT-3.dat<br>    4360DT-4.dat<br>    4360DT-5.dat<br>    4360DT-6.dat<br><br>    4360HET-1.dat<br>    4360HET-2.dat<br>    4360HET-3.dat<br>    4360HET-4.dat | Truck    Lateral Truck Position<br>Dump truck @ Y1 – good<br>Dump truck @ Y1 – good<br>Dump truck @ Y2 – good<br>Dump truck @ Y2 – good<br>Dump truck @ Y3 – good<br>Dump truck @ Y3 – good<br><br>HETS empty trailer @ Y2 (too fast no clicks)<br>HETS empty trailer @ Y2 (no clicks)<br>HETS empty trailer @ Y2 (good)<br>HETS empty trailer @ Y2 (good) |

| Item | Description |
|---|---|
| 4360HETM1-1.dat<br>4360HETM1-2.dat<br>4360HETM1-3.dat<br><br>4360M1-1.dat<br>4360M1-2.dat | HETS w/ M1A1 tank @ Y2 – missed first click<br>HETS w/ M1A1 tank @ Y2 – missed one click<br>HETS w/ M1A1 tank @ Y2 – good<br><br>M1 Tank @ Y2 – good<br>M1 Tank @ Y2 – good |

Table 3. Testing vehicle information (dump truck).

| Vehicle Type - Tandem rear-axle dump truck (see Figure 5) | |
|---|---|
| Gross Vehicle Weight (GVW) | 26380 kg |
| Wheel Rollout 5 Revs | 16.4 m |
| # Crawl Speed Passes | 6 |
| # High-Speed Passes/Speed | 0 |
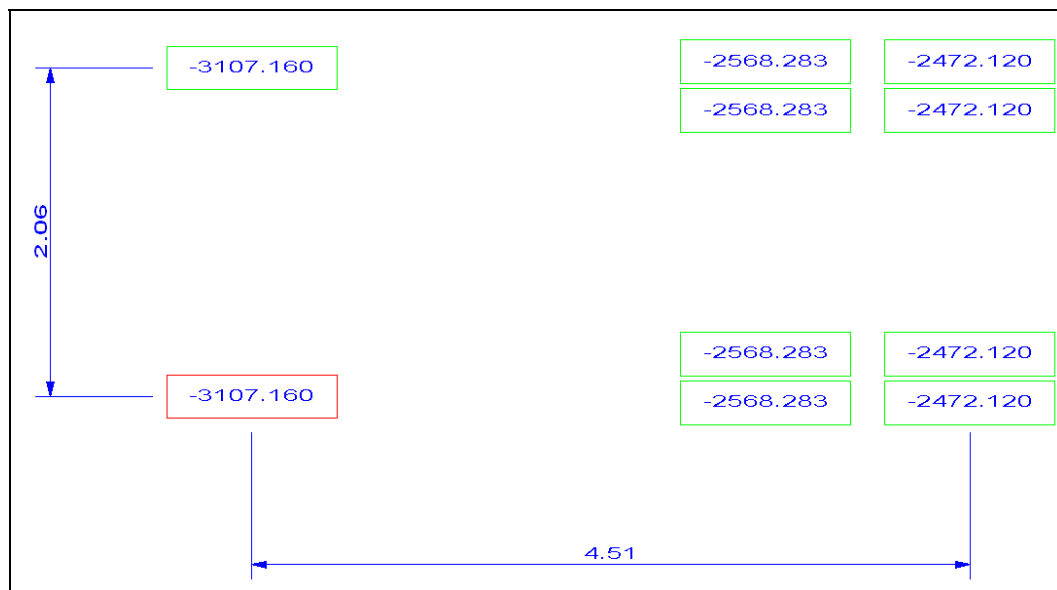
Figure 5. Tandem rear-axle dump truck footprint (measured in meters and kilograms).

Table 4. Testing vehicle information (HET with M1A1 tank).

| Vehicle Type – HETS with M1A1 Tank (see Figure 6) | |
|---|---|
| Gross Vehicle Weight (GVW) | 109400 kg |
| Wheel Rollout 5 Revs | 20.29 m |
| # Crawl Speed Passes | 3 |
| # High-Speed Passes /32 kph | 0 |
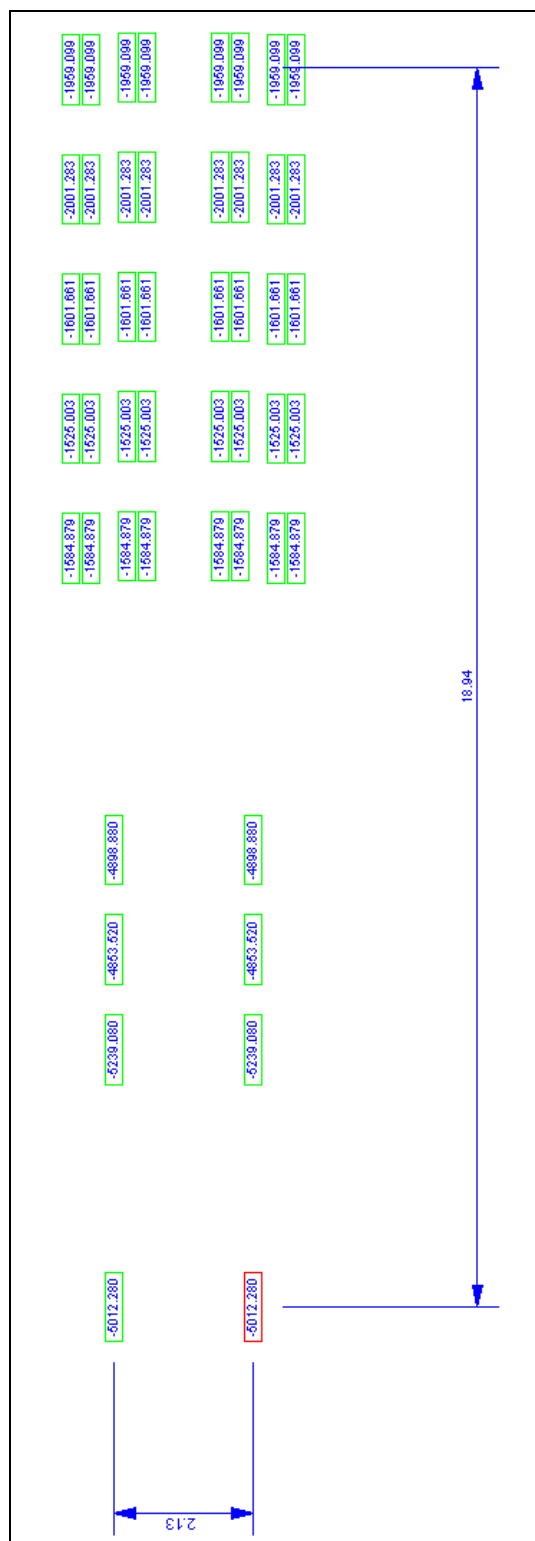


Figure 6. HET with M1A1 tank footprint.

Table 5. Testing vehicle information (empty HET).

| | Vehicle Type – Empty HET (see Figure 7) |
|---|---|
| Gross Vehicle Weight (GVW) | 46500 kg |
| Wheel Rollout 5 Revs | 16.4 m |
| # Crawl Speed Passes | 4 |
| # High-Speed Passes/Speed | 0 |
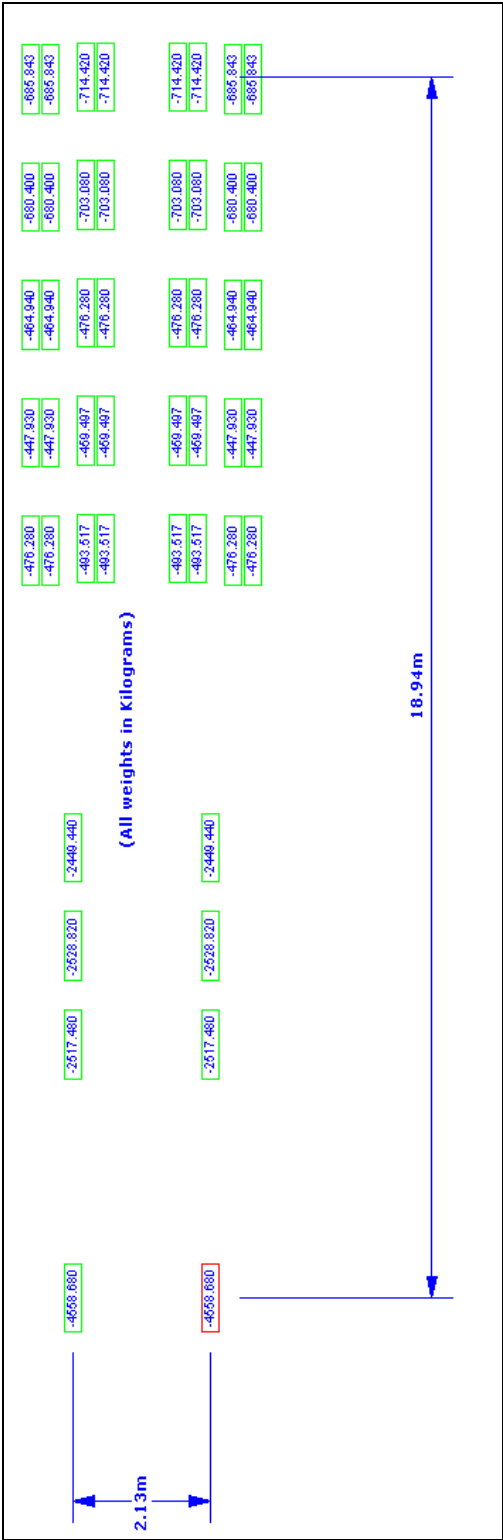


Figure 7. Empty HET footprint.

Table 6. Testing vehicle information (M1A1 tank).

| Vehicle Type – M1A1 Tank (see Figure 8) | |
|---|---|
| Gross Vehicle Weight (GVW) | 71300 kg |
| Wheel Rollout 10 Revs | 21.77 m |
| # Crawl Speed Passes | 2 |
| # High-Speed Passes/Speed | 0 |
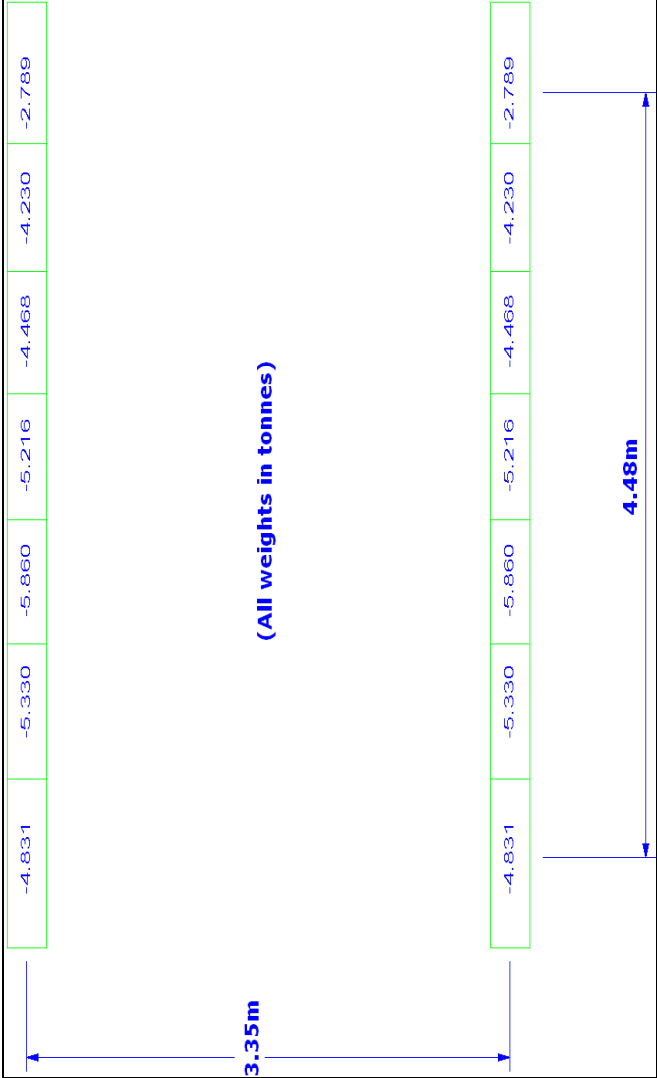


Figure 8. M1A1 tank footprint.

# 3   Investigation of Test Results

All of the field data were first examined graphically to determine quality and to provide a *qualitative* assessment of the structure's live-load response. Some of the indicators of data quality included reproducibility between identical truck crossings, elastic behavior (strains returning to zero after truck crossing), and any unusual-shaped responses that might indicate nonlinear behavior or possible gage malfunctions.

In addition to providing a data "quality check," the information obtained during the preliminary investigation was used to determine appropriate modeling procedures and helped establish the direction that the analysis should take. Several representative response histories are provided in Appendix A.

The following section contains comments based on examination of the load test data. In several cases, supporting data plots are referenced. The data plots typically contain a series legend providing an identification of the data series. In general, the legend contains the gage ID and the data file name. Within the data file name it is possible to determine the bridge ID, the load vehicle, and the pass number. A description of the truck path can be found in Figure 1 and in the field notes in Appendix B. The correlation between truck path and data file name is given in Table 2. Most of the measured data are presented in the form of stress histories in which the X-axis is shown as truck position. Stress values were obtained by simply multiplying the measured strains by the modulus of steel (200,000 MPa). The truck position value indicates the position of the vehicle's front axle with respect to the structure's origin (X = 0.0 in Figure 1).

## Data review for model calibration vehicle (dump truck)

### Reproducibility and linearity

Responses from identical truck paths were very reproducible, as shown in Figure 9. In addition, all stresses appeared to be linear with respect to load magnitude (truck position), and all stresses returned to zero, indicating that the structure was acting in a linear-elastic manner. The stress history plot shows the responses from two gages located at different parts of the
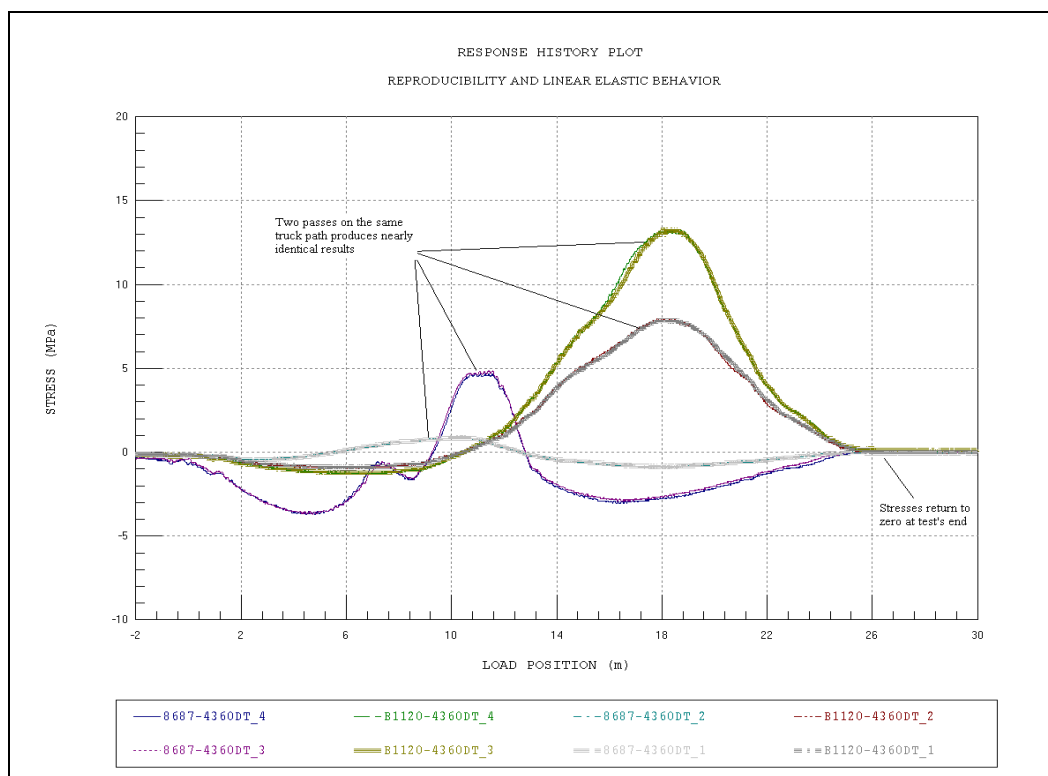
Figure 9. Reproducibility and linear-elastic response.

same beam-line. Data are shown for two truck paths. All of the stress histories had a similar degree of reproducibility and linearity, indicating that good quality data were obtained.

## Lateral distribution and symmetry

A good estimate of lateral distribution can be obtained by comparing the relative stress magnitudes of all beams at midspan, as shown in Figure 10. This data plot shows the midspan stress from each beam-line associated with the maximum midspan moment for three truck paths. From these results it is apparent that there is relatively good lateral distribution; the truck load is resisted by most or all of the beams, depending on the lateral truck position. It is also apparent that the responses are reasonably symmetric. The Y1 Path responses have a slightly greater magnitude than the Y3 Path responses, even though the truck paths were symmetric about the bridge center line. Further examination of data indicated the lack of symmetry was due to variations in the amount of end-restraint provided by the various beam supports. The level of distribution and degree of symmetry indicated that the bridge was responding in a normal fashion.
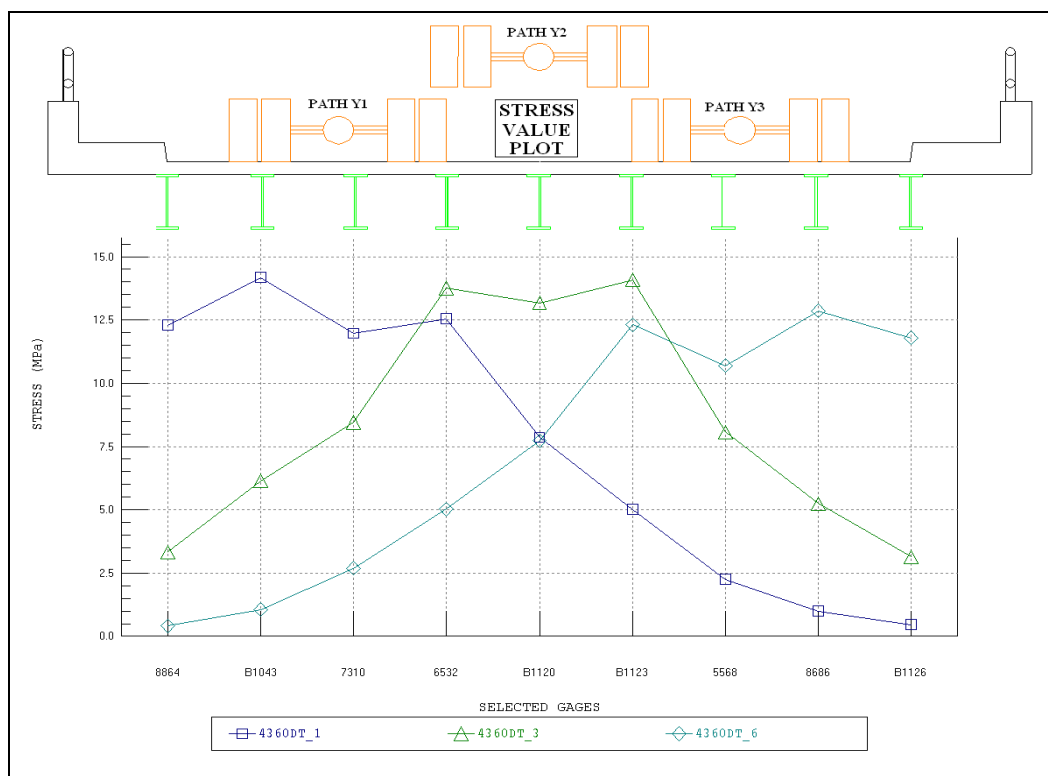
Figure 10. Lateral load distribution at midspan - paths Y1, Y2, and Y3.

**Neutral axis measurements**

Because strains (stresses) were measured at two depths on most instru-
mented cross sections, neutral axis locations (NA) were calculated using
the principles described in Appendix G. As expected, the NA locations
varied with the beam cross-section dimensions and deck thickness. The
exterior beams (B1 and B9) had NA values averaging 675 mm. Beams B2
and B8 were the first interior girders adjacent to the sidewalk and had
average NA values of 563 mm. The interior Type 1 beams (B4 and B6) had
NA values of approximately 500 mm, and the interior Type 2 beams (B3,
B5, and B7) had neutral axes at 488 mm. This information was used to
determine how the deck, sidewalk, and curbs interacted with the beams
and helped with the subsequent modeling procedures. The fact that Beam-
lines 2 and 8 had NA values higher than the other interior girders sug-
gested that the deck in the region next to the sidewalks was effectively
thicker than in the interior portion of the bridge. Photographs of the
bridge deck also indicated a thicker deck (approximately 250 mm). It is
likely that a 75-mm concrete overlay was applied to the deck. The variation
in NA values is likely due to the condition of the concrete overlay at vari-
ous locations on the deck. The concrete overlay adjacent to the sidewalks

was likely in better condition and was contributing to the effective deck thickness and composite beam stiffness.

## End-restraint

Two distinct stress response types were observed near the abutment. The first response displays no negative moment, indicating that the beam is experiencing minimal end-restraint. In this case, little rotational resistance or horizontal resistance was applied to the bottom flange. This would be similar to a theoretically simple beam support. The second response type, however, shows a large negative moment near the end of the beam while the truck is still on the bridge span. The negative flexure is an indication of significant end-restraint. The support details cannot provide a great deal of rotational restraint; however, a large horizontal force can be resisted by the bottom flange if the connection provides adequate restraint. Because the horizontal reaction was applied eccentric to the beam's neutral axis, negative moment was generated. Both response types can be clearly seen in Figure 11, which shows the stress histories of two gages near the abutment. The variation in end-restraint is likely due to differences in bolt tightness at the bearing plates. Because of this support
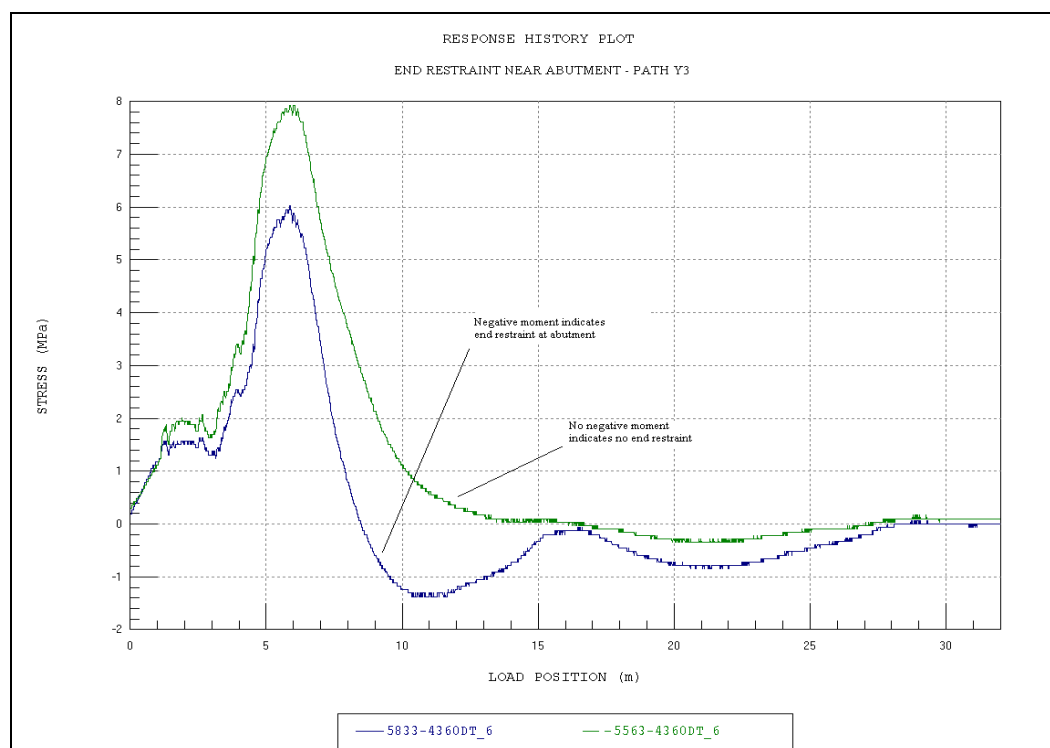


Figure 11. End-restraint near abutment.

detail and the fact that the degree of end-restraint varies from beam to beam, end-restraint should not be represented in subsequent load rating analyses. However, accurate evaluation of the end-restraint is required to accurately evaluate the effective beam and deck stiffness terms.

### Continuity

This structure exhibited notable load transfer from one span to the next. Figure 12 contains a stress history from a transducer located on Span 2 near the middle pier. The negative flexure that occurred while the truck was still on Span 1 indicated some type of load transfer across the pier. However, it was apparent that the beam was not acting like a continuous beam, because positive flexure occurred as soon as the truck traveled beyond the pier onto the span with the transducer. The occurrence of negative moment, after the truck had passed the gage location but was still on the span, indicated that significant end-restraint was provided by the beam bearing. The beams were not connected to one another, and the deck contained an expansion joint over the pier so there was no mechanism to provide flexural continuity over the pier. The source of load transfer was therefore the bottom flanges of the Span 1 and Span 2 beams sharing a common bearing plate. The bottom flanges were bolted to a steel bearing plate such that any horizontal displacement of one beam caused some horizontal displacement of the other beam. Because the bottom flanges are offset vertically from the beam neutral axis, any end-rotation caused horizontal displacement of the bottom flange. This occurrence was relatively consistent among all beam-lines. While the response was different from what is typically assumed by simple beam analyses, it was not an occurrence that should be relied upon for load rating. As with the beam end-restraints at the abutments, the unintended continuity must be realistically depicted during the model calibration so as to accurately assess other stiffness parameters, but then should be ignored for load rating calculations.

### Removed gages

A majority of top gages throughout the structure were placed very close to the neutral axis of the cross section, resulting in low stress responses (as shown in Figure 13). The low stress magnitudes are useful in that they help determine the location of the beam neutral axes, but they have little value for, and ultimately hinder, the automated model calibration process. As a result, these gages will not be considered in the model calibration.
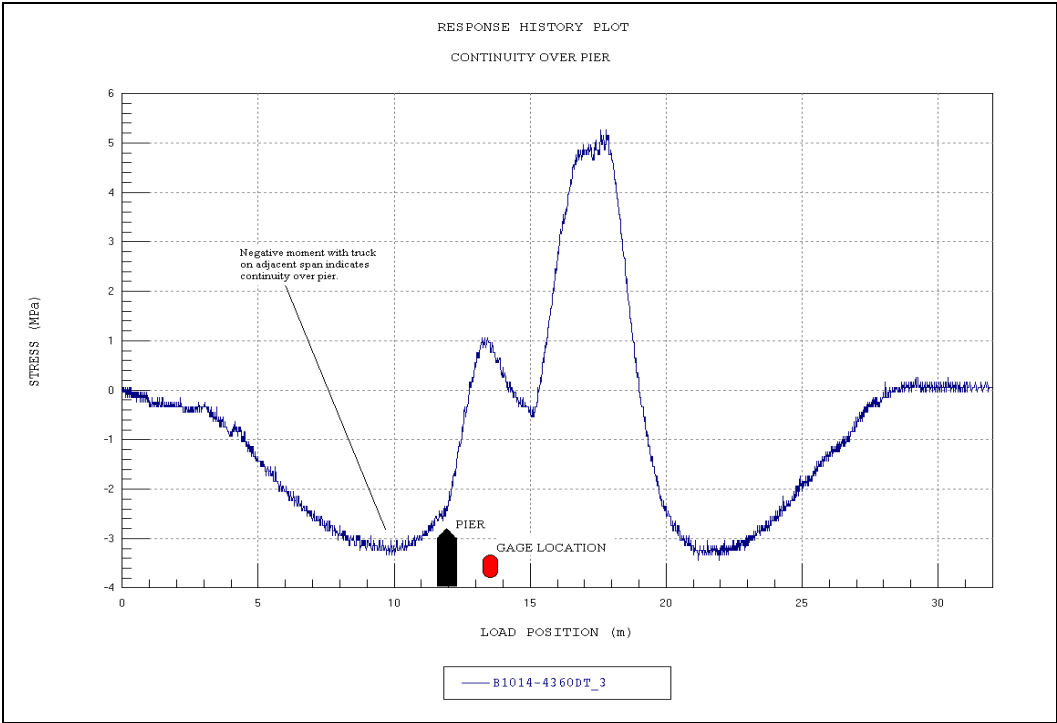
Figure 12. Continuity over pier.
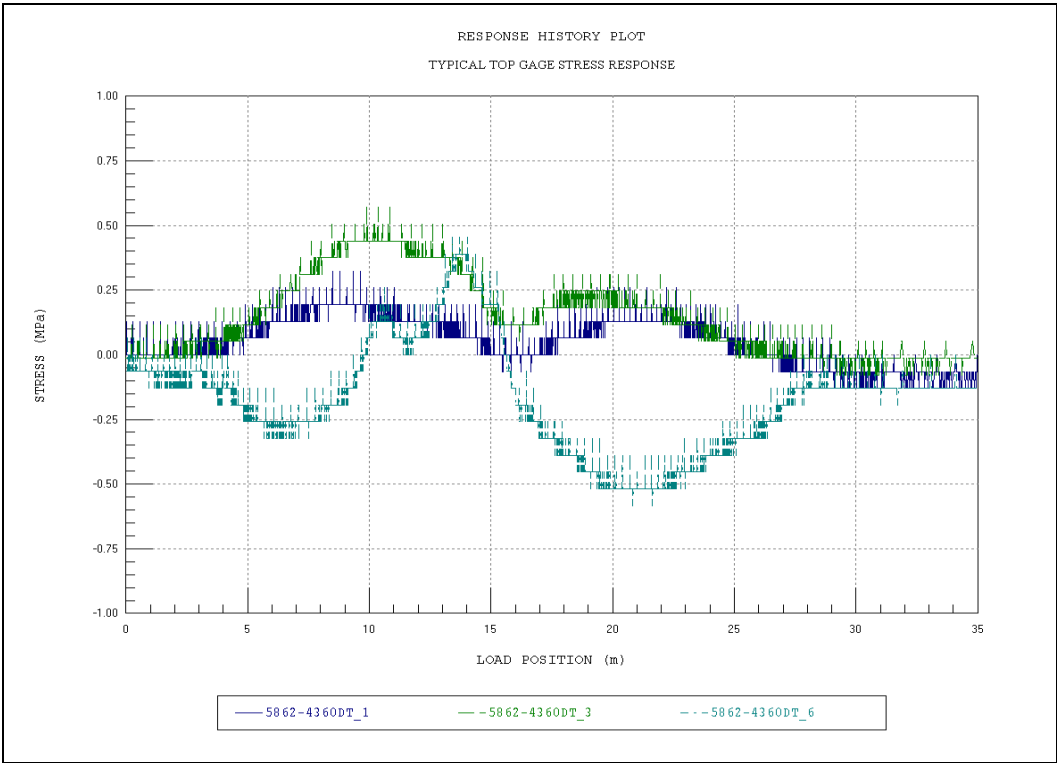


Figure 13. Typical stress magnitude at upper web gages – near neutral axis.

## Data review for military vehicle loads

In addition to the controlled load tests with the dump truck, tests were performed with a HETS loaded with an M1A1 tank, an empty HETS, and the M1A1 tank directly. As with the measurements obtained from the dump truck, the data from the military vehicles were examined for quality and as a qualitative measure of the structure's performance. Observations made from the various load tests are summarized below.

- All tests performed with the heavy military loads were duplicated to examine reproducibility. The same level reproducibility was obtained with the heavy loads as was achieved with the lighter dump truck. As shown in Figure 14, stresses returned to zero after each load cycle, indicating that all responses were linear-elastic. Reproducibility of the bottom flange stress distribution can also be observed in Figure 15.
- A primary goal of the test was to make direct comparisons of the HETS/M1 and M1 tank data. A comparison of a midspan stress history is shown in Figure 16. These data were from Beam 6, which was directly under one of the wheel lines for both vehicles. Stress distributions from the M1A1 loading and the HETS/M1 loading at section E are compared in Figure 17. This plot shows that use of the HETS reduces the overall cross-section moment and improves load distribution across the section.
- A maximum measured stress from all load tests (28.3 MPa) was generated by the M1A1 tank alone. The maximum and minimum stress responses for all tested vehicles can be seen in Table 7.
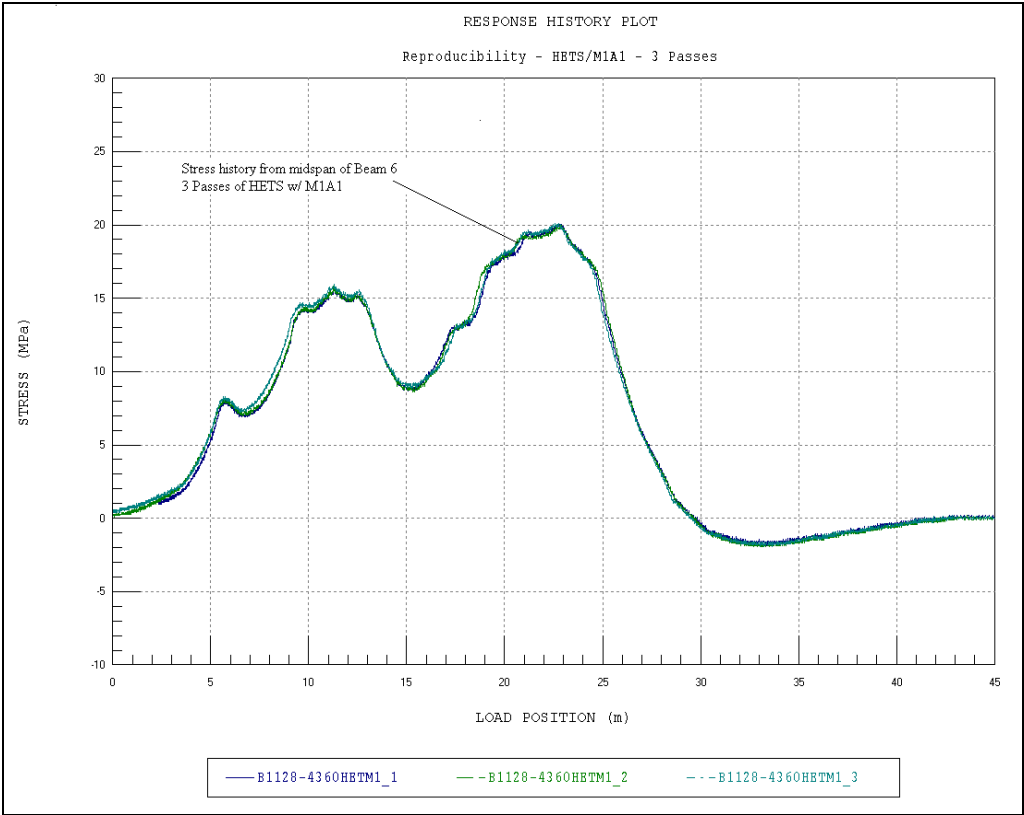
Figure 14. Reproducibility of HETS_M1A1 load tests.
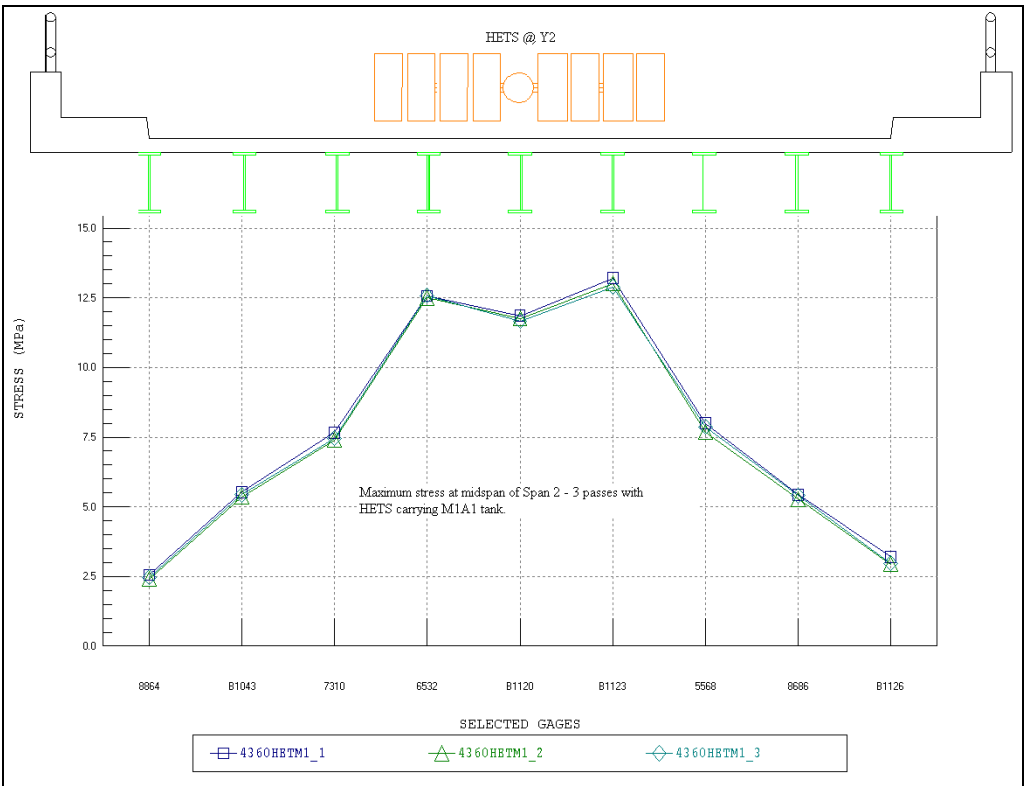


Figure 15. Reproducibility of lateral load distribution.
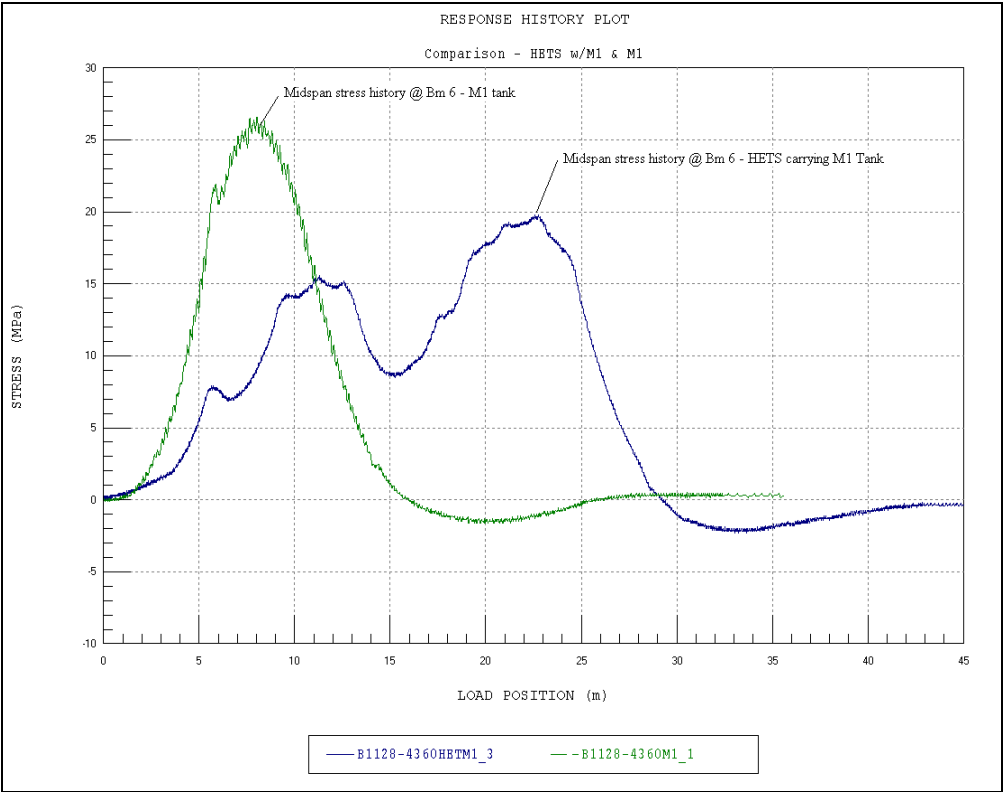
Figure 16. Comparison of midspan stress - HETS with M1 and direct loading of M1.
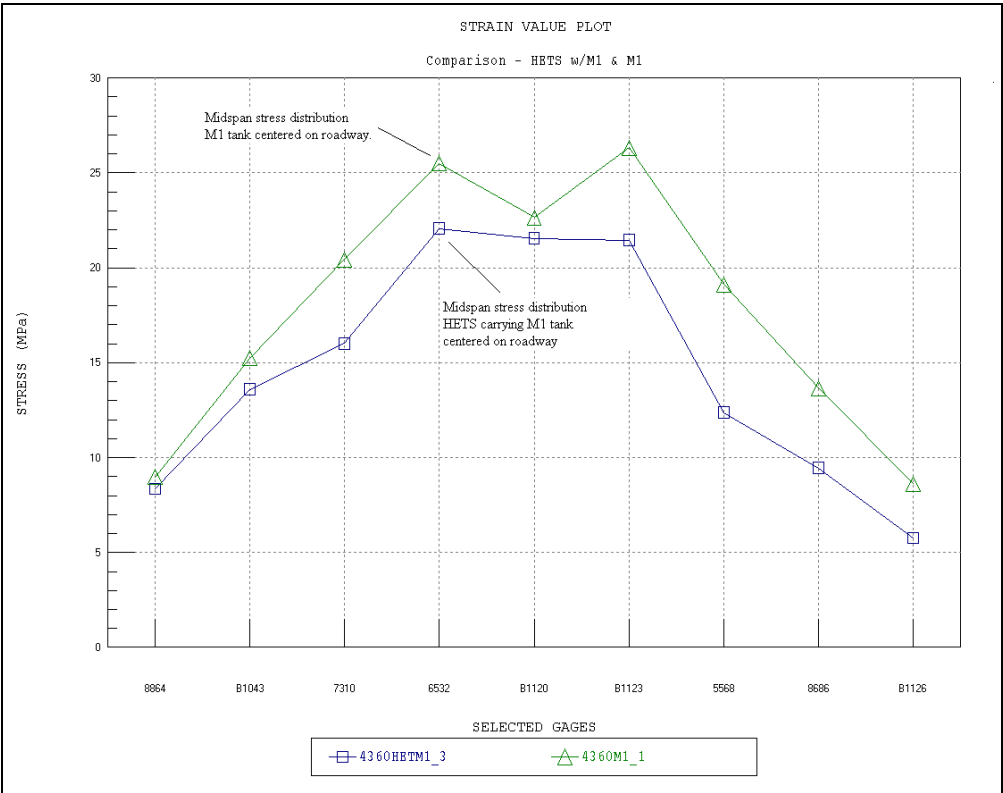


Figure 17. Lateral distribution of HETS with M1 tank and direct loading of M1 tank.

Table 7. Measured military vehicle stress values. (All values in megapascals, MPa.)

| Location | Transducer ID | HETS w/M1A1 Tank Stress, MPa | | Empty HETS Stress, MPa | | M1A1 Tank Stress, MPa | |
|---|---|---|---|---|---|---|---|
| | | Min | Max | Min | Max | Min | Max |
| Section A - B3 - Bottom | B1118 | -2.52 | 2.46 | -0.96 | 1.19 | -1.52 | 7.16 |
| Section A - B4 - Bottom | B1116 | -4.63 | 4.36 | -1.70 | 3.38 | -3.40 | 8.71 |
| Section A - B5 - Bottom | 4050 | -0.95 | 6.95 | -0.37 | 2.51 | -0.09 | 7.80 |
| Section A - B6 - Bottom | 5859 | -0.94 | 9.28 | -0.23 | 4.53 | -0.39 | 11.70 |
| Section A - B7 - Bottom | 5563 | -1.22 | 7.11 | -0.06 | 2.86 | -0.81 | 12.22 |
| Section A - B8 - Bottom | 5833 | -1.98 | 2.67 | -0.46 | 1.11 | -1.90 | 5.89 |
| Section A - B9 - Bottom | 7901 | -2.61 | 0.67 | -0.61 | 0.53 | -2.48 | 2.81 |
| Section A - B9 - Top | B1122 | -0.97 | 0.19 | -0.43 | 0.06 | -0.78 | 0.39 |
| Section B - B1 - Bottom | B1129 | -1.61 | 6.25 | -0.33 | 2.10 | -1.22 | 8.28 |
| Section B - B1 - Top | B1119 | -0.56 | 0.60 | -0.23 | 0.16 | -0.64 | 0.92 |
| Section B - B2 - Bottom | B1046 | -1.97 | 10.89 | -0.43 | 3.83 | -1.59 | 14.66 |
| Section B - B3 - Bottom | B1032 | -2.21 | 14.29 | -0.72 | 5.63 | -1.82 | 21.02 |
| Section B - B4- Bottom | B1095 | -2.53 | 20.75 | -0.68 | 7.68 | -1.95 | 28.29 |
| Section B - B5 - Bottom | B1094 | -2.67 | 20.73 | -0.61 | 8.08 | -1.81 | 25.01 |
| Section B - B6 - Bottom | B1128 | -2.29 | 19.75 | -0.49 | 8.65 | -1.59 | 26.57 |
| Section B - B6 - Top | B1191 | -4.36 | 0.29 | -0.93 | 0.33 | -4.45 | 0.19 |
| Section B - B7 - Bottom | 8865 | -2.14 | 13.21 | -0.65 | 5.38 | -1.80 | 22.35 |
| Section B - B7 - Top | B1100 | -3.66 | 0.19 | -1.08 | 0.17 | -4.08 | 0.35 |
| Section B - B8 - Bottom | B1097 | -1.69 | 8.72 | -0.47 | 3.33 | -1.48 | 14.38 |
| Section B - B8 - Top | B1133 | -0.88 | 0.10 | -0.37 | 0.12 | -0.53 | 0.54 |
| Section B - B9 - Bottom | B1125 | -1.54 | 5.19 | -0.29 | 2.15 | -1.43 | 9.21 |
| Section B - B9 - Top | 6327 | -0.35 | 0.49 | -0.12 | 0.27 | -0.51 | 1.18 |
| Section B - West Curb - Bottom | 6150 | -0.48 | 0.34 | -0.14 | 0.21 | -0.46 | 0.99 |
| Section B - West Curb - Top | B1127 | -3.81 | 0.10 | -0.62 | 0.74 | -4.78 | 0.39 |
| Section C - B3 - Bottom | 5560 | -3.96 | 3.40 | -1.11 | 1.39 | -3.18 | 8.62 |

| Location | Transducer ID | HETS w/M1A1 Tank Stress, MPa | | Empty HETS Stress, MPa | | M1A1 Tank Stress, MPa | |
|---|---|---|---|---|---|---|---|
| | | Min | Max | Min | Max | Min | Max |
| Section C - B4 - Bottom | 9065 | -5.45 | 4.10 | -2.49 | 2.76 | -4.45 | 9.60 |
| Section C - B5 - Bottom | 7906 | -5.19 | 1.99 | -2.50 | 0.77 | -3.90 | 5.44 |
| Section C - B6 - Bottom | 8687 | -7.76 | 2.15 | -3.54 | 1.09 | -5.97 | 7.05 |
| Section C - B7 - Bottom | 5698 | -3.05 | 2.06 | -1.12 | 1.00 | -2.65 | 8.50 |
| Section C - B8 - Bottom | 8688 | -1.77 | 2.28 | -0.66 | 0.99 | -1.83 | 6.26 |
| Section C - B9 - Bottom | 4118 | -0.39 | 3.39 | -0.02 | 1.43 | -0.14 | 5.29 |
| Section C - B9 - Top | 5862 | -0.31 | 0.92 | -0.06 | 0.45 | -0.04 | 1.13 |
| Section D - B1 - Bottom | 5854 | -0.25 | 4.50 | -0.12 | 1.66 | -0.78 | 5.75 |
| Section D - B1 - Top | 8267 | -0.13 | 0.64 | -0.06 | 0.32 | -0.15 | 0.81 |
| Section D - B2 - Bottom | 8860 | -0.93 | 3.80 | -0.51 | 1.15 | -1.87 | 5.61 |
| Section D - B3 - Bottom | 5696 | -3.08 | 4.08 | -1.08 | 1.46 | -3.30 | 7.86 |
| Section D - B4 - Bottom | B1088 | -7.14 | 2.50 | -2.84 | 1.64 | -4.88 | 6.85 |
| Section D - B5 - Bottom | B1044 | -5.92 | 2.55 | -2.17 | 1.26 | -4.72 | 5.18 |
| Section D - B6 - Bottom | B1014 | -9.18 | 2.32 | -3.70 | 1.70 | -6.22 | 6.78 |
| Section D - B7 - Bottom | 8863 | -2.38 | 3.60 | -1.22 | 1.24 | -3.47 | 8.38 |
| Section D - B8 - Bottom | 9020 | -1.41 | 3.33 | -0.51 | 1.28 | -2.12 | 5.58 |
| Section D - B9 - Bottom | 5564 | -0.72 | 2.63 | -0.14 | 1.28 | -0.71 | 4.25 |
| Section D - B9 - Top | 4123 | -0.21 | 0.54 | 0.00 | 0.37 | -0.09 | 0.84 |
| Section E - B1 - Bottom | 8864 | -0.72 | 8.53 | -0.35 | 2.45 | -1.76 | 10.03 |
| Section E - B1 - Top | B1045 | -0.53 | 0.99 | -0.40 | 0.36 | -0.74 | 1.35 |
| Section E - B2 - Bottom | B1043 | -1.04 | 13.88 | -0.71 | 4.10 | -2.14 | 16.61 |
| Section E - B2 - Top | B1132 | -0.64 | 0.52 | -0.33 | 0.44 | -0.72 | 0.73 |
| Section E - B3 - Bottom | 7310 | -1.28 | 16.12 | -0.65 | 5.15 | -2.28 | 21.36 |
| Section E - B3 - Top | 8984 | -4.78 | 0.08 | -2.07 | 0.08 | -4.93 | 0.10 |
| Section E - B4 - Bottom | 6532 | -1.56 | 22.05 | -0.85 | 7.75 | -2.69 | 26.51 |
| Section E - B4 - Top | 4079 | -5.09 | 0.07 | -2.10 | 0.18 | -6.06 | 0.25 |

| Location | Transducer ID | HETS w/M1A1 Tank Stress, MPa | | Empty HETS Stress, MPa | | M1A1 Tank Stress, MPa | |
|---|---|---|---|---|---|---|---|
| | | Min | Max | Min | Max | Min | Max |
| Section E - B5 - Bottom | B1120 | -1.71 | 21.71 | -0.90 | 7.14 | -2.75 | 23.63 |
| Section E - B5 - Top | B1087 | -3.76 | 0.20 | -1.52 | 0.16 | -3.86 | 0.10 |
| Section E - B6 - Bottom | B1123 | -1.64 | 21.54 | -0.88 | 7.24 | -2.74 | 27.09 |
| Section E - B6 - Top | B1139 | -3.58 | 0.00 | -1.74 | 0.10 | -3.40 | 0.17 |
| Section E - B7 - Bottom | 5568 | -1.38 | 12.56 | -0.69 | 4.50 | -2.12 | 19.37 |
| Section E - B7 - Top | 5565 | -2.48 | 0.05 | -0.63 | 0.06 | -2.72 | 0.13 |
| Section E - B8 - Bottom | 8686 | -1.02 | 9.58 | -0.51 | 3.12 | -1.77 | 13.97 |
| Section E - B8 - Top | 8861 | -0.81 | 0.07 | -0.30 | 0.04 | -0.67 | 0.20 |
| Section E - B9 - Bottom | B1126 | -0.96 | 6.15 | -0.44 | 2.25 | -1.65 | 9.20 |
| Section E - B9 - Top | B1190 | -0.27 | 0.89 | -0.21 | 0.27 | -0.50 | 1.24 |
| Section E - East Curb - Bottom | B1061 | -0.60 | 0.08 | -0.12 | 0.27 | -0.31 | 0.27 |
| Section E - West curb - Bottom | B1124 | -1.84 | 0.76 | -0.56 | 0.44 | -2.79 | 0.30 |
| Section E - West Curb - Top | B1062 | -4.66 | 0.24 | -0.96 | 0.64 | -5.74 | 1.06 |
| Maximum | | -9.18 | 22.05 | -3.70 | 8.65 | -6.22 | 28.29 |

# 4   Modeling, Analysis, and Data Correlation

## Discussion

Note that all of the above information was determined strictly by viewing the field data. The next step was to generate a representative finite element model, as shown in Figure 18. Both spans of the bridge were modeled, with each having identical construction. Details regarding the structure model and analysis procedures are provided in Table 8.
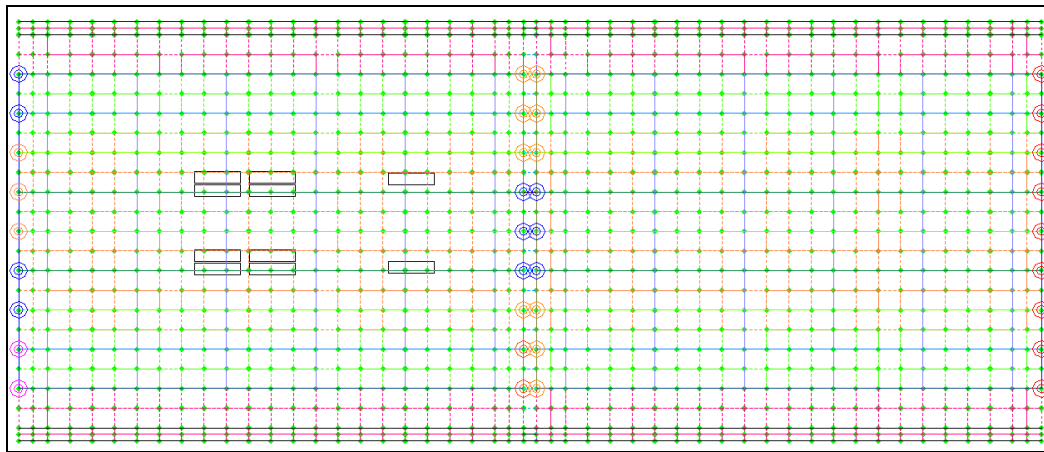


Figure 18. Finite element model of superstructure.

Once the model was developed, the load testing procedures were essentially "reproduced" within the analyses. A two-dimensional (2-D) "footprint" of the loading vehicle was applied to the model along the same paths by which the actual test vehicle crossed the bridge. A direct comparison of strain values was then made between the analytical predictions and the experimentally measured results. The initial model was then "calibrated" by modifying various properties and boundary conditions until the results matched those measured in the field. A complete outline of this process is provided in Appendix G. Table 8 provides a summary of the model details and parameters.

Table 8. Analysis and model details.

| Parameter | Description |
|---|---|
| Analysis Type | Linear-elastic finite element - stiffness method. |
| Model Geometry | Planar-grid composed of shell elements, beam elements, and springs. |
| Nodal Locations | Nodes placed at all bearing locations.<br>Nodes at all four corners of each shell element. |
| Model Components | Shells for all slab elements.<br>Beam elements for stringers, diaphragms, and guardrails.<br>Springs elements at each support.<br>Axial link elements to transfer horizontal reactions from one beam to the next over the pier. |
| Live Load | 2-D footprint of test truck consisting of 10 vertical point loads. The truck path was simulated by series of load cases with truck moving at 0.61-m increments. |
| Dead Load | Self-weight of structure plus weight of guardrail uprights and pipe attached to the exterior of the structure. |
| Number of Load Case Positions Compared | 51 x 3 lateral load paths = 153 load case positions compared. |
| Total Number of Strain Comparisons | 46 strain points x 153 load positions = 7038 strain comparisons. |
| Model Statistics | 1250    Nodes<br>2203    Elements<br>24        Cross section/material types<br>153     Load cases<br>46      Gage locations |
| Adjustable Parameters for Model Calibration | 1.  Axial springs at abutments and piers, $F_x$<br>2.  Moment springs at abutments and piers, $M_y$<br>3.  Slab Young's modulus, $E$<br>4.  Curb moment of inertia, $I_x$<br>5.  Sidewalk/curb Young's modulus, $E$<br>6.  Link stiffness, $E$ |

## Model calibration results

### Deck stiffness

The deck stiffness for this structure increased slightly from the initial value as a result of the parameter optimization. The deck thickness at the interior portion of the bridge was assumed to be 175 mm as specified in the design plans. It was observed in the field that a concrete overlay of approximately 75 mm was present. The increase in the effective modulus was likely due to the contribution of the overlay on the overall slab depth. The effective deck modulus values are not assumed to be the accurate representations of the concrete modulus. The values include the effects of the reinforcing steel, flexural cracks, and any dimensional errors. The goal of obtaining an accurate effective modulus was primarily to obtain a correct

lateral load distribution for the bridge. The same effective modulus was used for the deck and the sidewalk. The slab thickness was increased along the edge of the deck and at the sidewalks.

## Abutment and pier springs

The abutment and pier springs were optimized in both the axial and rotational directions. It was found that a significant amount of end-restraint was present at the abutments and the piers. The degree of end-restraint varied from beam to beam. Because of the variability, the observed support stiffness should not be used in subsequent load rating analyses. However, realistic assessment of the beam bearings was necessary to accurately model the beam and deck stiffness.

## Curb moment of inertia

The moment of inertia ($I_x$) of the curb was initially allowed to adjust ±20% to account for the presence of the steel pipe railing. After optimization, it was observed that the high eccentricity of the railing increased the moment of inertia of the curb more than expected. The moment of inertia was optimized a second time to more accurately reflect the eccentricity of the railing. Both the eccentricity of the steel pipe railing and the stiffness of the curb contributed to extra-stiff exterior girders. Even after two optimizations of the curb stiffness and one optimization of the sidewalk/deck stiffness, the exterior girders are still slightly stiffer than the calibrated model results. This is a reasonable solution since the overall effect results in a slightly more conservative model. The effective curb stiffness should be reduced for the load rating model because minor damage of the railing would reduce its contribution to the curb stiffness.

## Link stiffness

In an attempt to model the unintended continuity over the pier, link elements were used to effectively connect the bottom flanges of the beams. An effective axial stiffness was used to obtain the desired load transfer from one span to the next. As with the end-restraints, the accurate assessment of the continuity was necessary to accurately evaluate other stiffness parameters, but the degree of continuity is not likely reliable over the long term or with heavy loads. Therefore, these link elements should not be used in the load rating analysis.

Following the optimization procedures, the model produced a 0.9857 correlation. The parameter and model accuracy values used in the initial model and obtained for the final model are provided in Table 9. See Appendix G for a description of each error value.

Table 9. Model accuracy and parameter values.

| Modeling Parameter | Initial Model Value | Final Model Value |
|---|---|---|
| **Beam Springs** Note: All springs have eccentricity of -739.8 mm from center of deck. | | |
| S Abutment Springs - Strong (Translational – X)     (kN/mm) | 0 | 780.19 |
| S Abutment Springs - Strong (Rotational – Y)     (kN-m/rad) | 0 | 51588.88 |
| S Abutment Springs - Weak (Translational – X)     (kN/mm) | 0 | 5.30 |
| S Abutment Springs - Weak (Rotational – Y)     (kN-m/rad) | 0 | 51588.88 |
| Pier Springs - Strong (Translational – X)     (kN/mm) | 0 | 19.77 |
| Pier Springs - Strong (Rotational – Y)     (kN-m/rad) | 0 | 37974.20 |
| Pier Springs - Weak (Translational – X)     (kN/mm) | 0 | 6.81 |
| Pier Springs - Weak (Rotational – Y)     (kN-m/rad) | 0 | 37974.20 |
| N Abutment Springs (Translational – X)     (kN/mm) | 0 | 98.23 |
| N Abutment Springs (Rotational – Y)     (kN-m/rad) | 0 | 51588.88 |
| **Stiffness, $E$** | | |
| Sidewalk     (MPa) | 22063 | 23270 |
| Deck     (MPa) | 22063 | 23270 |
| Curb     (MPa) | 22063 | 23270 |
| Link – Strong     (MPa) | 199948 | 670170 |
| Link – Weak     (MPa) | 199948 | 460087 |
| **Moment of Inertia, $I_x$** | | |
| Curb     (mm$^4$) | 2426 x 10$^7$ | 7624 x 10$^6$ |
| **Error Parameters** | Initial Model Value | Final Model Value |
| Absolute Error | 47159.6 | 13183.8 |
| Percent Error | 37.6% | 2.9% |
| Scale Error | 15.7% | 2.3% |
| Correlation Coefficient | 0.9261 | 0.9857 |

In addition to the dump truck, the analysis was run on the calibrated model with the empty HETS, a HETS with an M1A1 tank, and an M1A1 tank alone. Data correlation between the model and the measured data was performed for each of the load vehicles tested. Model accuracy results are provided in Table 10. Overall, the correlation was 0.975 or greater, so it

can be concluded that the model is not specific to any particular load configuration and can be used to represent responses from any live-load situation.

Table 10. Military vehicle accuracy and parameter values.

| Error Parameters | Empty HETS | HETS with M1A1 Tank | M1A1 Tank |
|---|---|---|---|
| Absolute Error | 3843.8 | 7595.4 | 6271.8 |
| Percent Error | 6.1% | 3.9% | 4.6% |
| Scale Error | 12.8% | 8.9% | 9.1% |
| Correlation Coefficient | 0.9754 | 0.9810 | 0.9775 |

# 5   Load Rating Procedures and Results

## Procedures

The goal of producing an accurate model was to better predict the structure's behavior when subjected to design or rating loads. This approach is essentially identical to standard load rating procedures (Manual for Condition Evaluation and Load and Resistance Factor Rating of Highway Bridges, AASHTO 2003), except that a "field-verified" model is used to predict shears and moments instead of a typical beam analysis combined with load distribution factors. (See Appendix H for a detailed outline of the load rating procedures.)

Once the finite element model was calibrated to field conditions, any items thought to be unreliable over the life of the structure were removed from the model. In the case of Bridge S-4360, all end-restraint and continuity variables were set to zero (simple supports). The curb stiffness was also reduced to remove the effect of the guard rail. This procedure was done to ensure that the analysis performed for the load ratings would remain conservative if any of the secondary stiffness parameters changed with load magnitude or over time. For example, the load ratings will not be affected by a reduction in bolt tension at the supports or a damaged guard rail.

Shear and moment capacities were calculated using LRFD Bridge Design Specifications (AASHTO 2004) and the AASHTO (2003) Manual. For this structure, a condition factor of "fair" was selected, based on the National Bridge Inventory rating of 6 reported in the 2005 Bridge Inspection Report provided by the U.S. Army Corps of Engineers. For a list of the load and resistance factors, please refer to Table H4 and Table H5 (Appendix H).

The beam moment capacities were based on composite action between the steel beams and the concrete deck. This assessment was based on shear connector details shown in the renovation plans (29 May 1984) and determined from the load test data. It was assumed that the composite action was available for live load only. Therefore, the structure's dead load was applied to a noncomposite model, and stresses were computed at all extreme fibers. The composite moment capacities were calculated by subtracting the noncomposite dead-load stresses from the yield stress and

multiplying the difference by the composite section modulus of each section [(Yield stress – Dead-load stress) * $S_{XC}$]. The composite moment capacities were used in the load rating calculations to resist all live loads and superimposed dead loads. The superimposed dead loads applied to the composite models consisted of the roadway wearing surface, the railings, and the conduits suspended from the bridge.

Since the shear capacities were dependent only on the steel web properties and not the composite action of the deck and beams, the shear capacities were not separated into noncomposite and composite values. The calculated positive moment capacity and shear capacity based on each unique stringer section can be seen in Table 11 and Table 12. A construction date for the original structure was unknown. The structure was renovated in 1984. A yield stress of 248 MPa was used for all member capacities, based on the AASHTO Manual for Condition Evaluation of Bridges, 2nd ed. (for bridges built after 1963).

Load ratings were computed for several AASHTO and military vehicles. The configuration and layout of all the vehicles used in the load rating is provided in Appendix H. The applied load paths for each of the loading vehicles are described in Table 13. For the standard-width vehicles, two-lane loading could be applied, resulting in a multi-lane presence factor of 1.00. Only single-lane loading could be considered for the wide military vehicles (axle widths greater than 3 m). As per AASHTO LRFD specifications, the single-lane load conditions were multiplied by a factor of 1.2. For all military vehicles except the Palletized Load System (PLS), only single-lane loading could be achieved. An impact factor of 33% was applied to all live-load responses.

Table 11. LRFD positive moment loading, section properties and capacity for noncomposite and composite sections.

| Beam Section | $M_{DL\ Factored}$ kN-m | $Y_{nc}$ mm | $Ix_{nc}$ mm$^4$ | $Sx_{btm}$-$nc$ mm$^3$ | $\sigma_{DLbtm}$ mPa | $Y_c$ mm | $Ix_c$ mm$^4$ | $Sx_{btm}\ c$ mm$^3$ | $\sigma_{Capacity}$ mPa | $M_{LL}$ Capacity kN-m |
|---|---|---|---|---|---|---|---|---|---|---|
| G_1 | 137.50 | 306.4 | 8.542E+08 | 2.788E+06 | 39.5 | 536.194 | 2.237E+09 | 4.173E+06 | 208.8 | 871.0 |
| G_2 | 153.47 | 298.5 | 1.342E+09 | 4.497E+06 | 27.3 | 489.204 | 3.098E+09 | 6.333E+06 | 220.9 | 1399.0 |
| G1_Exterior | 223.73 | 306.4 | 8.542E+08 | 2.788E+06 | 64.2 | 590.296 | 2.594E+09 | 4.395E+06 | 184.0 | 808.7 |

Where:
$M_{DL}$ = maximum dead-load moment from a finite element analysis multiplied by a dead-load factor of 1.25 (AASHTO 3.4.1)

$Ync$, $Yc$ = locations of the neutral axes for the noncomposite and composite sections

$Sx$-$nc$, $Sx$-$c$ = section modulus values for the noncomposite and composite sections

$\sigma_{DL}$ = maximum tensile stress at the bottom flange due to dead-load

$\sigma_{cap}$ = live-load tensile stress capacity of the bottom flange of the composite section

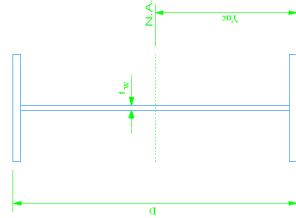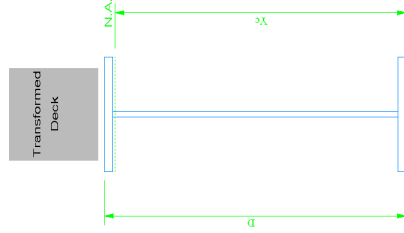$M_{LL\ cap}$ = yield-based live-load capacity of the composite section
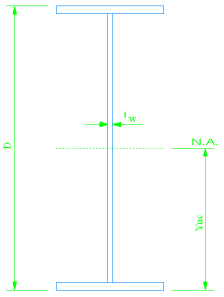
Table 12. LRFD beam shear capacity.

| Beam Section | $D$ mm | $t_w$ mm | $V_p$ kN | $D/t_w$ | $C$ | $V_n$ kN |
|---|---|---|---|---|---|---|
| G_1 | 612.775 | 12.7 | 1120.3 | 48.3 | 1 | 1120.3 |
| G_2 | 596.9 | 15.875 | 1364.2 | 37.6 | 1 | 1364.2 |
| G1_Exterior | 612.775 | 12.7 | 1120.3 | 48.3 | 1 | 1120.3 |



Where:
$Vp$ = plastic shear force = $0.58 * F_y D t_w$ (ASHTO 6.10.9.2)
$C$ = ratio of shear bucking resistance to shear yield strength and is a function of $D/t_w$ (AASHTO 6.19.9.3)
$Vn$ = nominal shear capacity

Table 13. Load path locations.

| Rating Vehicle | Paths | Location |
|---|---|---|
| HS-20, HS-26, HS-30, Type 3, Type 3-3, Type 3S2, PLS | 1 | 0.61 m from edge of east curb |
| | 2 | 0.61 m from edge of west curb |
| | 3 | Driver side wheel on center line |
| | 4 | Passenger side wheel on center line |
| | 5 | Combined paths: 1 & 3 |
| | 6 | Combined paths: 2 & 4 |
| HETS, M1A1 Tank, MCL60, MLC70 | 1 | 0.61 m from edge of east curb |
| | 2 | 0.61 m from edge of west curb |
| | 3 | Center line of roadway |

## Load rating results

Table 14 presents the load and resistance factors used in the load rating calculations. An example computation of an inventory and operating load rating factor is provided for section beam type G1_Exterior:

Table 14. Rating factor calculation for HS-20.

| Moment capacity available for superimposed dead-load and live-load at Section G_Standard | $M_{Cap}$ | 808.7 | kN-m |
|---|---|---|---|
| Superimposed dead-load applied to composite model—wearing surface and railing | DW | 75.69 | kN-m |
| Live-load effect (HS-20) | LL | 113.47 | kN-m |
| Resistance factor for steel in flexure | $\Phi_b$ | 1.00 | |
| Condition factor (good) | $\varphi_c$ | 1.00 | |
| System factor (multiple girders) | $\varphi_s$ | 1.00 | |
| LRFD load factor for structural components and attachments | $\gamma_{DC}$ | 1.25 | |
| Live-load factor | $\gamma_{LL}$ | 1.75<br>1.35 | Inventory<br>Operating |
| Dynamic influence (impact) factor | IM | 1.33 | |
| Using Equation H1:<br>$RF_{Inv}$ = [(1.0)(1.0)(808.7) – (1.25 * 75.69)] / (1.75 * 113.47 * 1.33) = **2.70**<br>$RF_{Opr}$ = [(1.0)(1.0)(808.7) – (1.25 * 75.69)] / (1.35 * 113.47 * 1.33) = **3.50** | | | |

**Calculated load rating factors for the structure are presented in Table 15– Table 29. All load ratings were controlled by positive moment at the exterior girders. Maximum live- and dead-load values for each member group are provided with the rating values. Note that the associated dead load may change slightly because the critical element changes slightly with live-load condition.**

Table 15. Vehicle rating factors and responses – HS-20.

| | Responses [kN-m] | | Inventory | Operating |
|---|---|---|---|---|
| Location | Dead-load | Live-load | RF | RF |
| G_1_Ext | 75.69 | 113.47 | 2.70 | 3.50 |
| G_1_Int | 50.85 | 108.67 | 3.19 | 4.14 |
| G_2_Int | 34.53 | 157.00 | 3.71 | 4.81 |

Table 16. Vehicle rating factors and responses – HS-26.

| | Responses [kN-m] | | Inventory | Operating |
|---|---|---|---|---|
| Location | Dead-load | Live-load | RF | RF |
| G_1_Ext | 75.69 | 147.51 | 2.08 | 2.69 |
| G_1_Int | 50.85 | 141.27 | 2.45 | 3.18 |
| G_2_Int | 34.53 | 204.10 | 2.85 | 3.70 |

Table 17. Vehicle rating factors and responses – HS-30.

| Location | Responses [kN-m] | | Inventory | Operating |
| | Dead-load | Live-load | RF | RF |
| --- | --- | --- | --- | --- |
| G_1_Ext | 75.69 | 170.20 | 1.80 | 2.33 |
| G_1_Int | 50.85 | 163.00 | 2.13 | 2.76 |
| G_2_Int | 34.53 | 235.50 | 2.47 | 3.21 |

Table 18. Vehicle rating factors and responses – Type 3.

| Location | Responses [kN-m] | | Inventory | Operating |
| | Dead-load | Live-load | RF | RF |
| --- | --- | --- | --- | --- |
| G_1_Ext | 75.78 | 88.35 | 3.47 | 4.50 |
| G_1_Int | 52.02 | 84.52 | 4.10 | 5.31 |
| G_2_Int | 32.96 | 124.97 | 4.67 | 6.05 |

Table 19. Vehicle rating factors and responses – Type 3-3.

| Location | Responses [kN-m] | | Inventory | Operating |
| | Dead-load | Live-load | RF | RF |
| --- | --- | --- | --- | --- |
| G_1_Ext | 73.81 | 73.16 | 4.21 | 5.46 |
| G_1_Int | 52.11 | 69.85 | 4.96 | 6.43 |
| G_2_Int | 32.93 | 103.93 | 5.61 | 7.27 |

Table 20. Vehicle rating factors and responses – Type 3S2.

| Location | Responses [kN-m] | | Inventory | Operating |
| | Dead-load | Live-load | RF | RF |
| --- | --- | --- | --- | --- |
| G_1_Ext | 76.71 | 82.25 | 3.72 | 4.82 |
| G_1_Int | 52.53 | 78.94 | 4.38 | 5.68 |
| G_2_Int | 34.50 | 117.63 | 4.95 | 6.42 |

Table 21. Vehicle rating factors and responses – M1A1 tank.

| Location | Responses [kN-m] | | Inventory | Operating |
| | Dead-load | Live-load | RF | RF |
| --- | --- | --- | --- | --- |
| G_1_Ext | 76.80 | 248.63 | 1.23 | 1.59 |
| G_1_Int | 52.53 | 213.01 | 1.62 | 2.10 |
| G_2_Int | 50.53 | 249.04 | 2.30 | 2.98 |

Table 22. Vehicle rating factors and responses – empty HET.

| Location | Responses [kN-m] | | Inventory | Operating |
| | Dead-load | Live-load | RF | RF |
|---|---|---|---|---|
| G_1_Ext | 76.16 | 59.48 | 5.15 | 6.68 |
| G_1_Int | 52.55 | 58.07 | 5.96 | 7.73 |
| G_2_Int | 50.16 | 79.21 | 7.25 | 9.40 |

Table 23. Vehicle rating factors and responses – HET with M1A1 tank.

| Location | Responses [kN-m] | | Inventory | Operating |
| | Dead-load | Live-load | RF | RF |
|---|---|---|---|---|
| G_1_Ext | 76.60 | 173.58 | 1.76 | 2.28 |
| G_1_Int | 52.46 | 161.15 | 2.15 | 2.79 |
| G_2_Int | 50.53 | 222.66 | 2.58 | 3.34 |

Table 24. Vehicle rating factors and responses – Korean HET with K1 tank.

| Location | Responses [kN-m] | | Inventory | Operating |
| | Dead-load | Live-load | RF | RF |
|---|---|---|---|---|
| G_1_Ext | 76.71 | 180.92 | 1.69 | 2.19 |
| G_1_Int | 52.46 | 159.45 | 2.17 | 2.81 |
| G_2_Int | 50.56 | 201.00 | 2.86 | 3.71 |

Table 25. Vehicle rating factors and responses – PLS.

| Location | Responses [kN-m] | | Inventory | Operating |
| | Dead-load | Live-load | RF | RF |
|---|---|---|---|---|
| G_1_Ext | 76.71 | 137.49 | 2.23 | 2.89 |
| G_1_Int | 52.53 | 130.51 | 2.65 | 3.44 |
| G_2_Int | 34.50 | 198.66 | 2.93 | 3.80 |

Table 26. Vehicle rating factors and responses – MLC60-wheeled.

| Location | Responses [kN-m] | | Inventory | Operating |
| | Dead-load | Live-load | RF | RF |
|---|---|---|---|---|
| G_1_Ext | 75.69 | 155.44 | 1.97 | 2.55 |
| G_1_Int | 51.91 | 147.23 | 2.35 | 3.05 |
| G_2_Int | 49.19 | 171.97 | 3.34 | 4.33 |

Table 27. Vehicle rating factors and responses – MLC60-tracked.

| Location | Responses [kN-m] | | Inventory | Operating |
| | Dead-load | Live-load | RF | RF |
|---|---|---|---|---|
| G_1_Ext | 76.80 | 210.27 | 1.46 | 1.89 |
| G_1_Int | 52.53 | 188.78 | 1.83 | 2.37 |
| G_2_Int | 50.56 | 232.37 | 2.47 | 3.20 |

Table 28. Vehicle rating factors and responses – MLC70-wheeled.

| Location | Responses [kN-m] | | Inventory | Operating |
| | Dead-load | Live-load | RF | RF |
|---|---|---|---|---|
| G_1_Ext | 75.69 | 177.78 | 1.73 | 2.24 |
| G_1_Int | 52.53 | 168.61 | 2.05 | 2.66 |
| G_2_Int | 49.25 | 196.15 | 2.93 | 3.80 |

Table 29. Vehicle rating factors and responses – MLC70-tracked.

| Location | Responses [kN-m] | | Inventory | Operating |
| | Dead-load | Live-load | RF | RF |
|---|---|---|---|---|
| G_1_Ext | 76.80 | 235.69 | 1.30 | 1.69 |
| G_1_Int | 52.53 | 210.89 | 1.64 | 2.13 |
| G_2_Int | 50.56 | 262.42 | 2.19 | 2.84 |

# 6   Conclusions and Recommendations

Load test results indicated that the bridge was responding in a normal linear-elastic manner for all applied conditions. There was no indication of any type of distress during any of the load test procedures. Direct comparison of results from the different load configurations showed that the M1A1 tank produced the highest flexural stresses. Flexural stresses produced by the M1A1 tank were approximately 20 to 25% greater than the stresses generated by HETS transporting the M1A1. Stress history plots and lateral distribution plots showed that the HETS was very effective at spreading the load and reducing the overall load effect on the structure.

An accurate grid model was obtained for the bridge, which further indicated that all load responses were in fact linear. A conservative version of the calibrated model was used to compute load rating factors using the AASHTO LRFR method. Load rating results verified the conclusion that the HETS is a preferred method of transporting the M1 tank over the bridge. The bridge, however, was designed for heavy military loads, as the M1 tank can cross the bridge within Inventory (design) stress limits.

It should be noted that no high-speed tests were performed during the testing process. It is suggested that heavy military vehicles travel at crawl speeds when crossing the bridge to ensure proper loading. The location of the bridge is such that high-speed crossings are not feasible, since an intersection occurs immediately after the bridge.

Efforts were made to ensure the load rating had an acceptable degree of conservatism beyond the standard load factors. However, it should be noted that the load ratings are valid only while the bridge remains in its current condition. Any significant loss of member cross section due to deterioration or damage would require additional load rating. No effort was made during the load test or subsequent load ratings to evaluate the abutments, piers, or any substructure components.

# References

American Association of State Highway and Transportation Officials. 2003. *Manual for the condition evaluation and load and resistance factor rating (LRFR) of highway bridges.* Washington, DC.

_____. 2004. *AASHTO LRFD bridge design specifications.* 3d ed. (includes 2005 and 2006 Interims). Washington, DC.

Commander, B. 1989. An improved method of bridge evaluation: Comparison of field test results with computer analysis. MS thesis, Univ. of Colorado, Boulder.

Gerstle, K. H., and M. H. Ackroyd. 1990. Behavior and design of flexibly-connected building frames. *Engineering Journal, AISC* 27(1):22-29.

Goble, G., J. Schulz, and B. Commander. 1992. Load prediction and structural response. Final Report, FHWA DTFH61-88-C-00053. Boulder, CO: University of Colorado.

Lichtenstein, A. G. 1995. *Bridge rating through nondestructive load testing.* Technical Report NCHRP Project 12-28(13)A. National Cooperative Highway Research Program.

Schulz, J. L. 1989. Development of a digital strain measurement system for highway bridge testing. MS thesis, Univ. of Colorado, Boulder.

_____. 1993. In search of better load ratings. *Civil Engineering, ASCE* 63(9):62–65.

# Appendix A: Measured and Computed Strain Comparisons

While statistical terms provide a means of evaluating the relative accuracy of various modeling procedures or help determine the improvement of a model during a calibration process, the best conceptual measure of a model's accuracy is by visual examination of the response histories. The following graphs contain measured and computed stress histories from each truck path. In each graph the continuous lines represent the measured stress at the specified gage location as a function of truck position as it traveled across the bridge. In all cases, the measured stress is the product of the measured strain and the modulus of steel (200,000 MPa). Computed stresses are shown as markers at discrete truck intervals in the same color as the test stress curve.

The following data comparisons indicate that an accurate model was established—certainly within the applicable load factors used for load rating. In general, the analytical results overpredicted the measurements but, on occasion, did underpredict the measurements. A certain amount of error can be expected under the best of conditions. Two of the factors that typically result in differences between measured and calculated responses are described below.

- Variations between the actual truck paths and the modeled path will always exist.
- The real structure will always exhibit secondary response behavior that cannot be simulated by a 2-D grid model. For example, localized behavior due to the vertical pressure of the wheel loads can have a substantial effect on the measurements. An extremely refined 3-D model of the beams would be required to simulate this type of response.

End-restraints provided by beam bearings that are intended to be simple supports are often highly variable and nonlinear. These end-restraints are simulated as well as possible with linear springs, but are generally removed from the model prior to load rating.
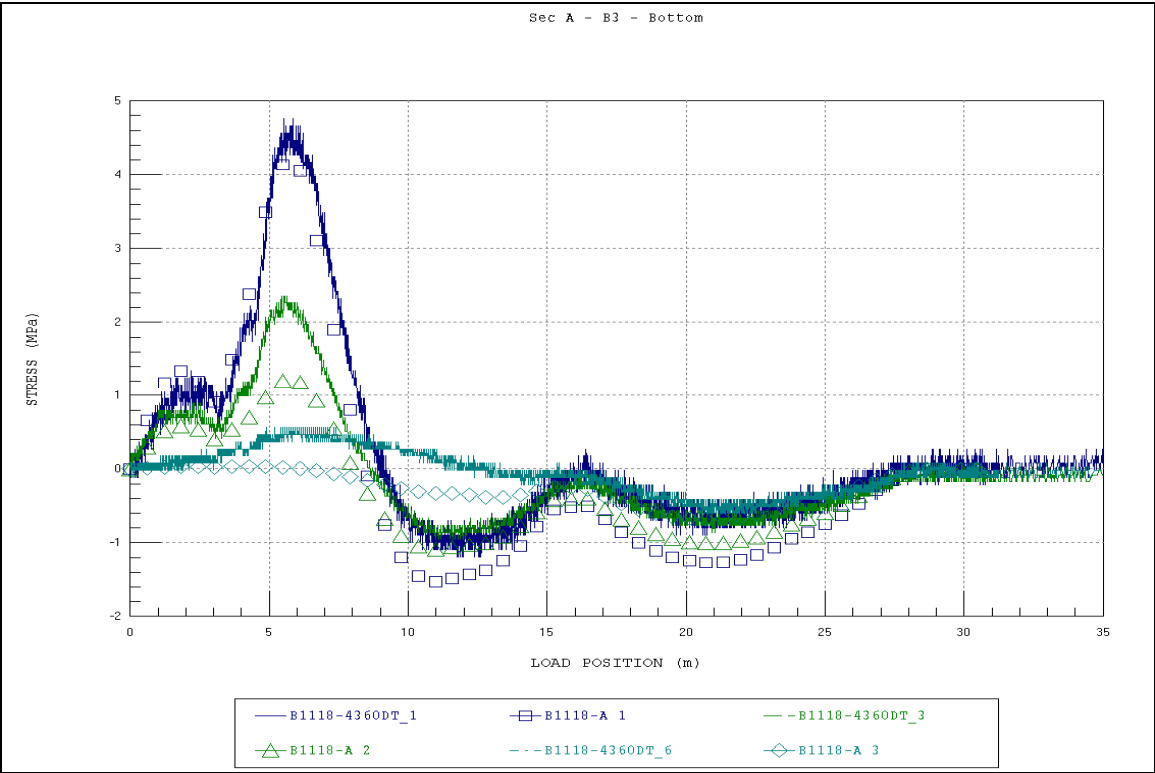
## Test truck
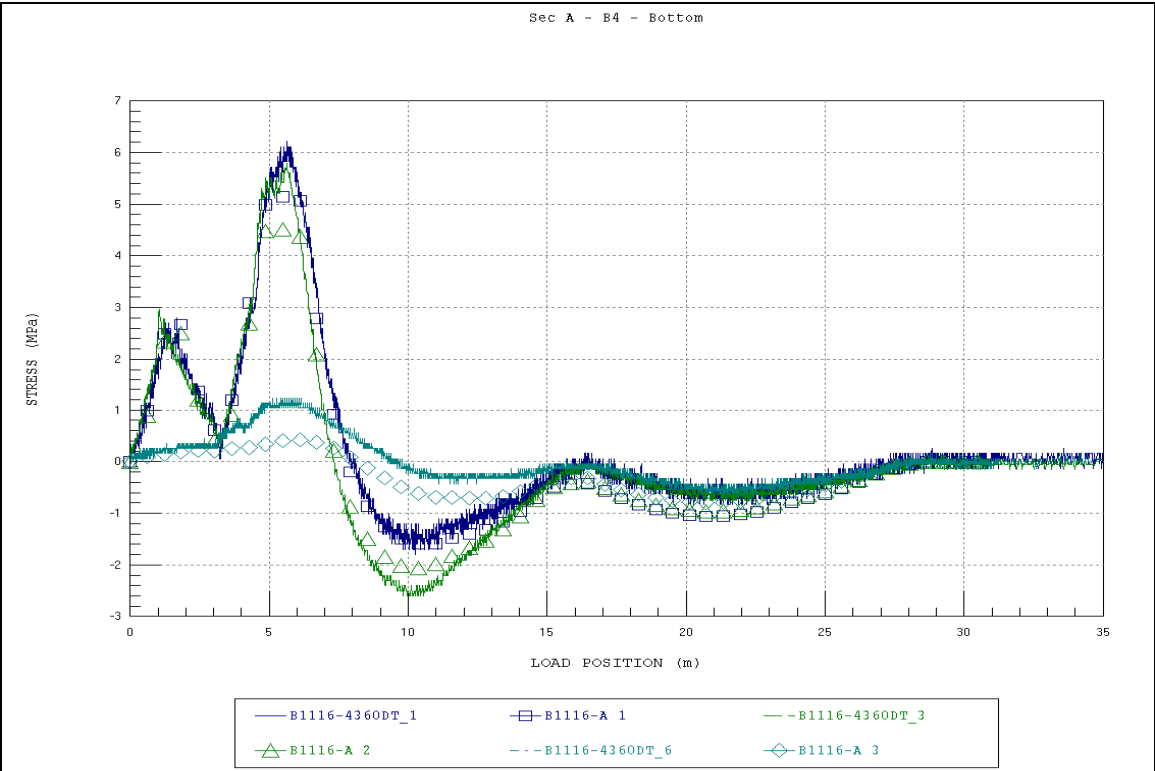


Figure A1. Section A – B3 – Bottom.
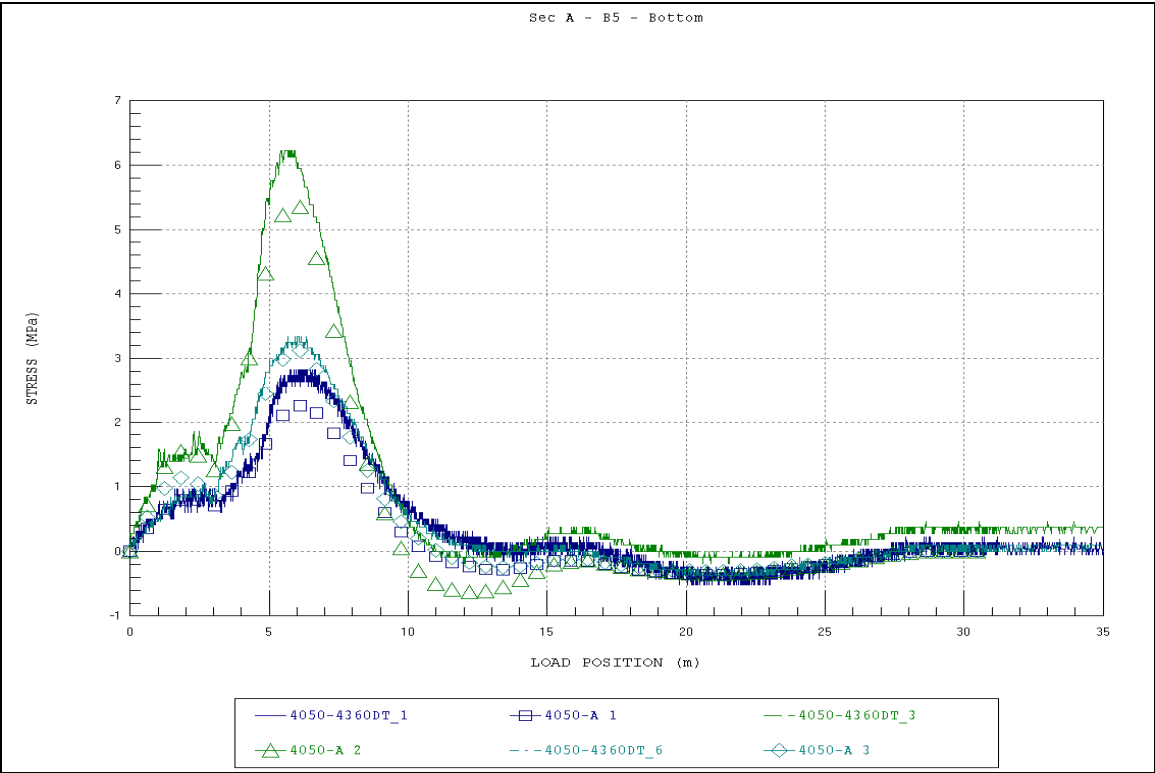


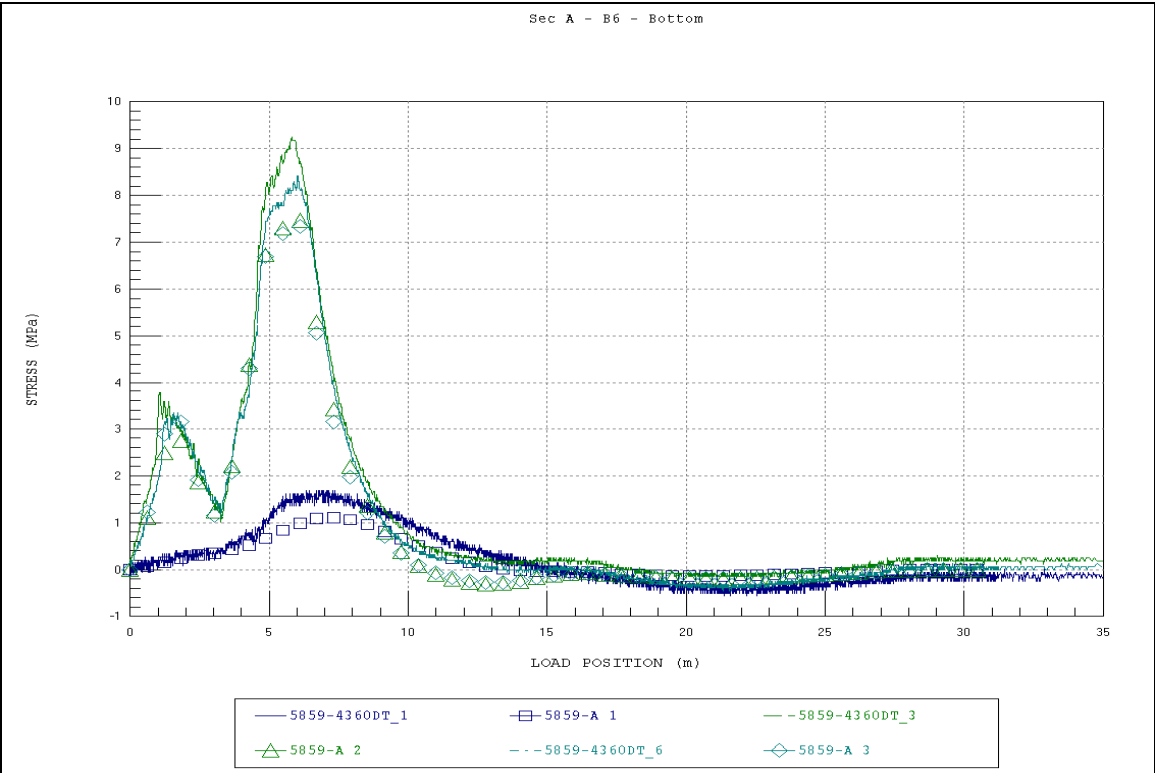Figure A2. Section A – B4 – Bottom.

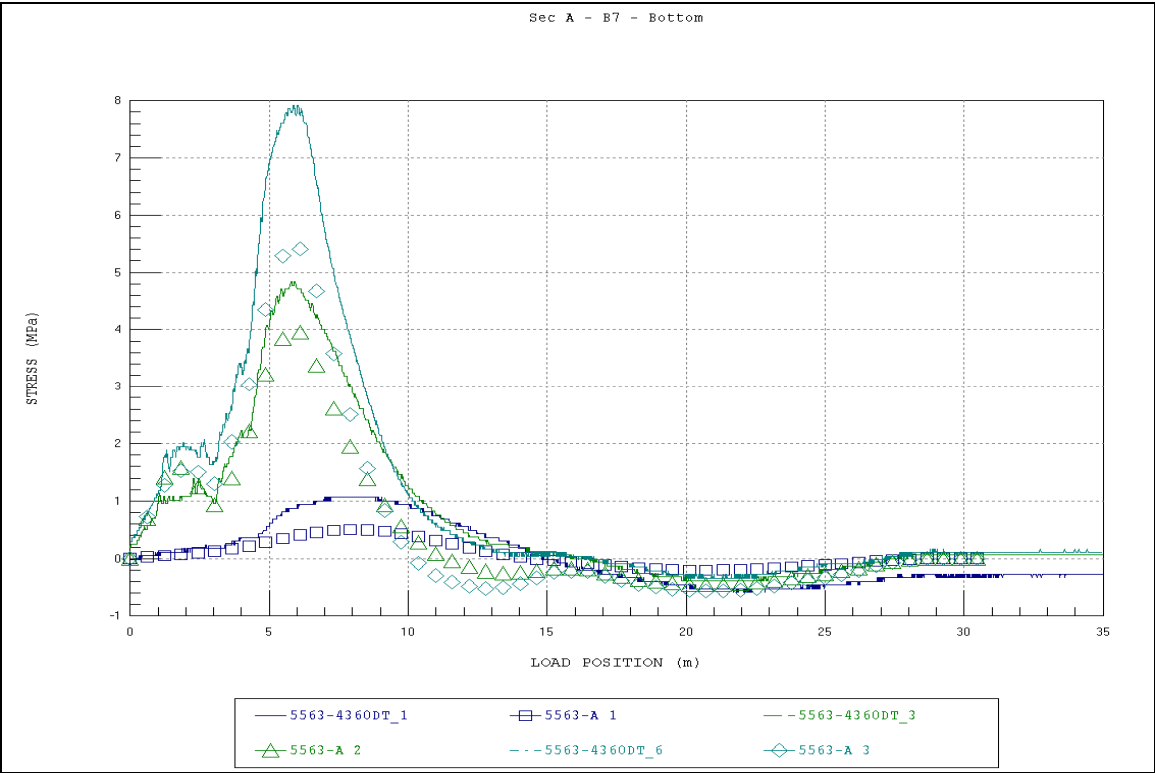Figure A3. Section A – B5 – Bottom.



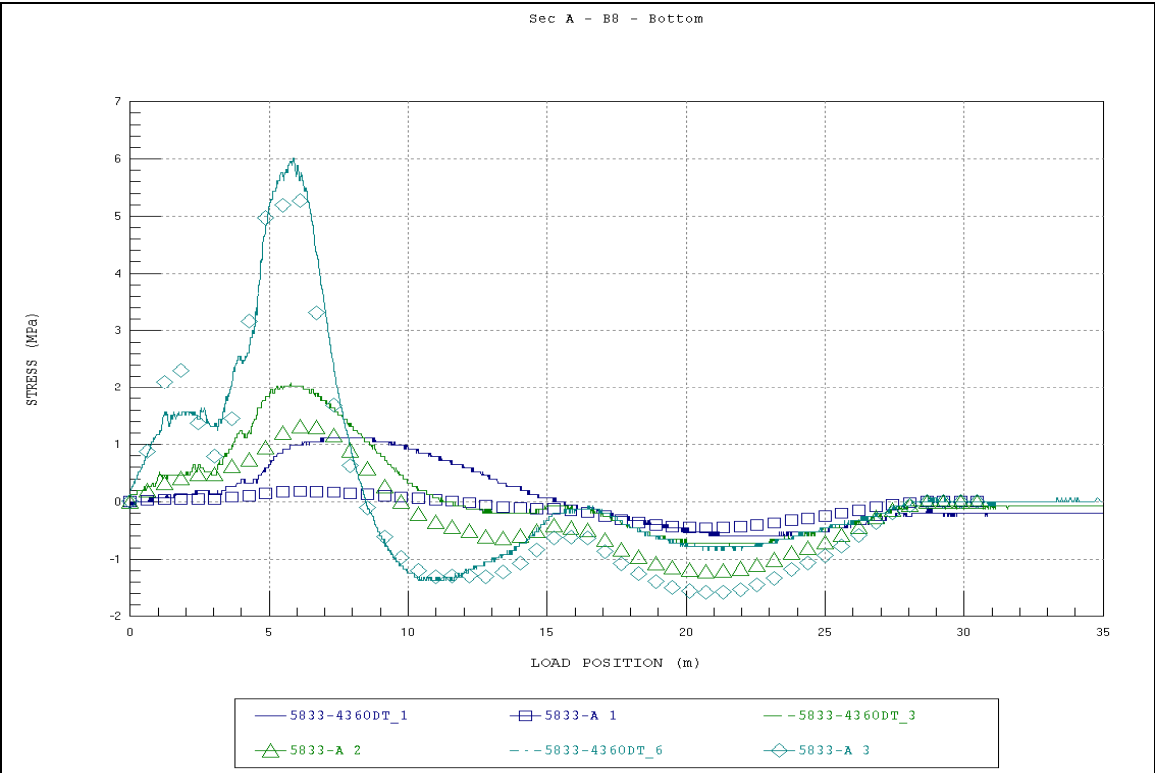Figure A4. Section A – B6 – Bottom.

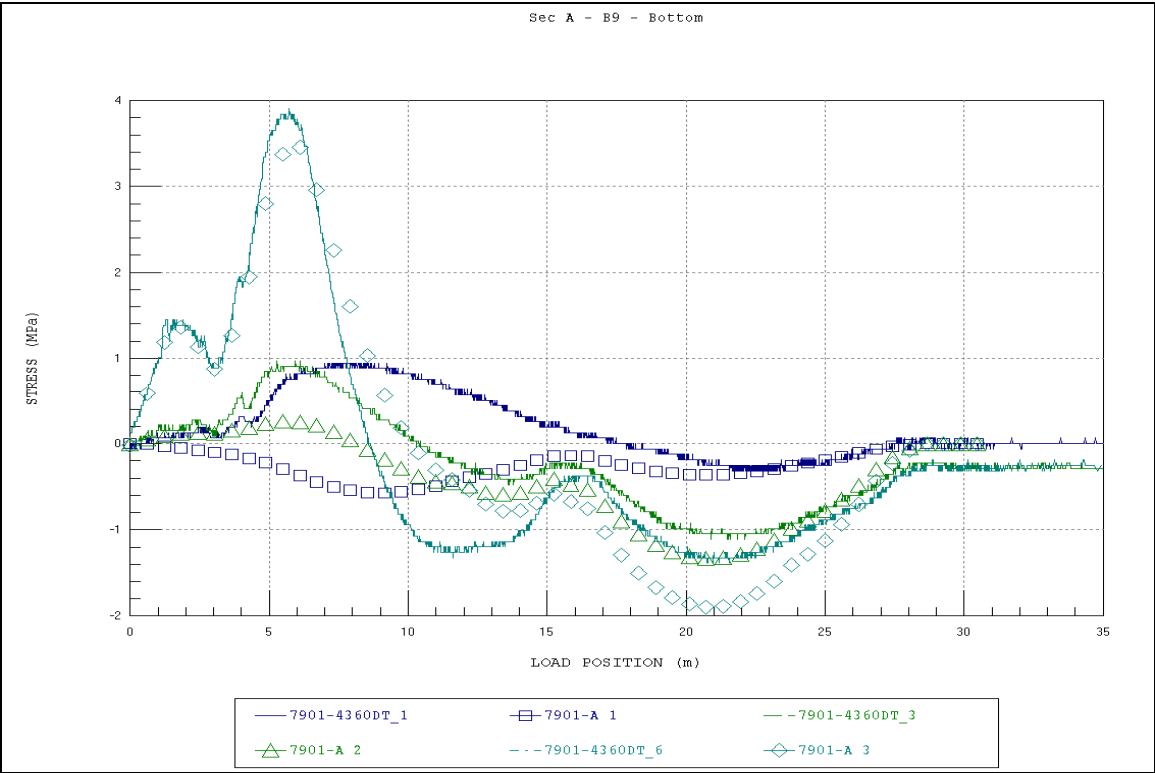Figure A5. Section A – B7 – Bottom.



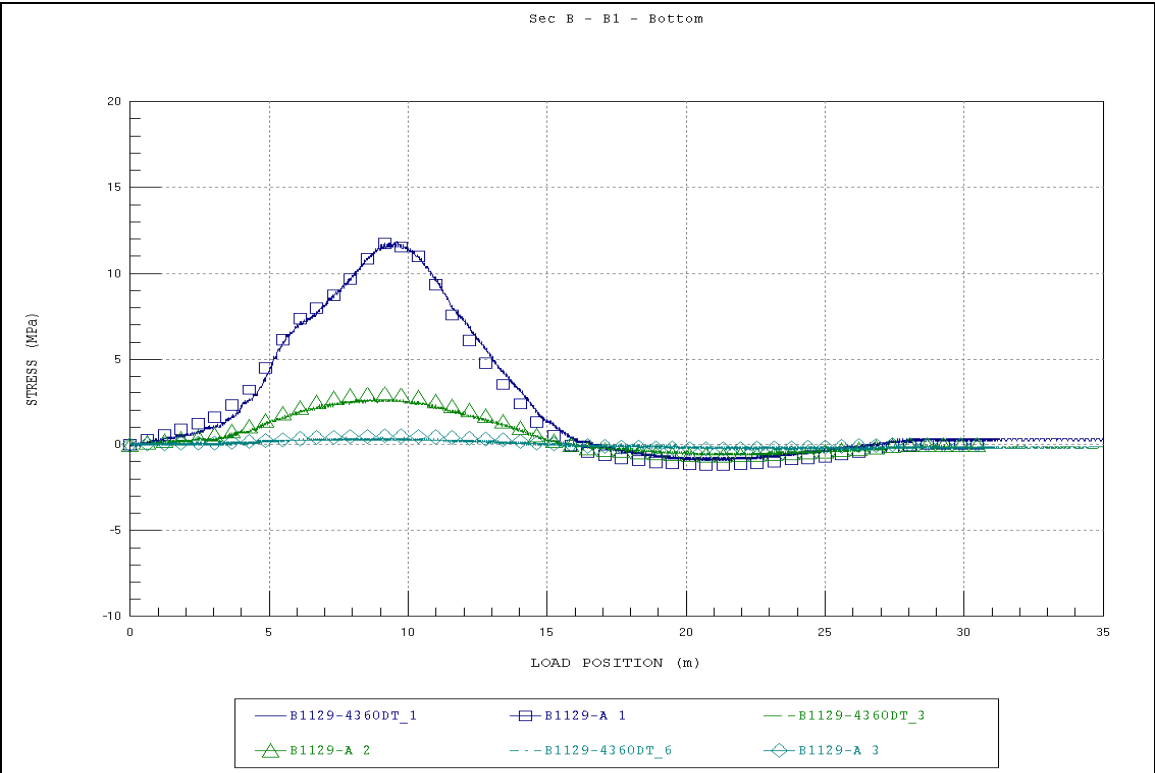Figure A6. Section A – B8 – Bottom.

Figure A7. Section A – B9 – Bottom.
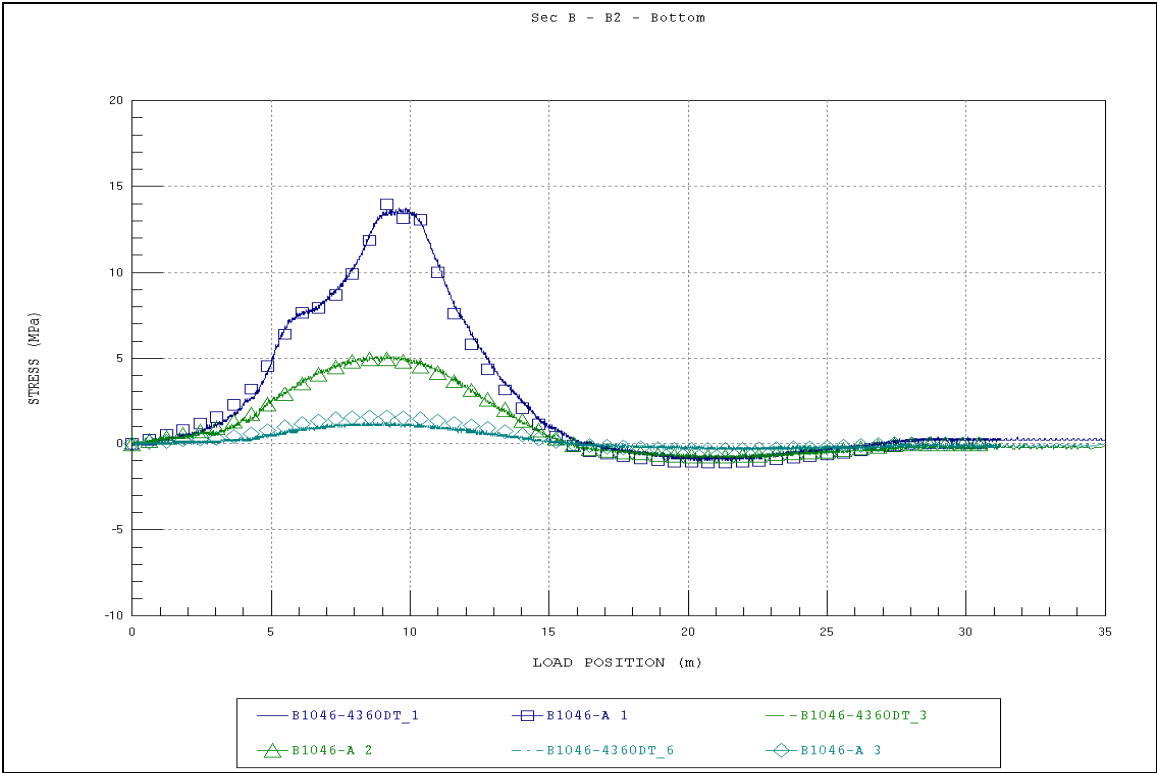


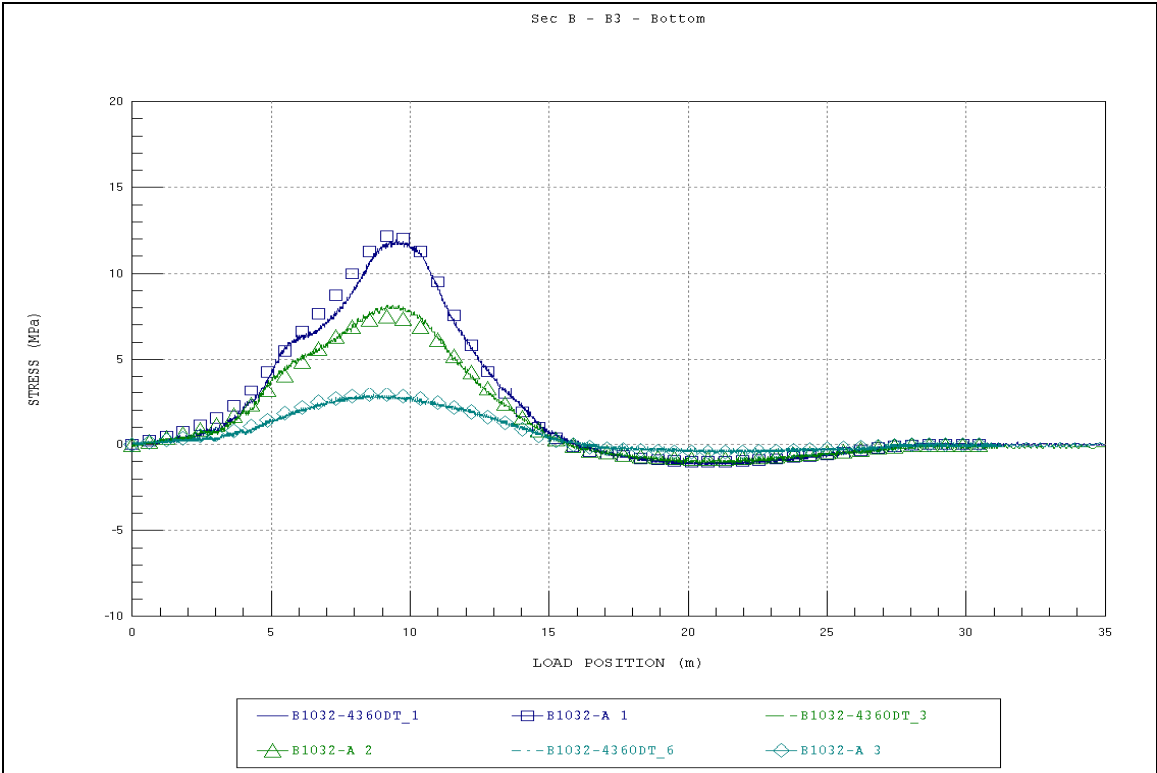Figure A8. Section B – B1 – Bottom.

Figure A9. Section B – B2 – Bottom.
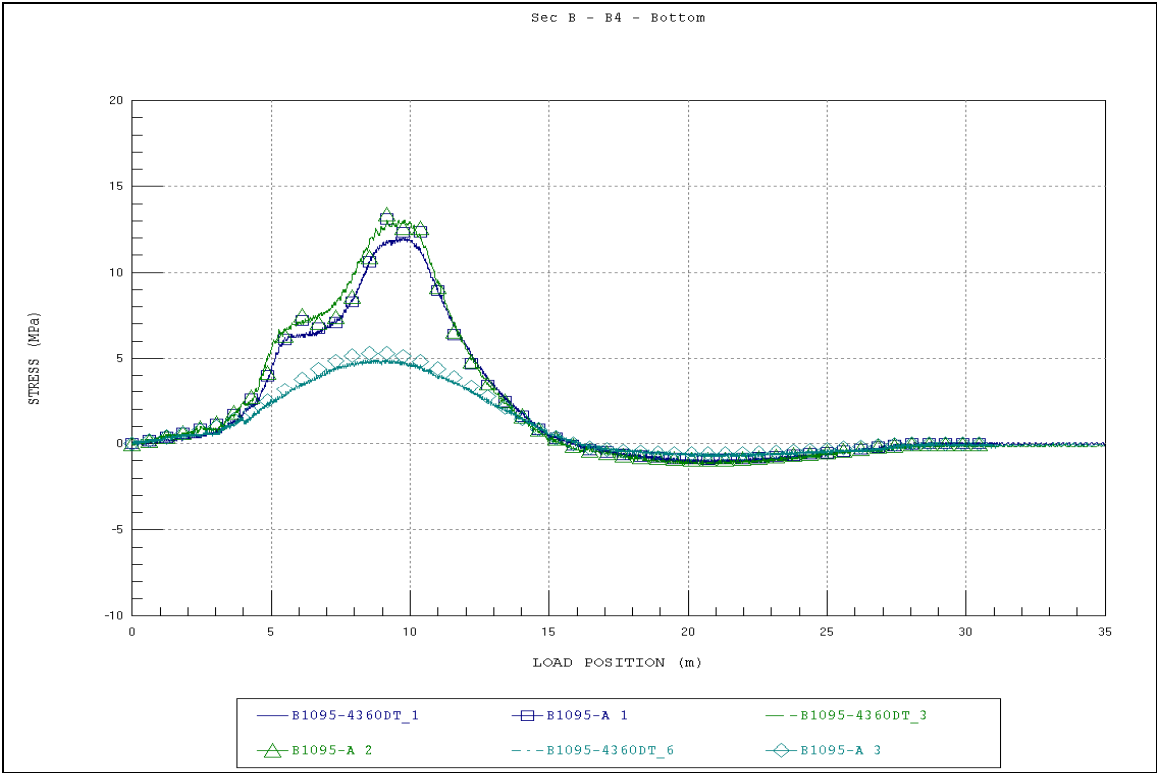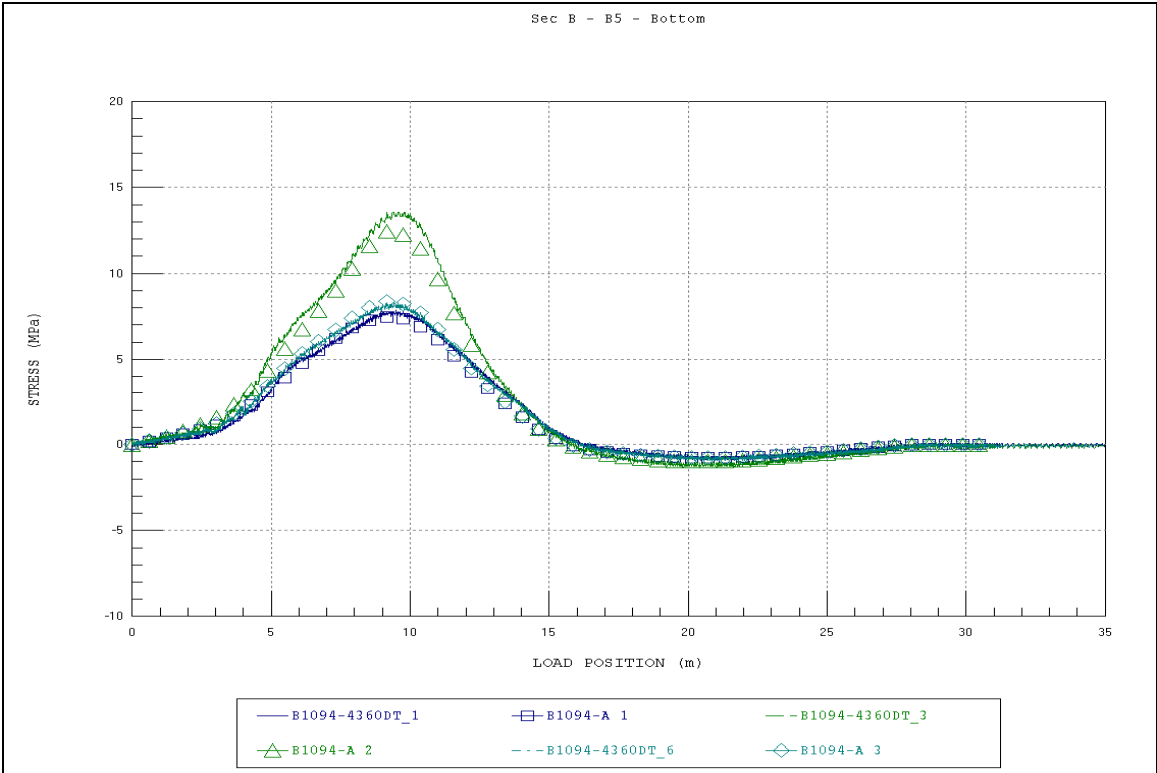


Figure A10. Section B – B3 – Bottom.

Figure A11. Section B – B4 – Bottom.



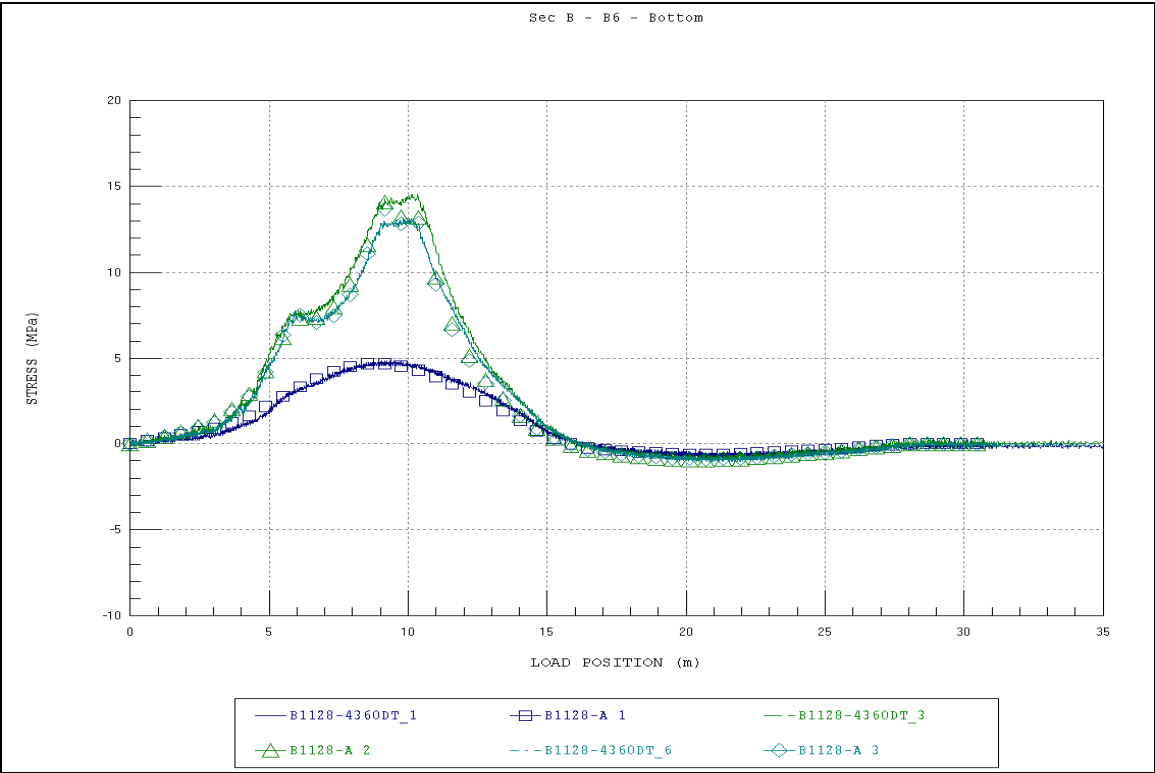Figure A12. Section B – B5 – Bottom.
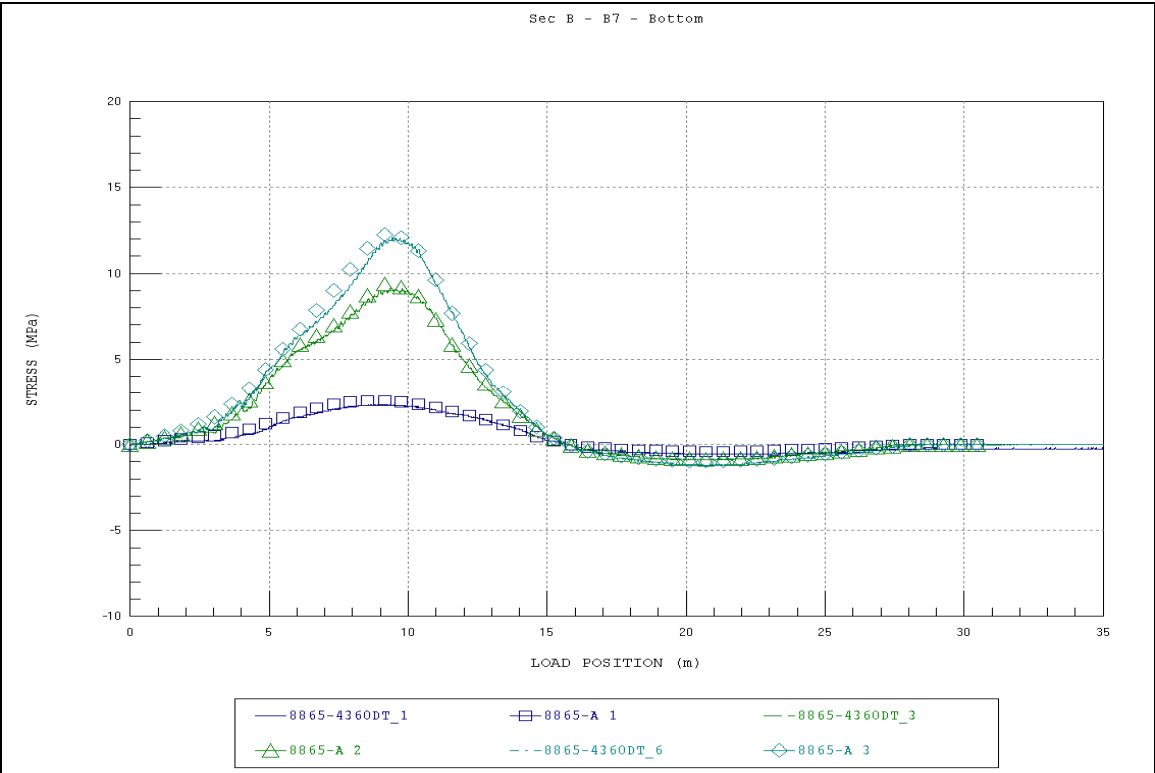
Figure A13. Section B – B6 – Bottom.



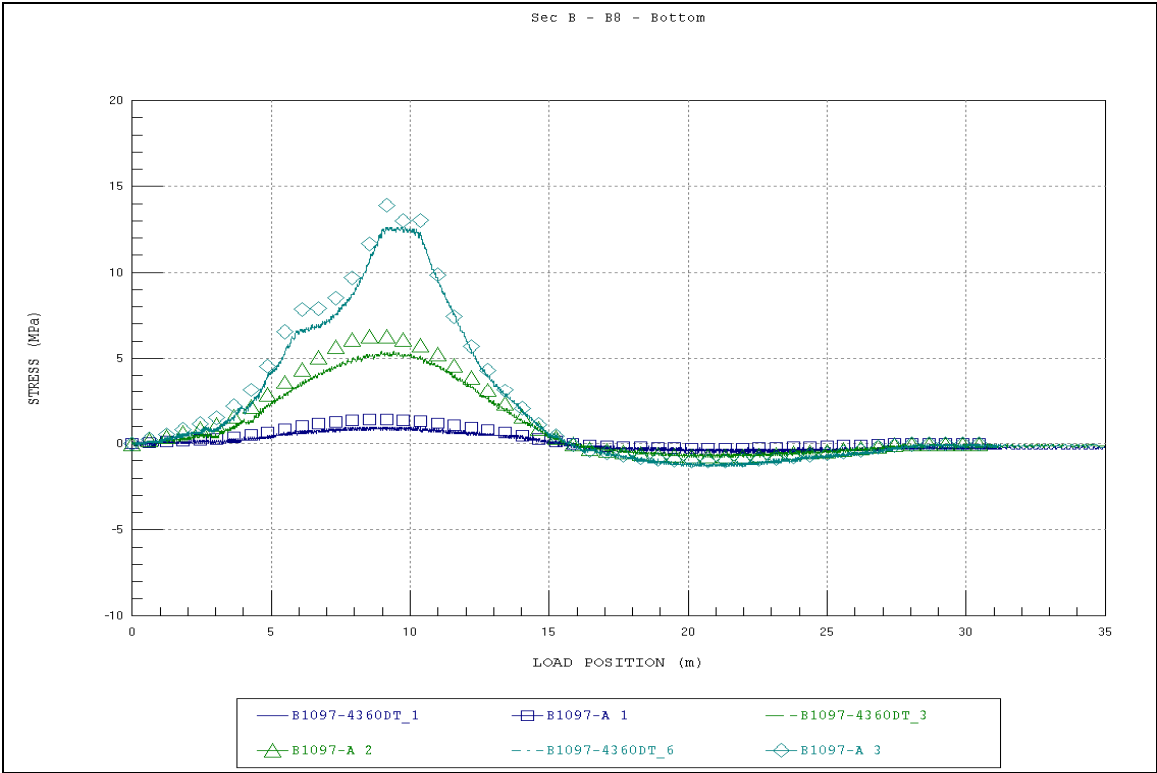Figure A14. Section B – B7 – Bottom.

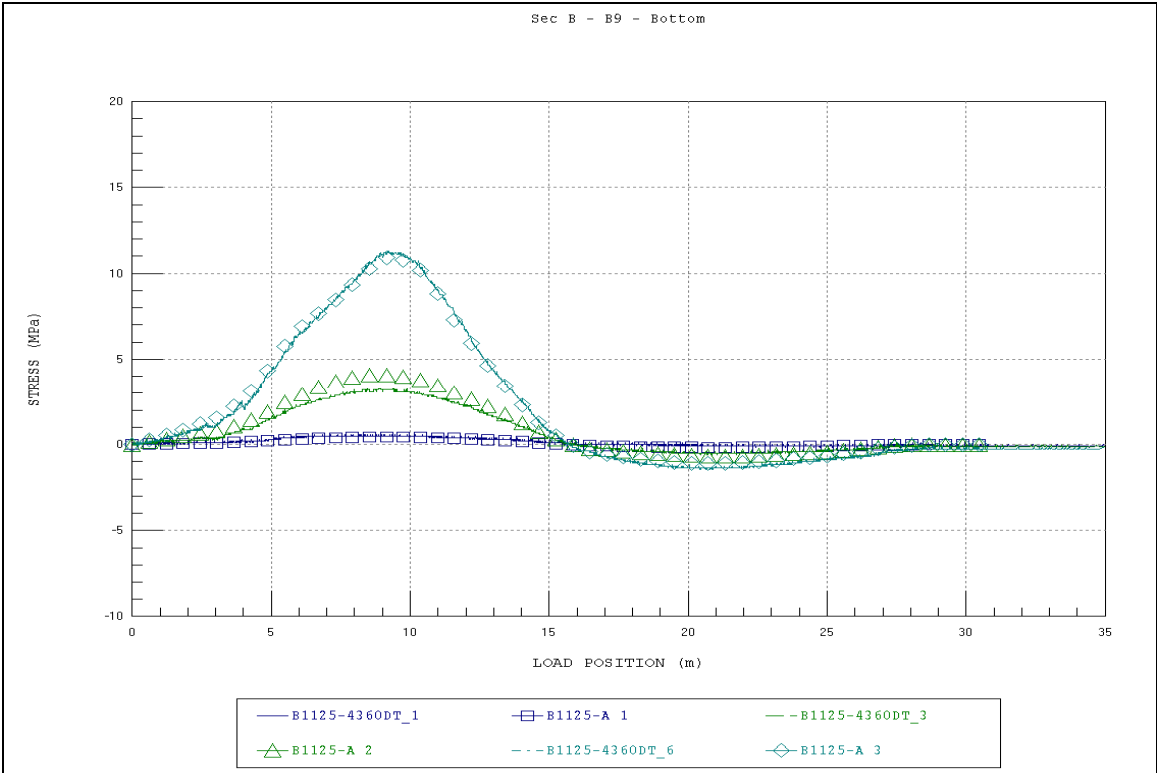Figure A15. Section B – B8 – Bottom.
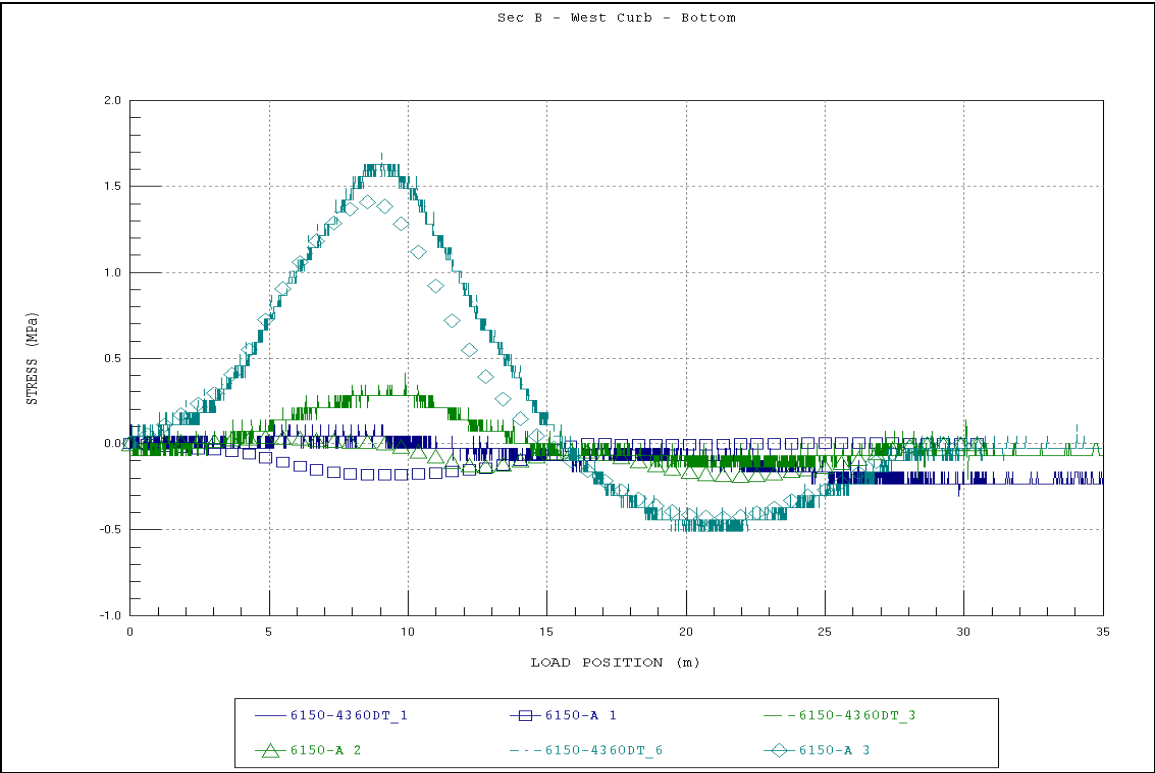


Figure A16. Section B – B9 – Bottom.

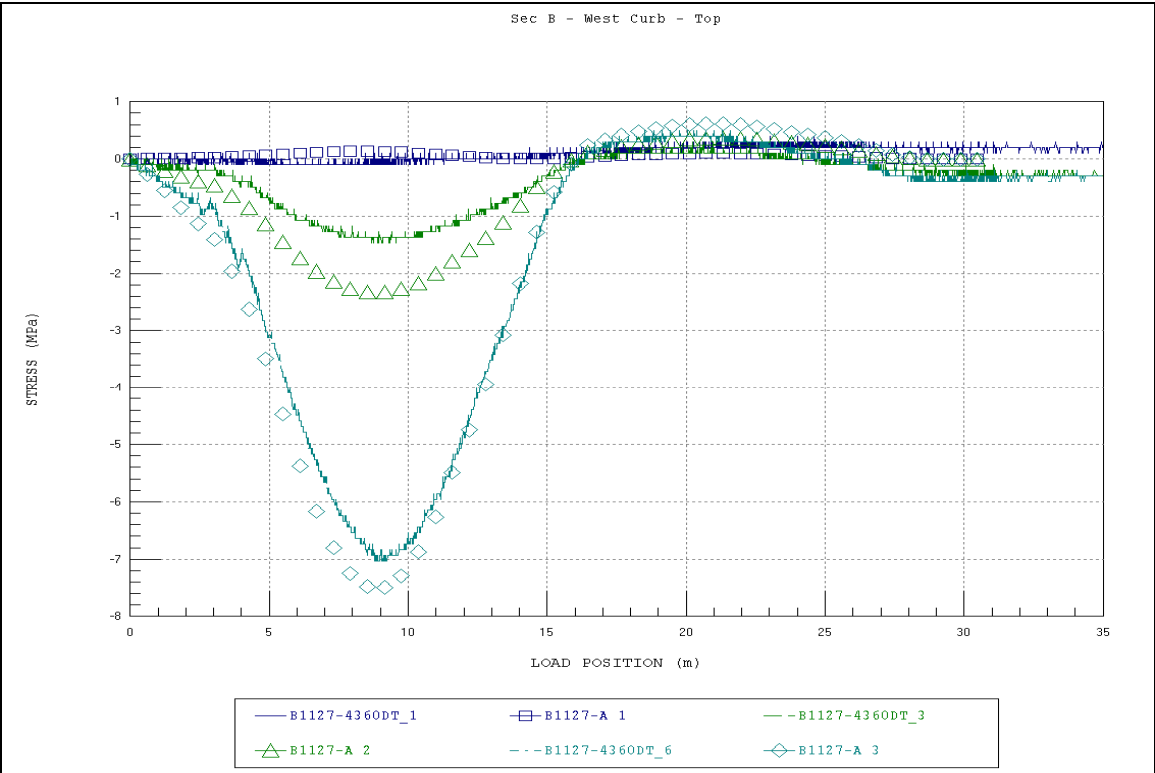Figure A17. Section B – West Curb – Bottom.



Figure A18. Section B – West Curb – Top.

Figure A19. Section C – B3 – Bottom.
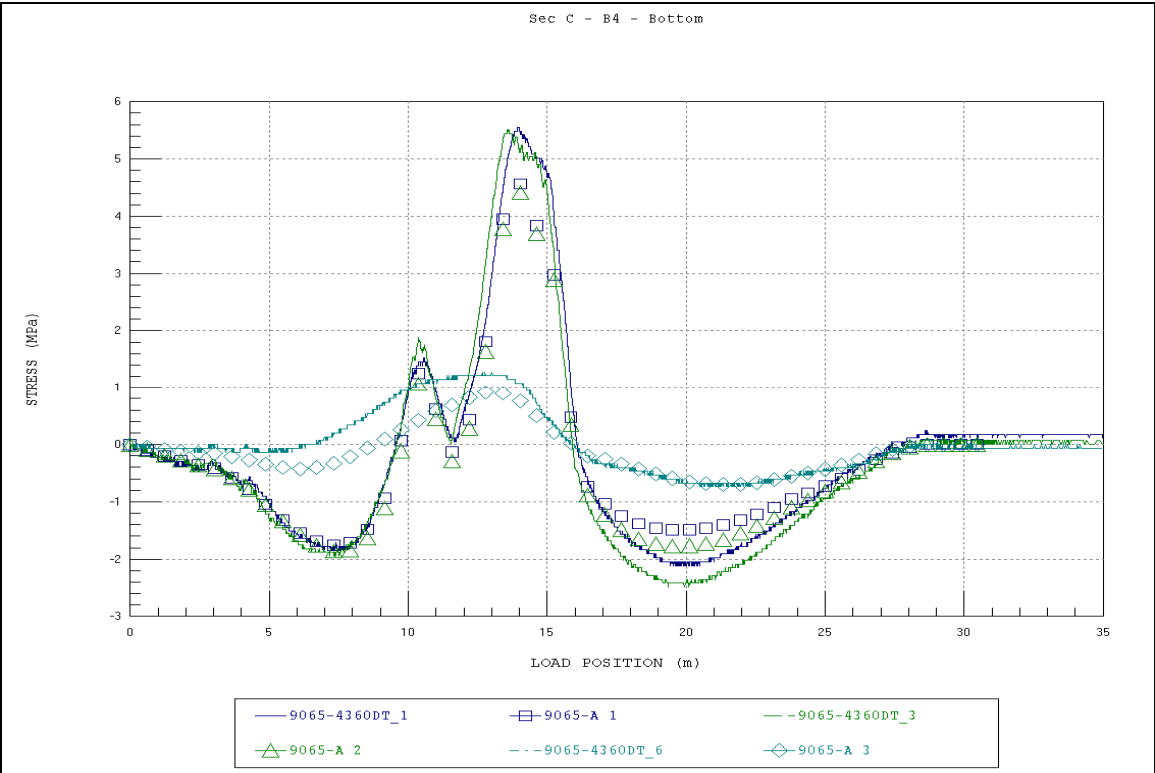


Figure A20. Section C – B4 – Bottom.
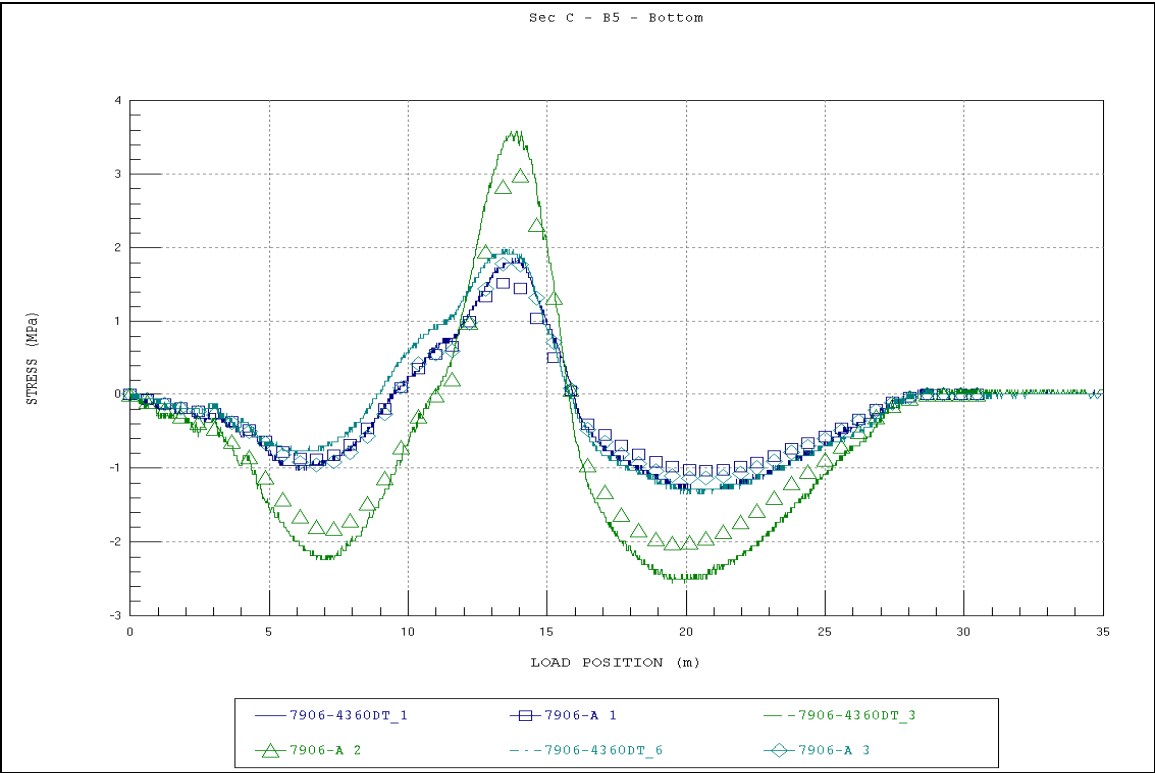
Figure A21. Section C – B5 – Bottom.
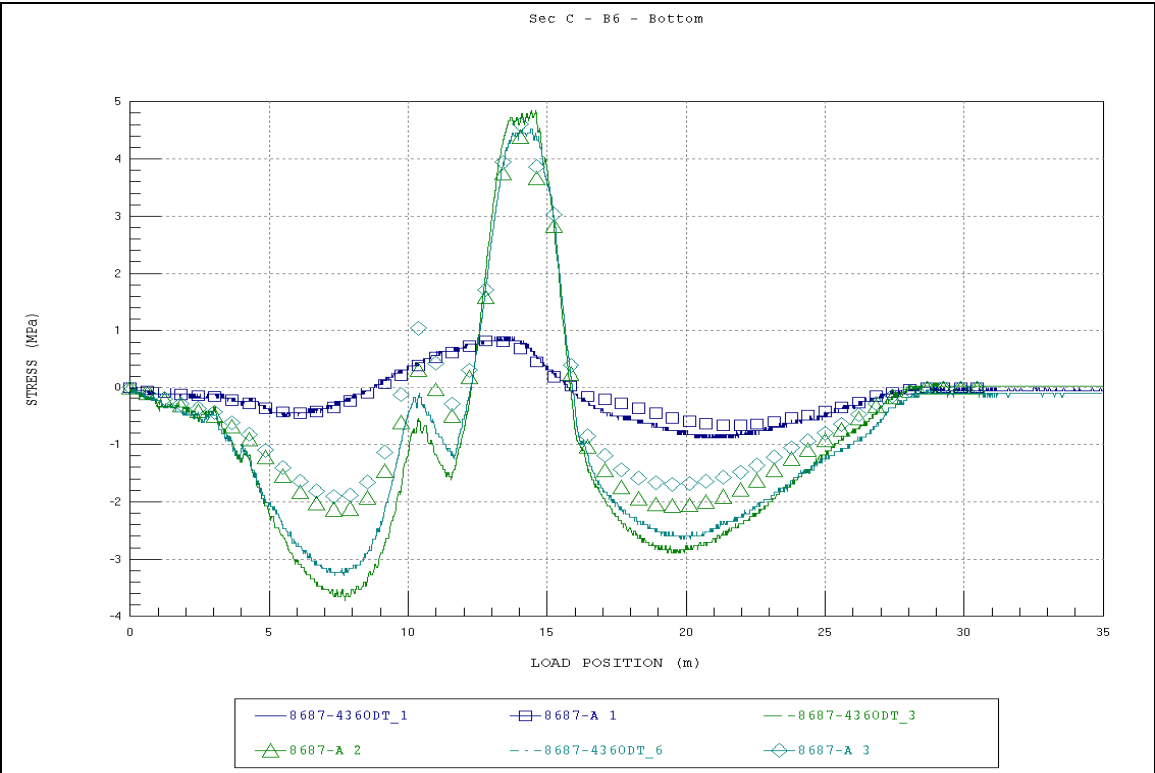


Figure A22. Section C – B6 – Bottom.
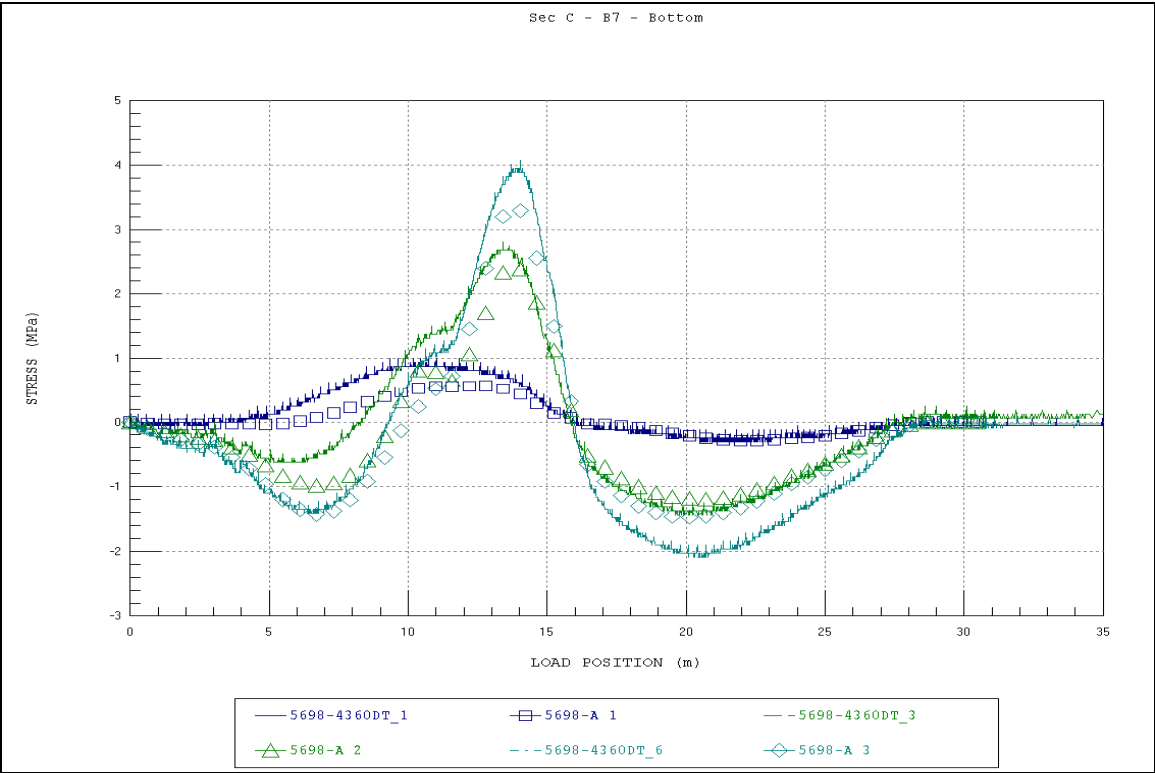
Figure A23. Section C – B7 – Bottom.



Figure A24. Section C – B8 – Bottom.

Figure A25. Section C – B9 – Bottom.



Figure A26. Section D – B1 – Bottom.
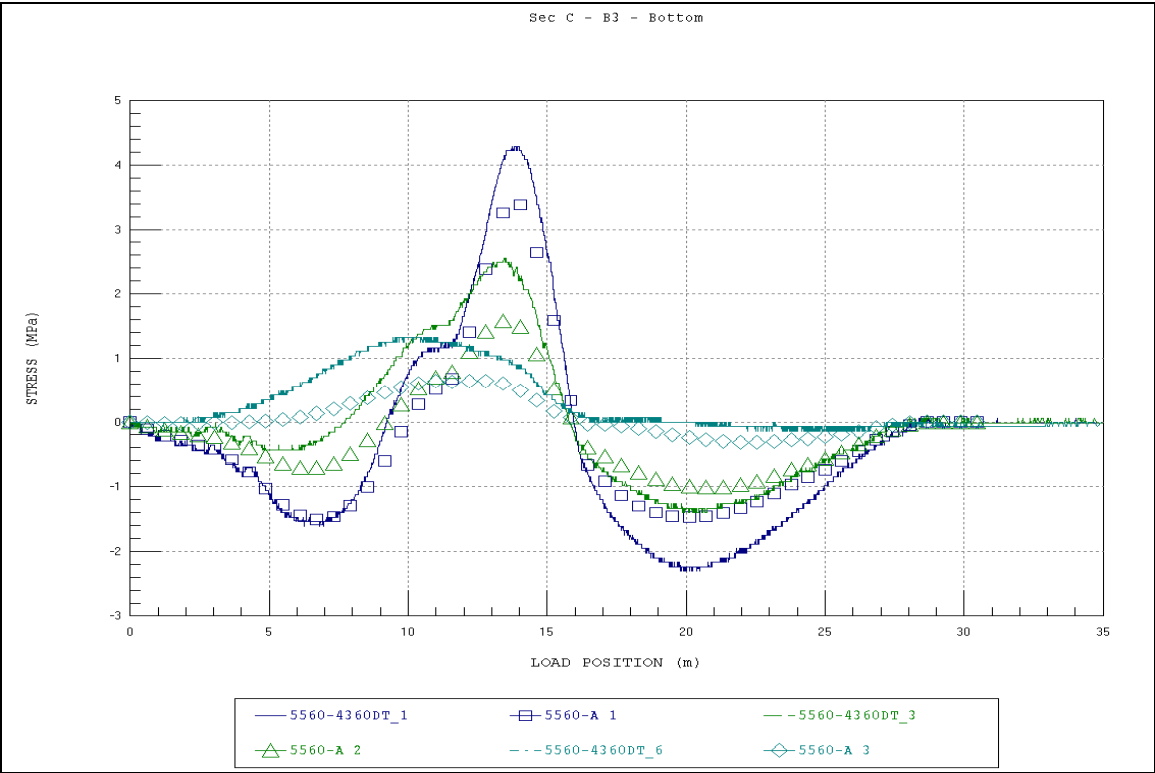
Figure A27. Section D – B2 – Bottom.



Figure A28. Section D – B3 – Bottom.

Figure A29. Section D – B4 – Bottom.



Figure A30. Section D – B5 – Bottom.

Figure A31. Section D – B6 – Bottom.
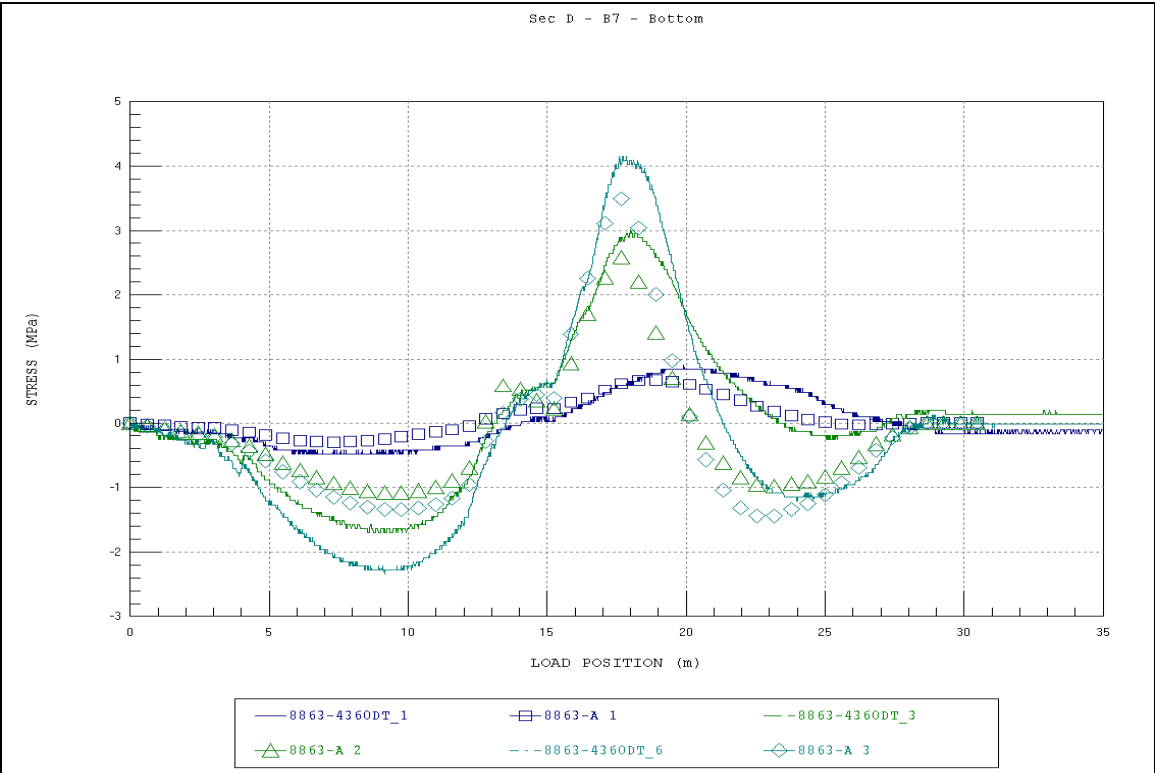


Figure A32. Section D – B7 – Bottom.
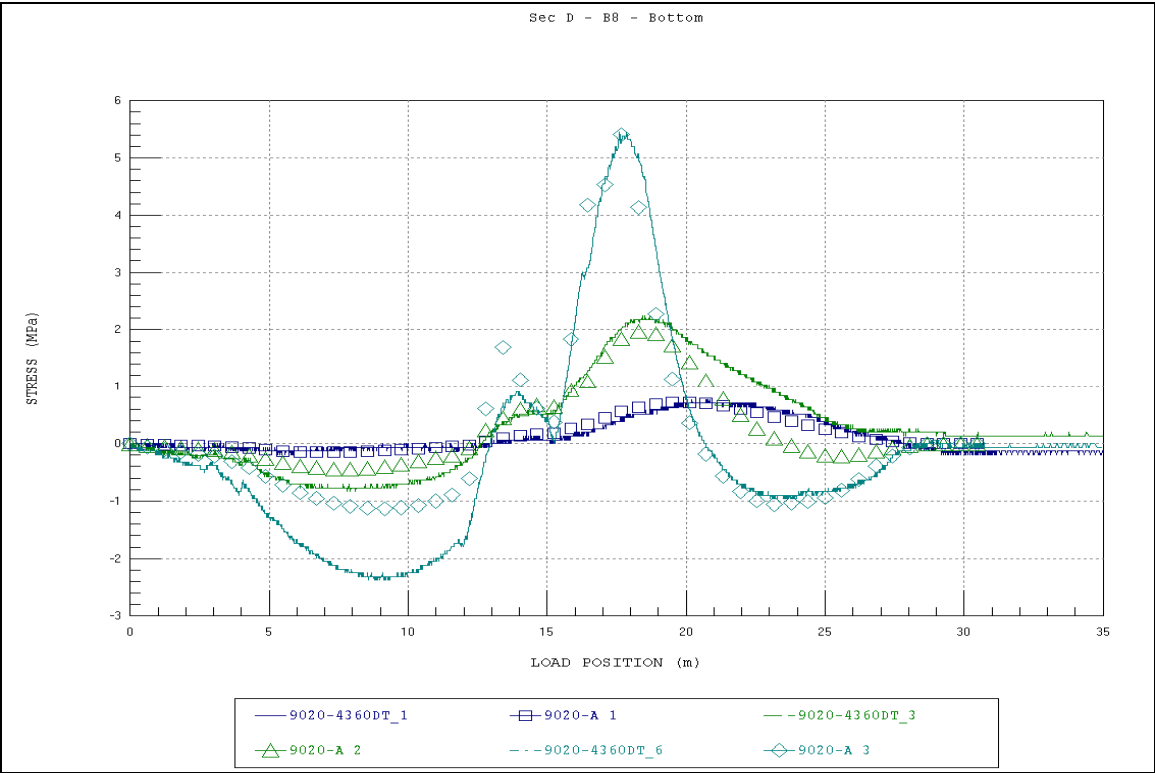
Figure A33. Section D – B8 – Bottom.



Figure A34. Section D – B9 – Bottom.

Figure A35. Section E – East Curb – Bottom.



Figure A36. Section E – B1 – Bottom.
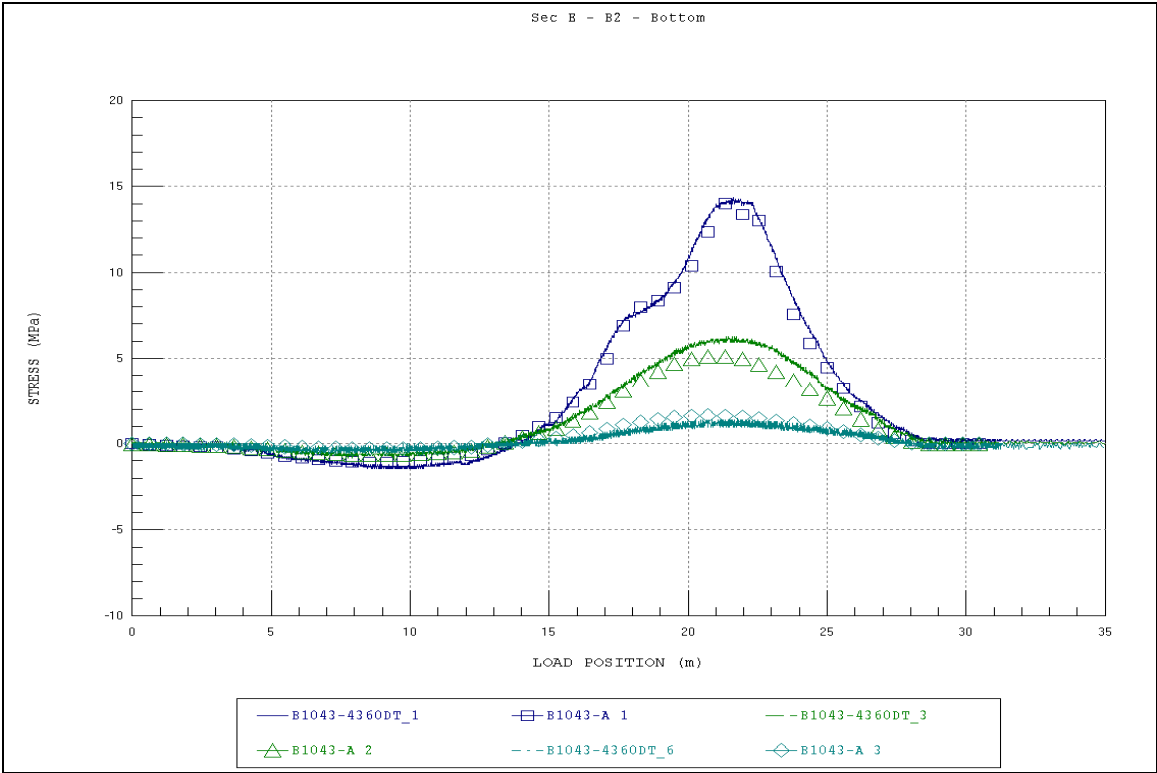
Figure A37. Section E – B2 – Bottom.
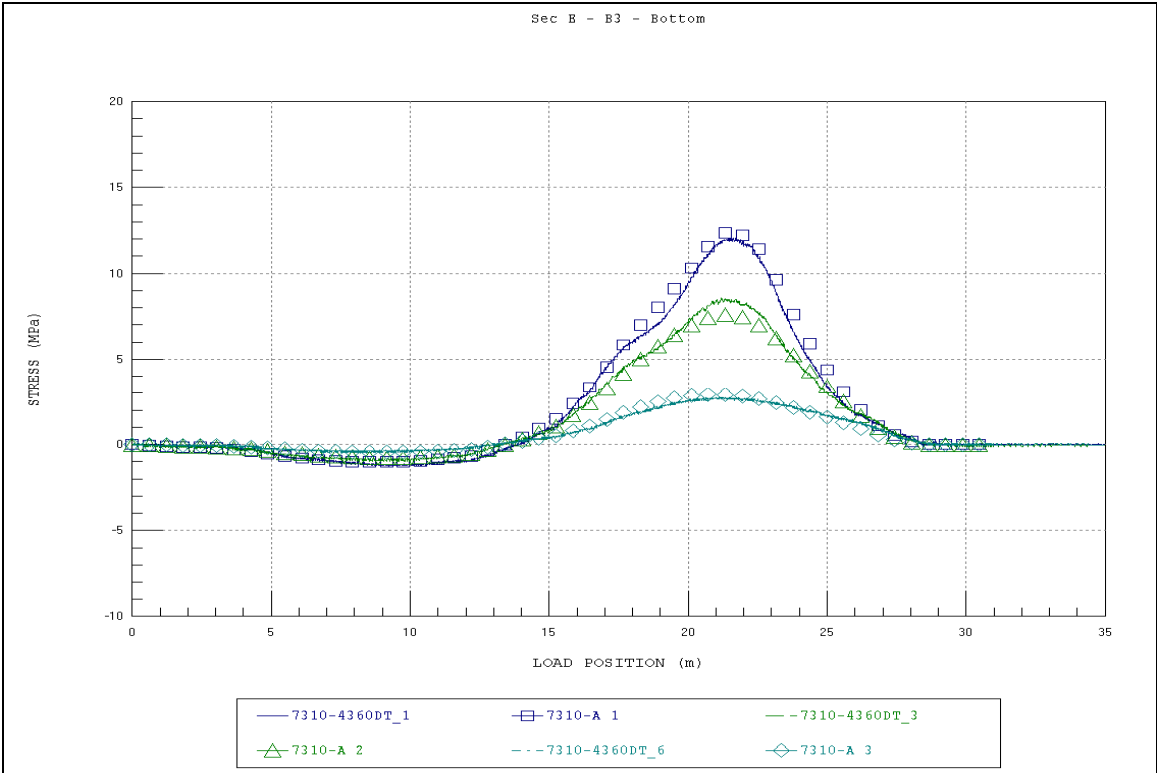


Figure A38. Section E – B3 – Bottom.
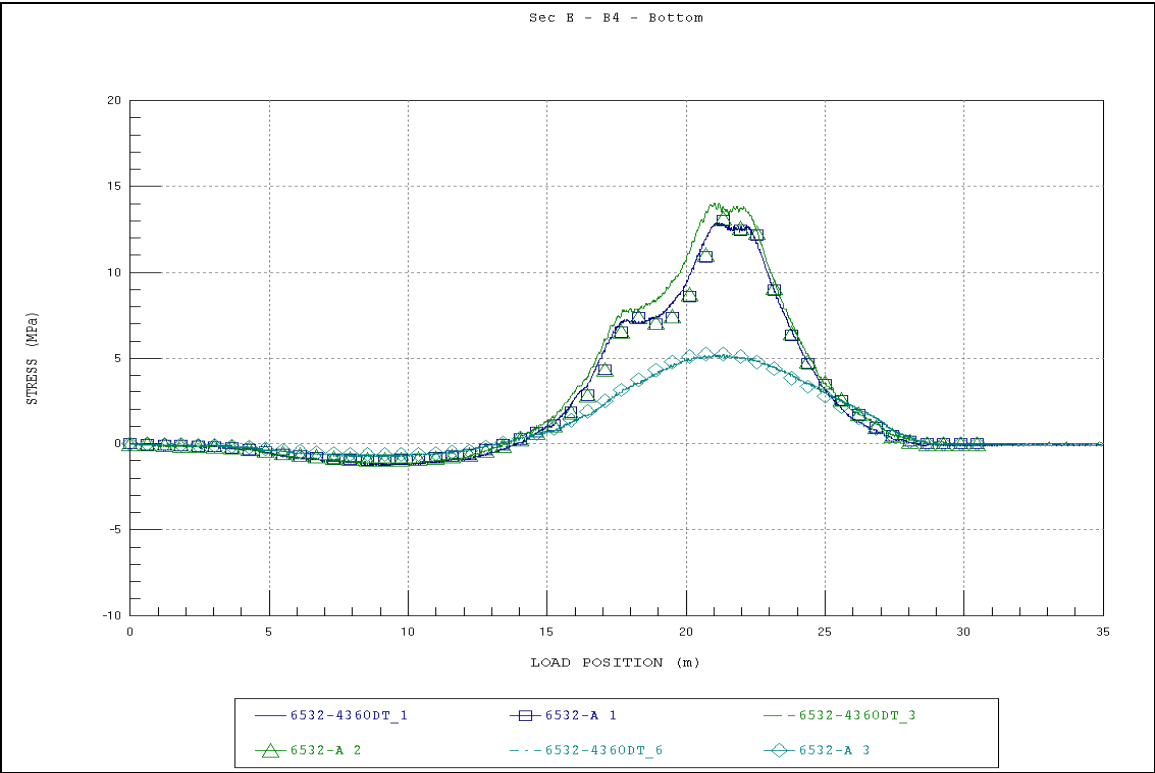
Figure A39. Section E – B4 – Bottom.
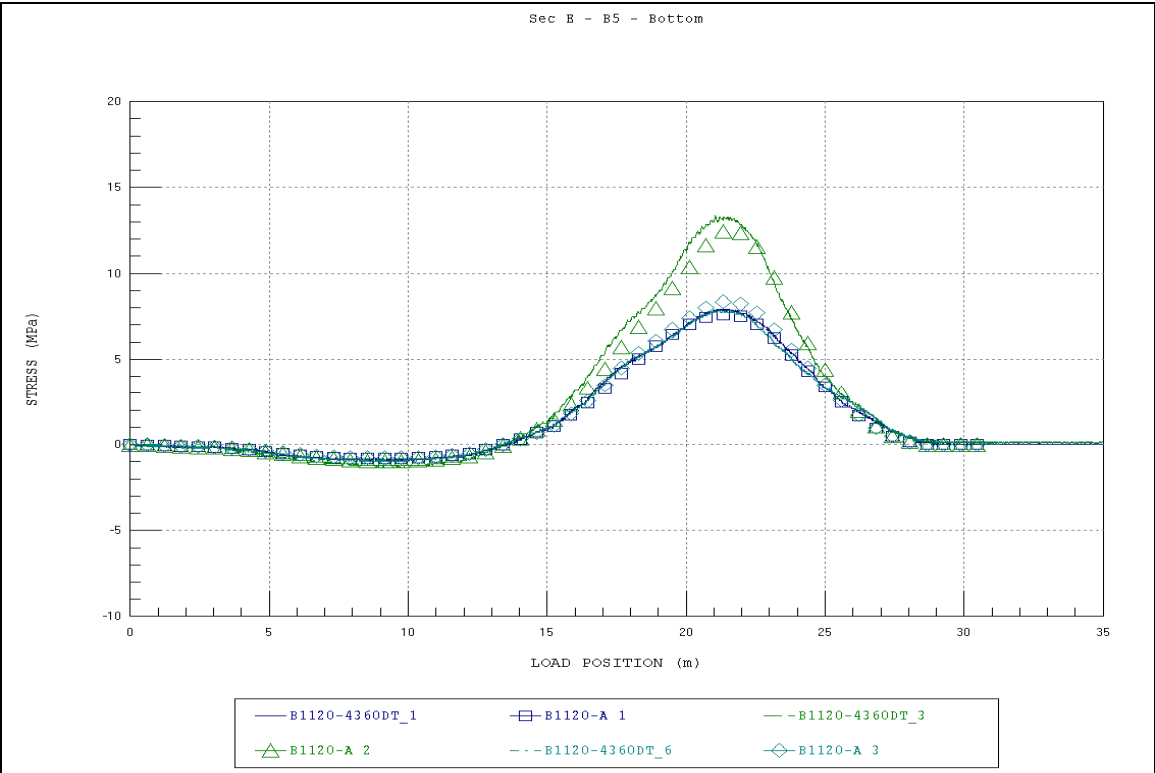


Figure A40. Section E – B5 – Bottom.
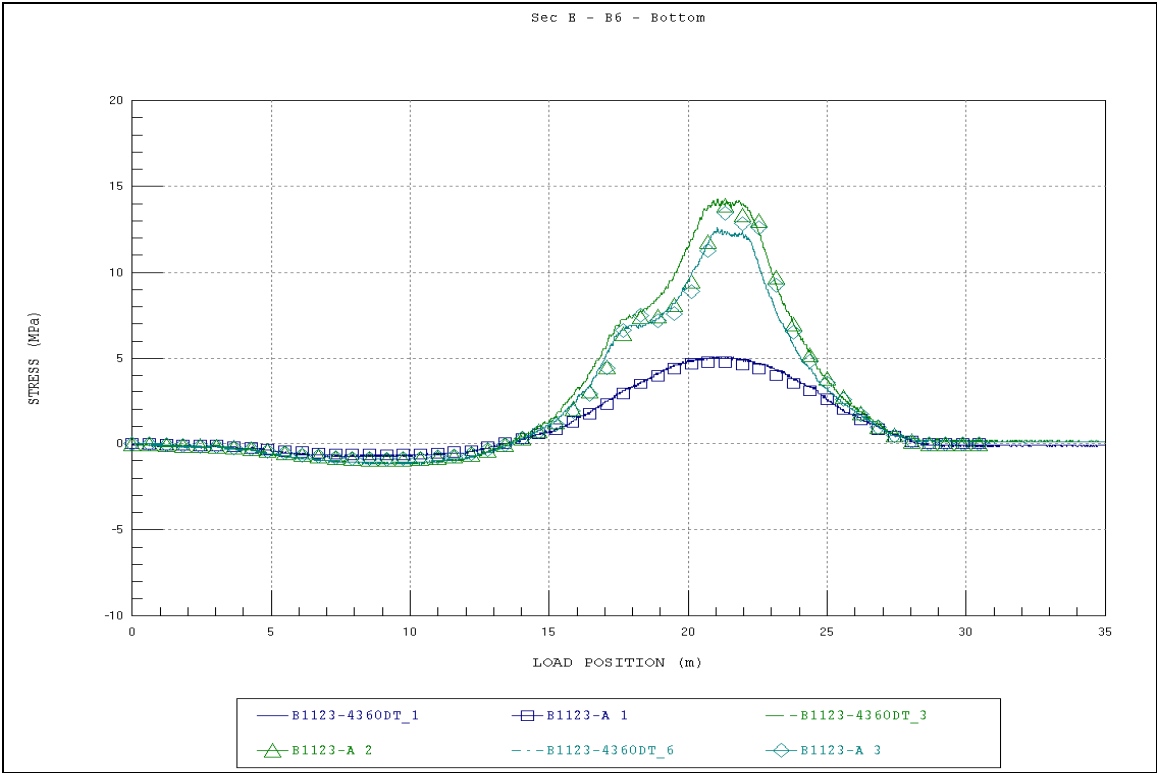
Figure A41. Section E – B6 – Bottom.
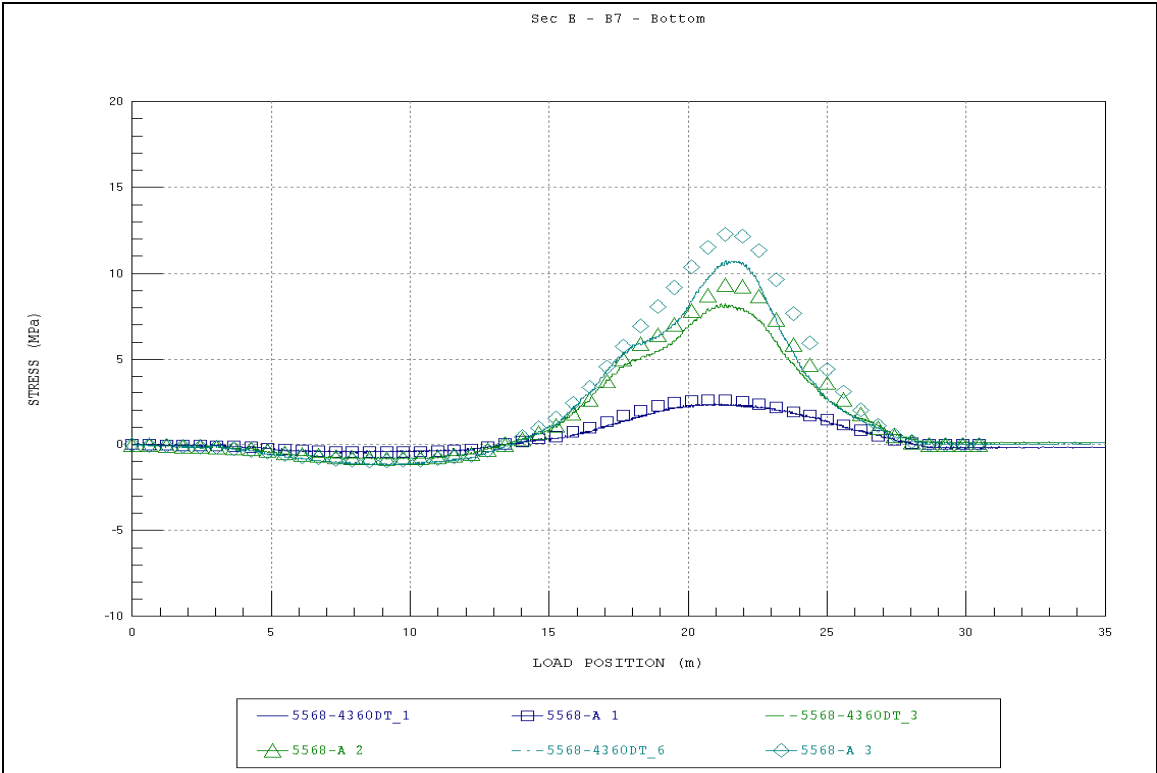


Figure A42. Section E – B7 – Bottom.
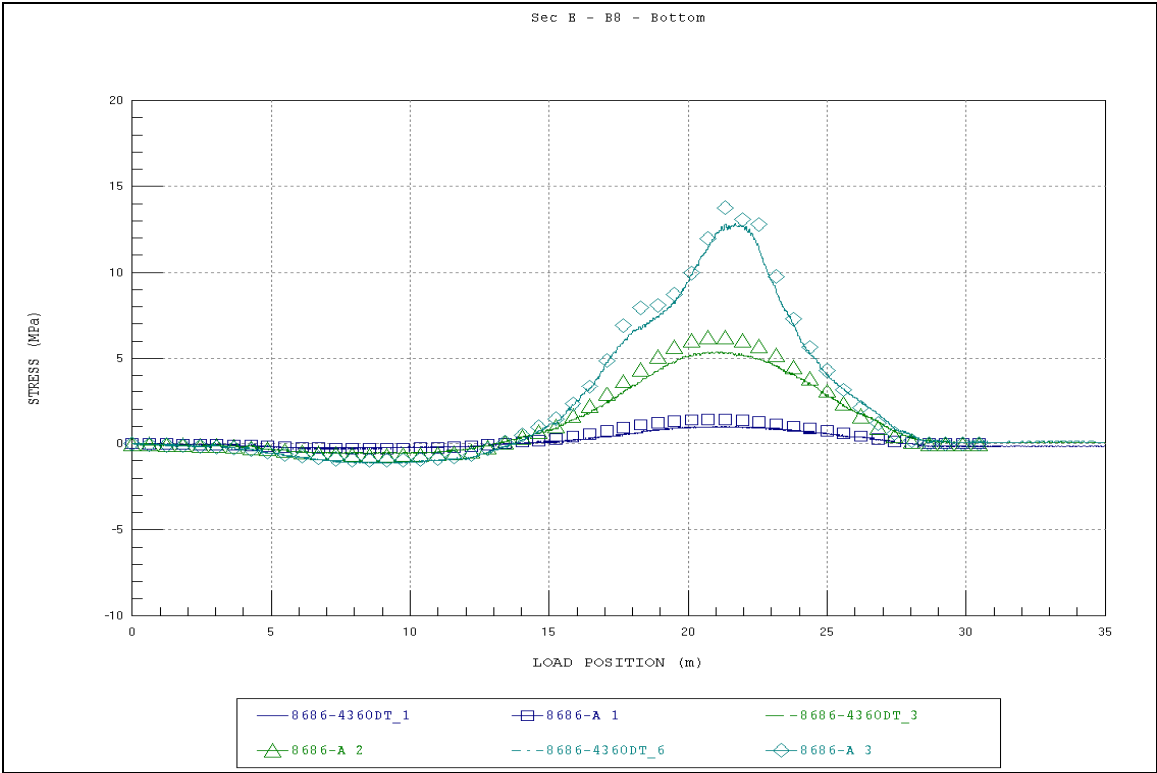
Figure A43. Section E – B8 – Bottom.
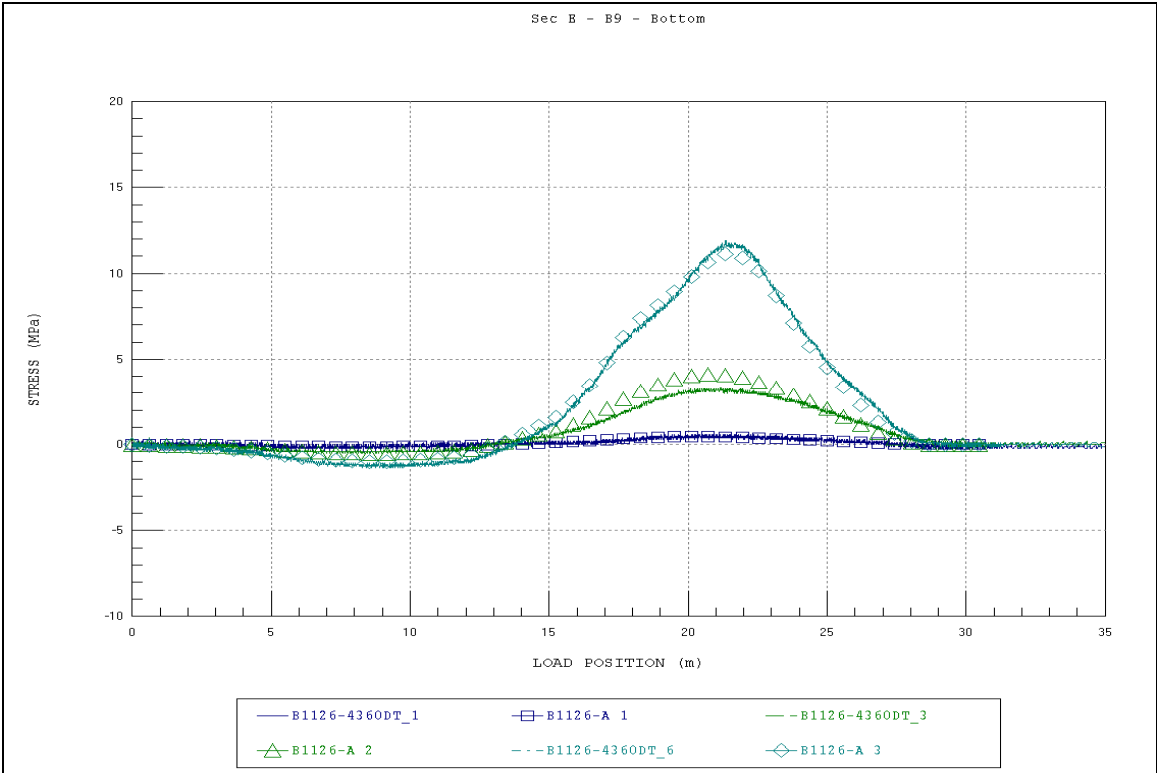


Figure A44. Section E – B9 – Bottom.
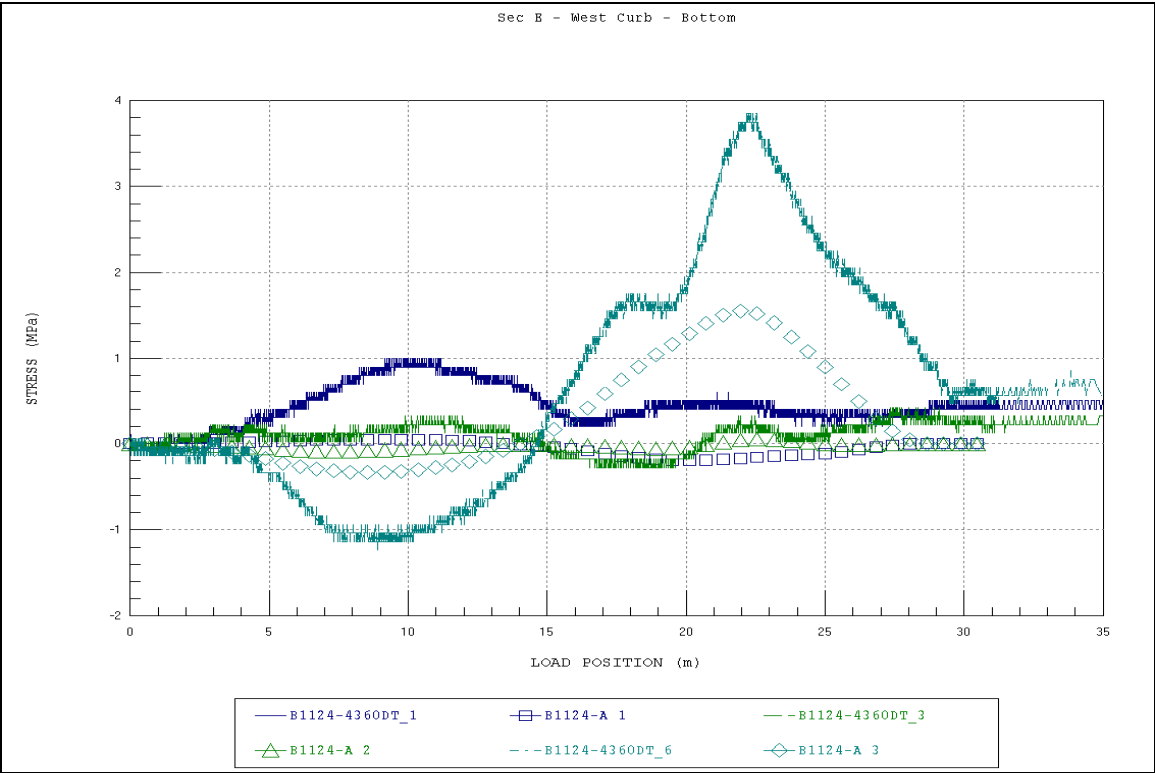
Figure A45. Section E – West Curb – Bottom.
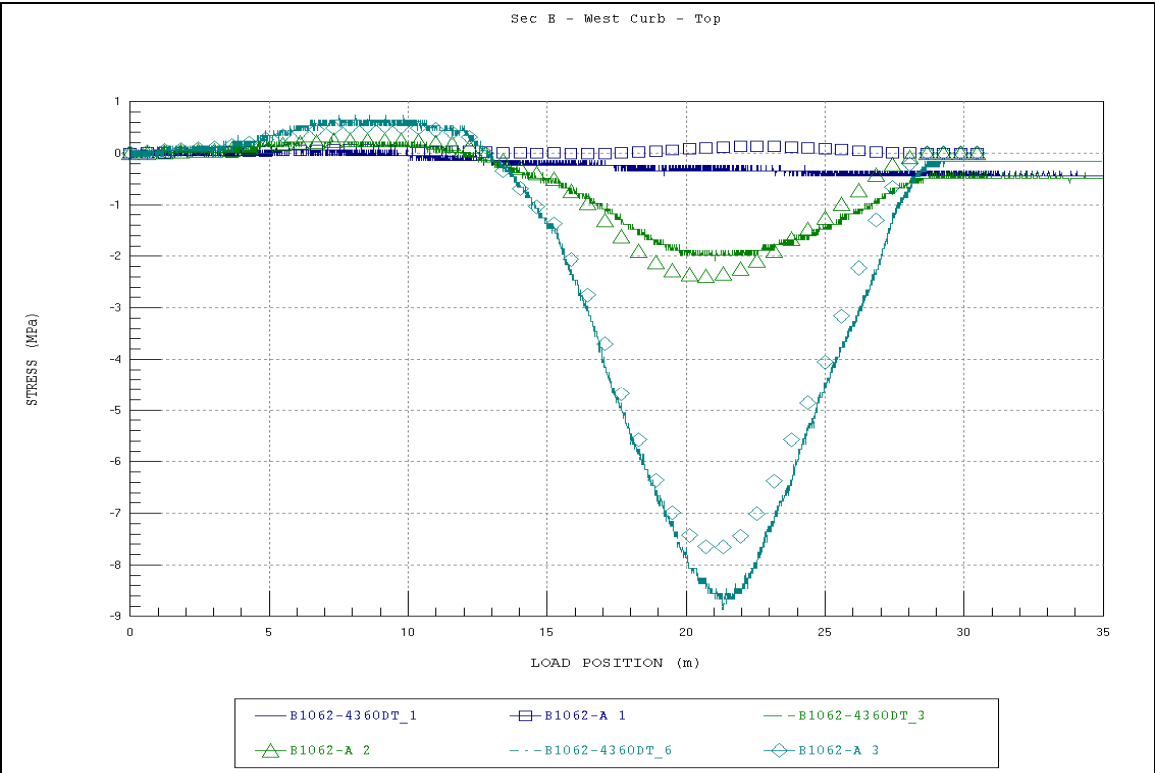


Figure A46. Section E – West Curb – Top.

## Empty HETS
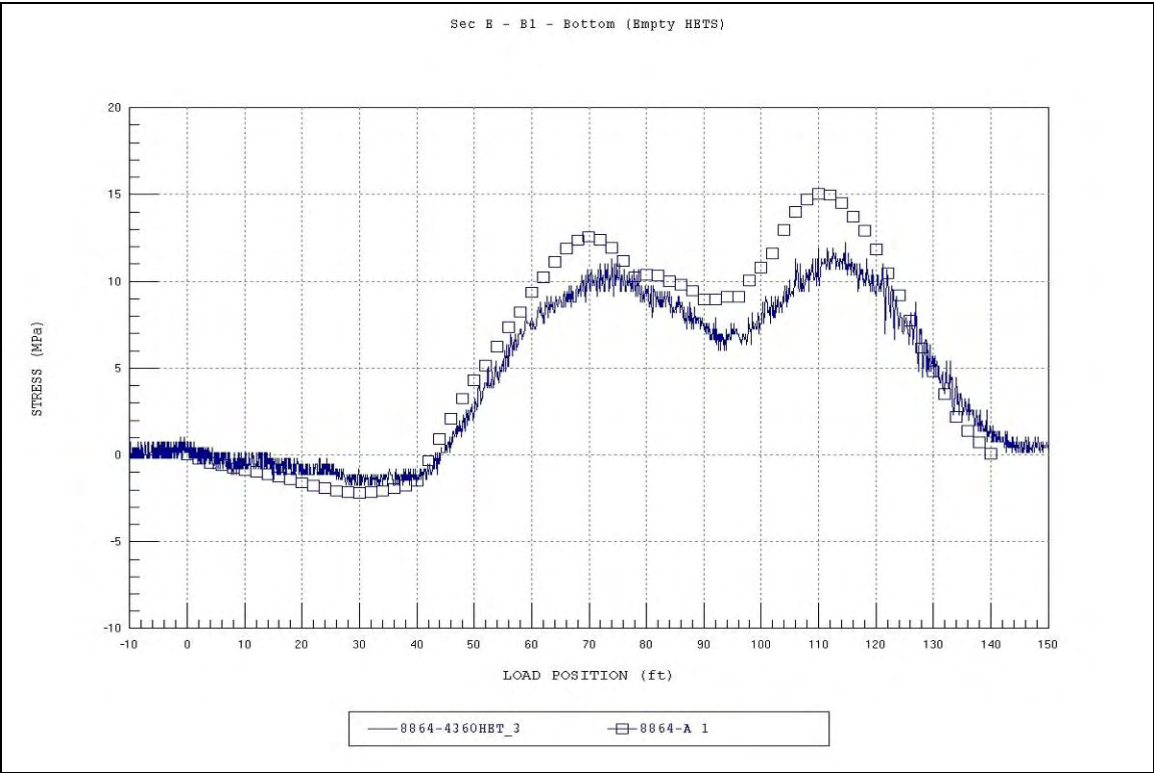


Figure A47. Section E – B1 – Bottom.
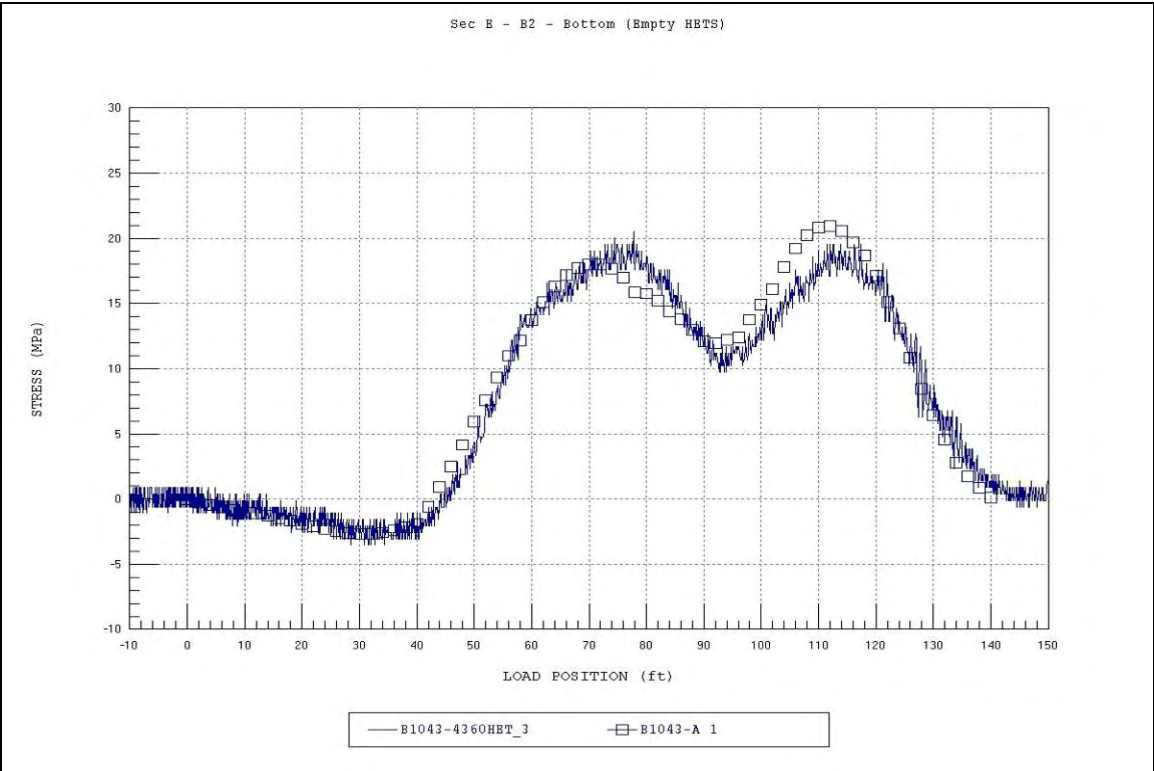


Figure A48. Section E – B2 – Bottom.
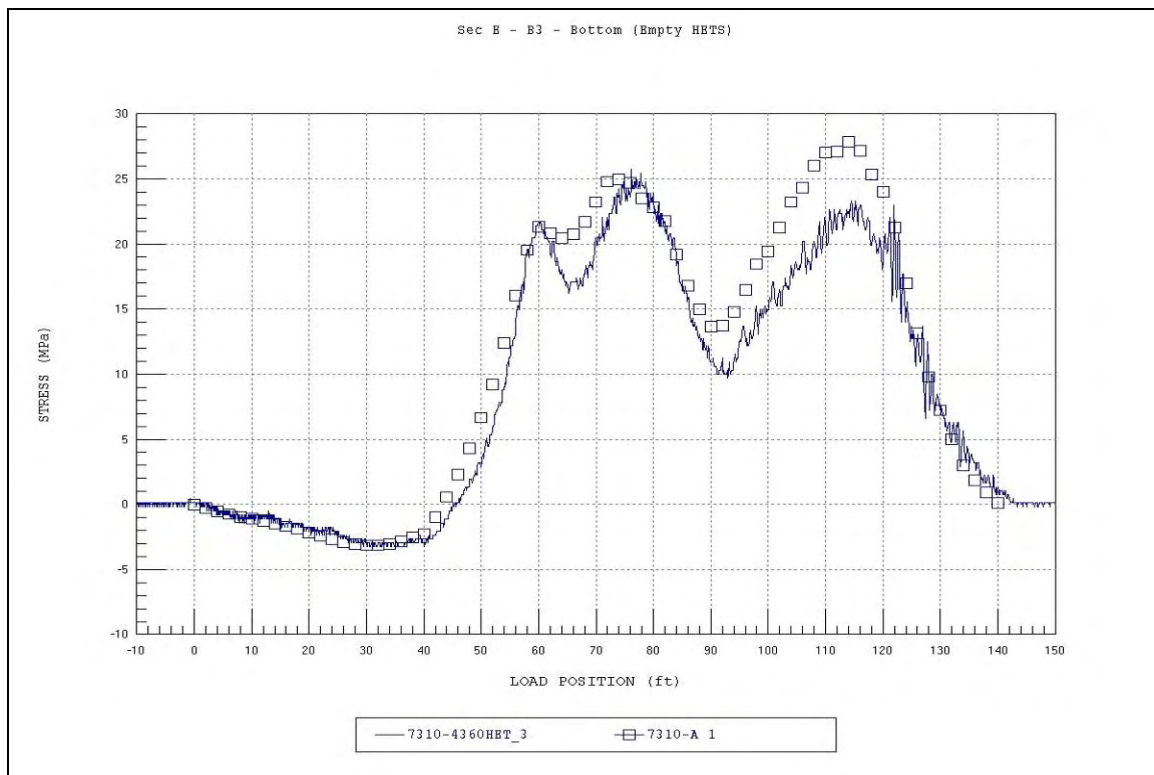
Figure A49. Section E – B3 – Bottom.
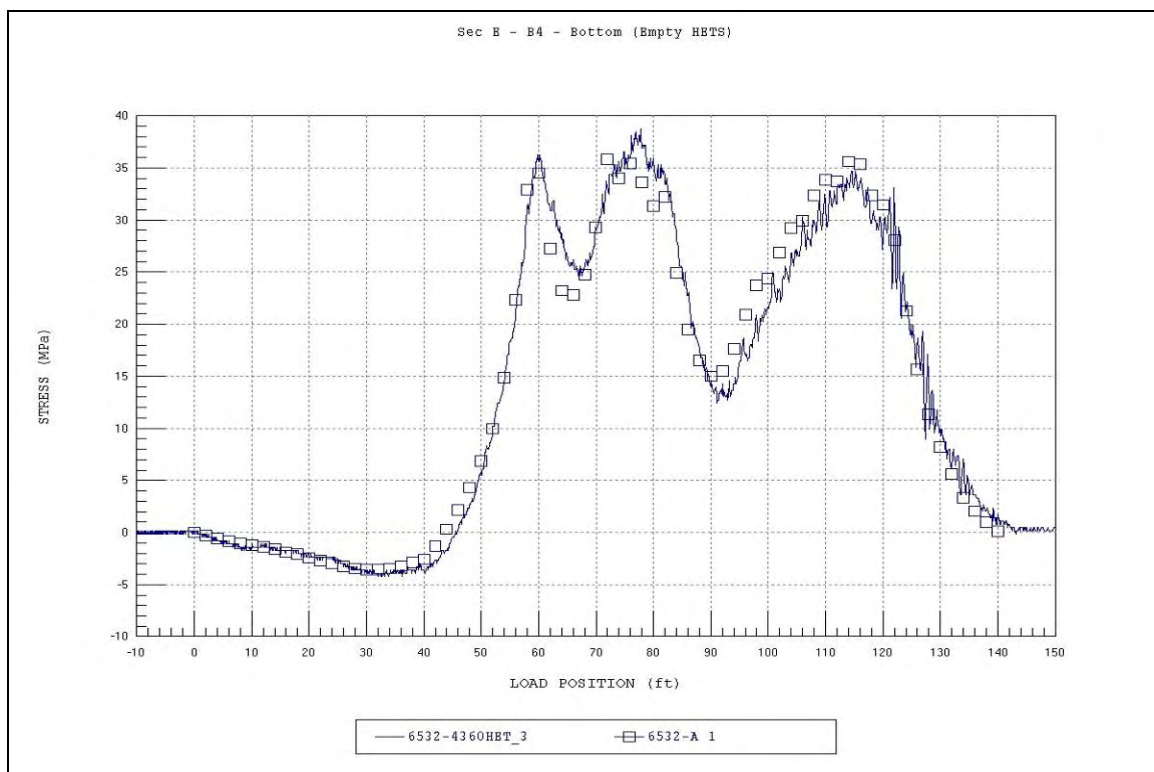


Figure A50. Section E – B4 – Bottom.
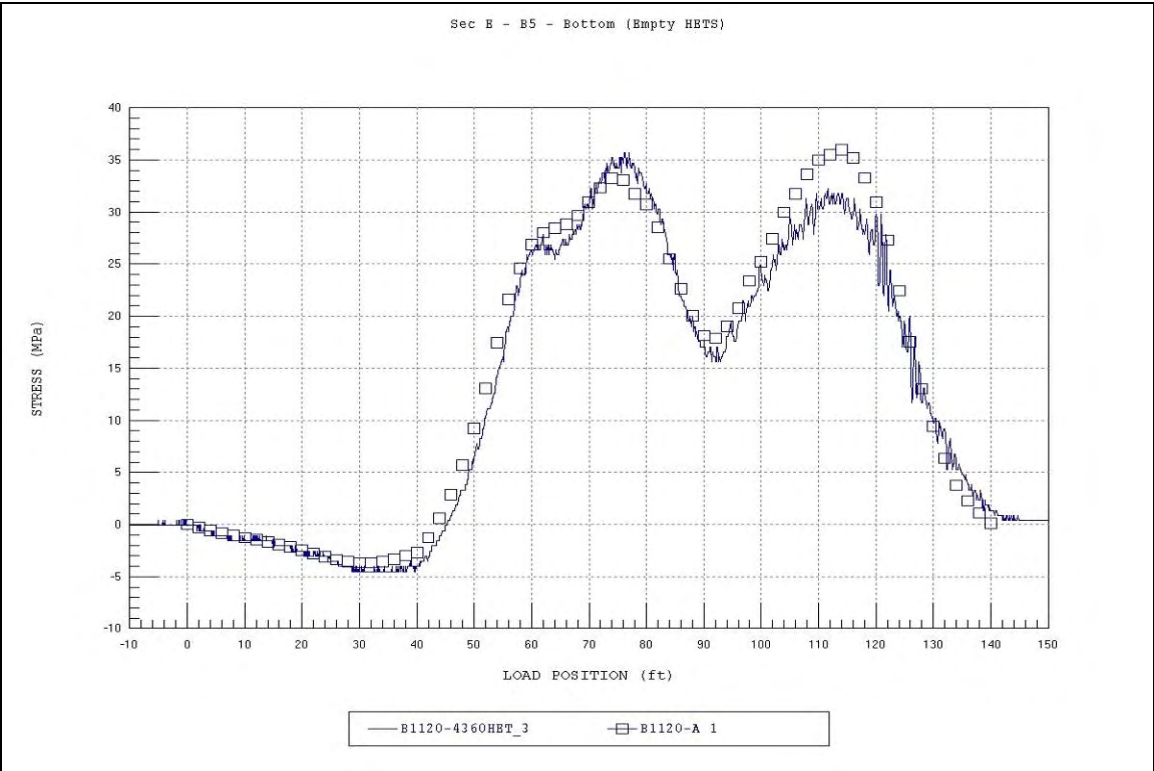
Figure A51. Section E – B5 – Bottom.
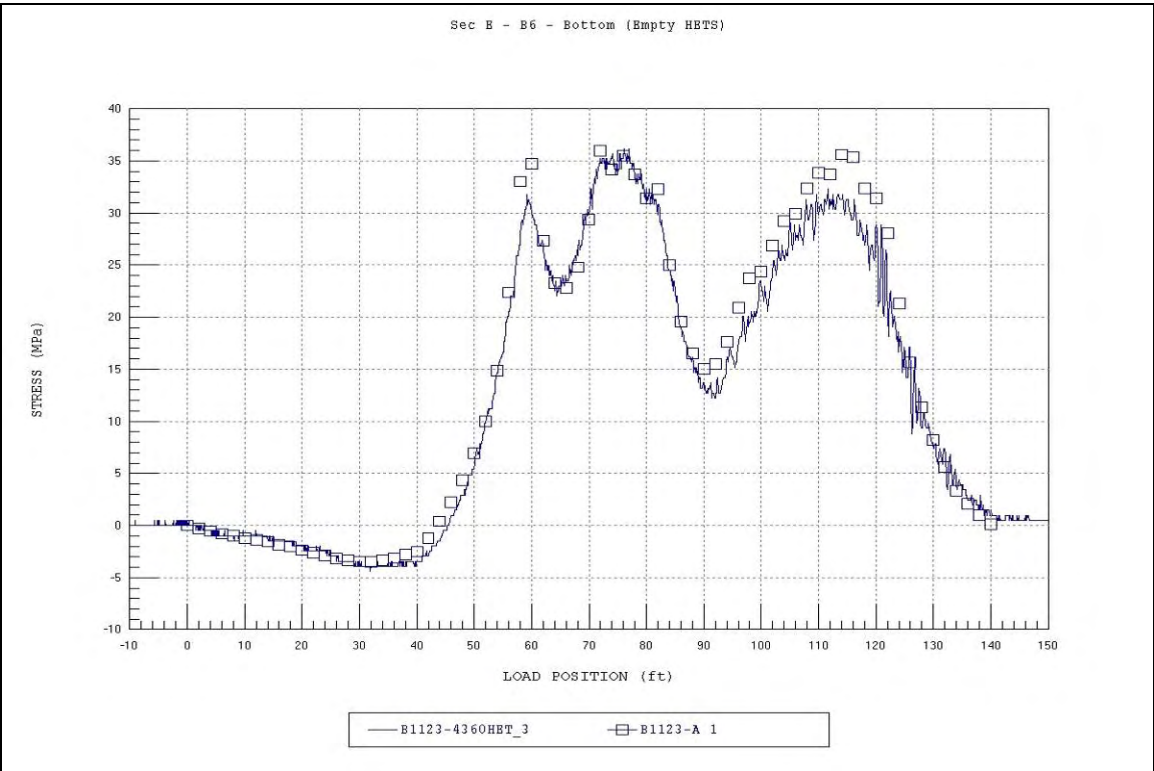


Figure A52. Section E – B6 – Bottom.
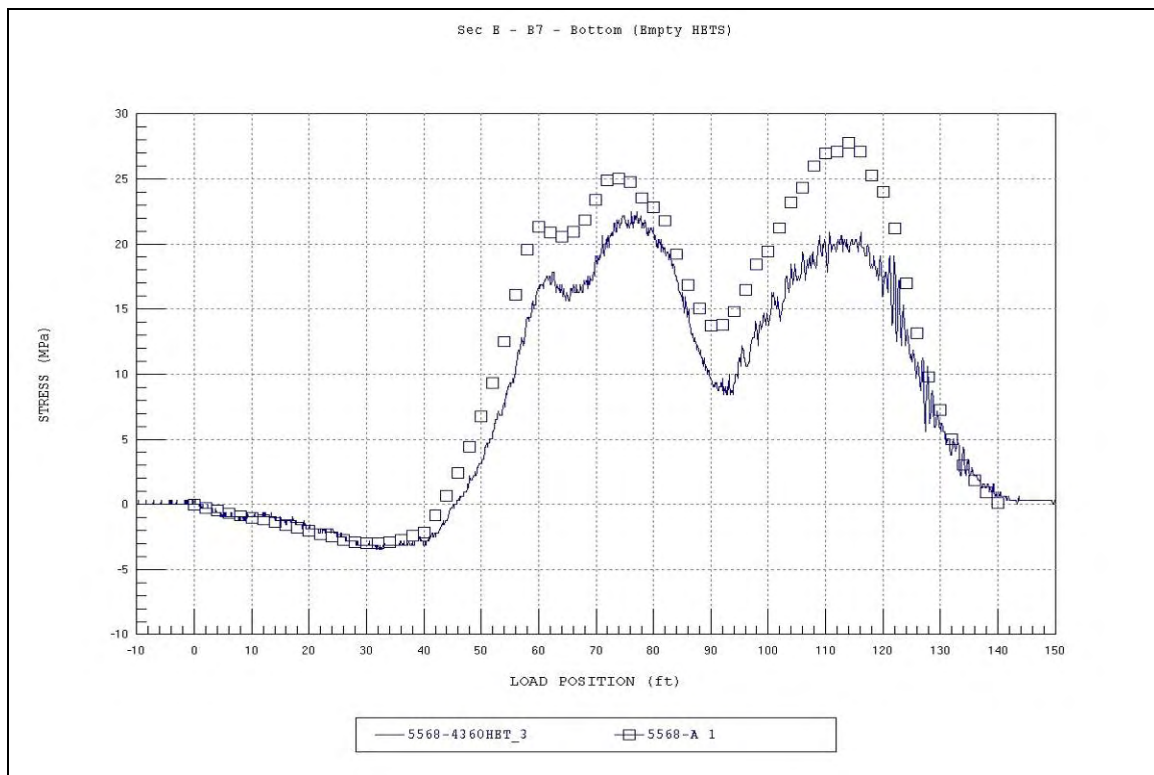
Figure A53. Section E – B7 – Bottom.
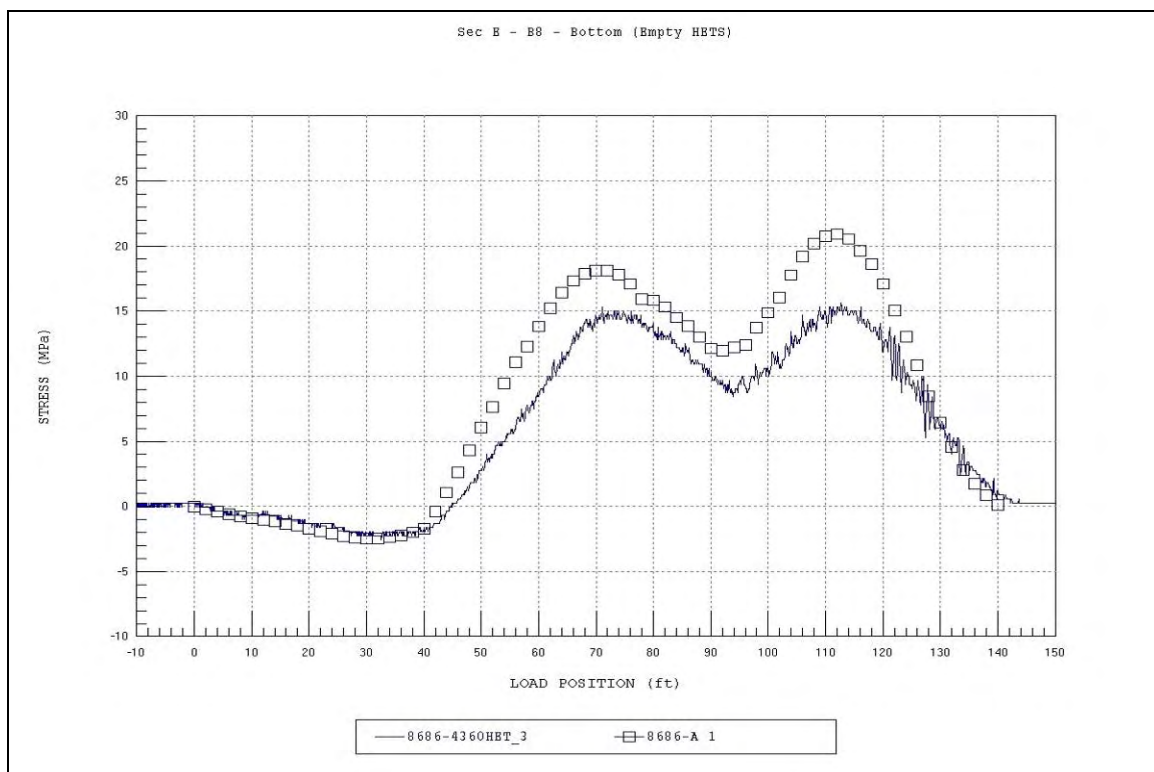


Figure A54. Section E – B8 – Bottom.
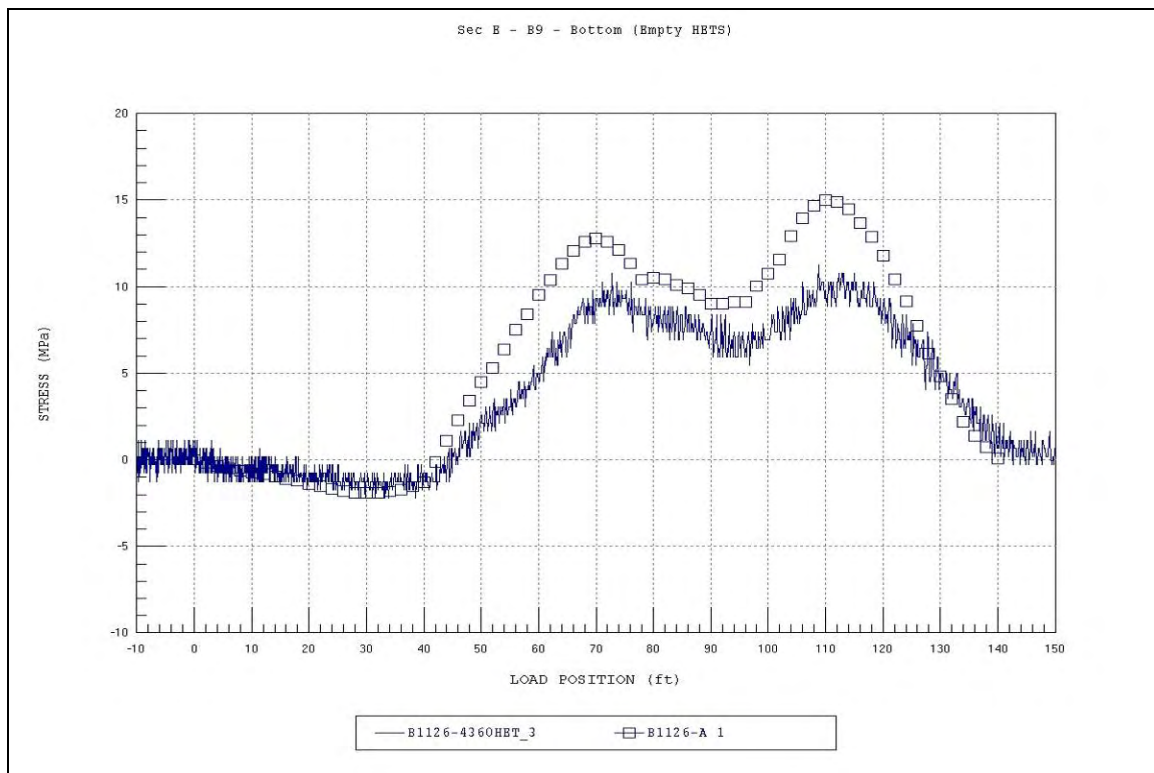
Figure A55. Section E – B9 – Bottom.

## HETS with M1
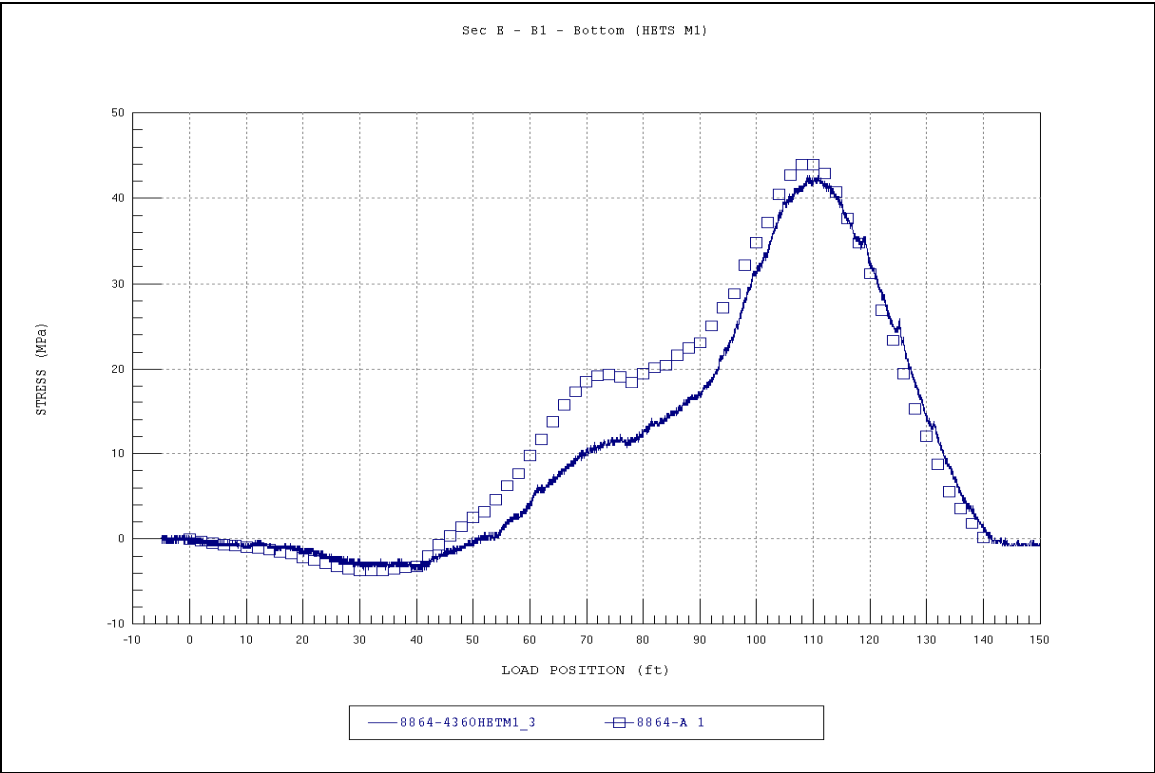


Figure A56. Section E – B1 – Bottom.
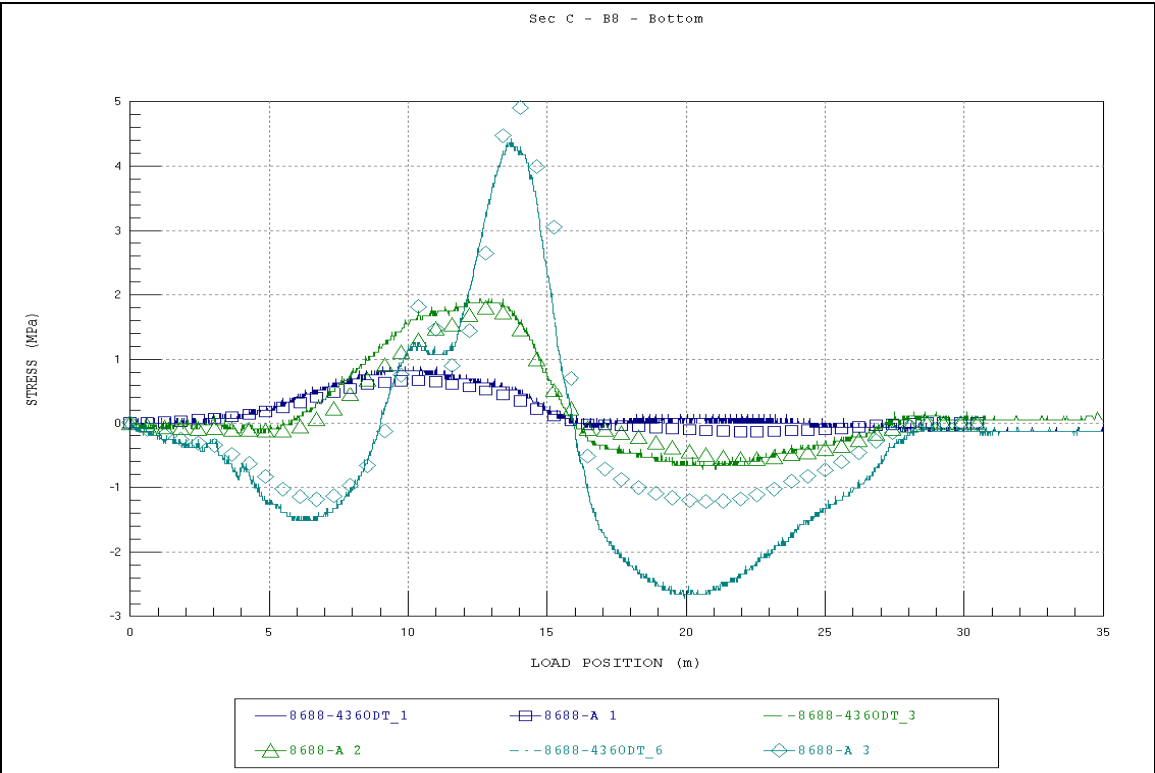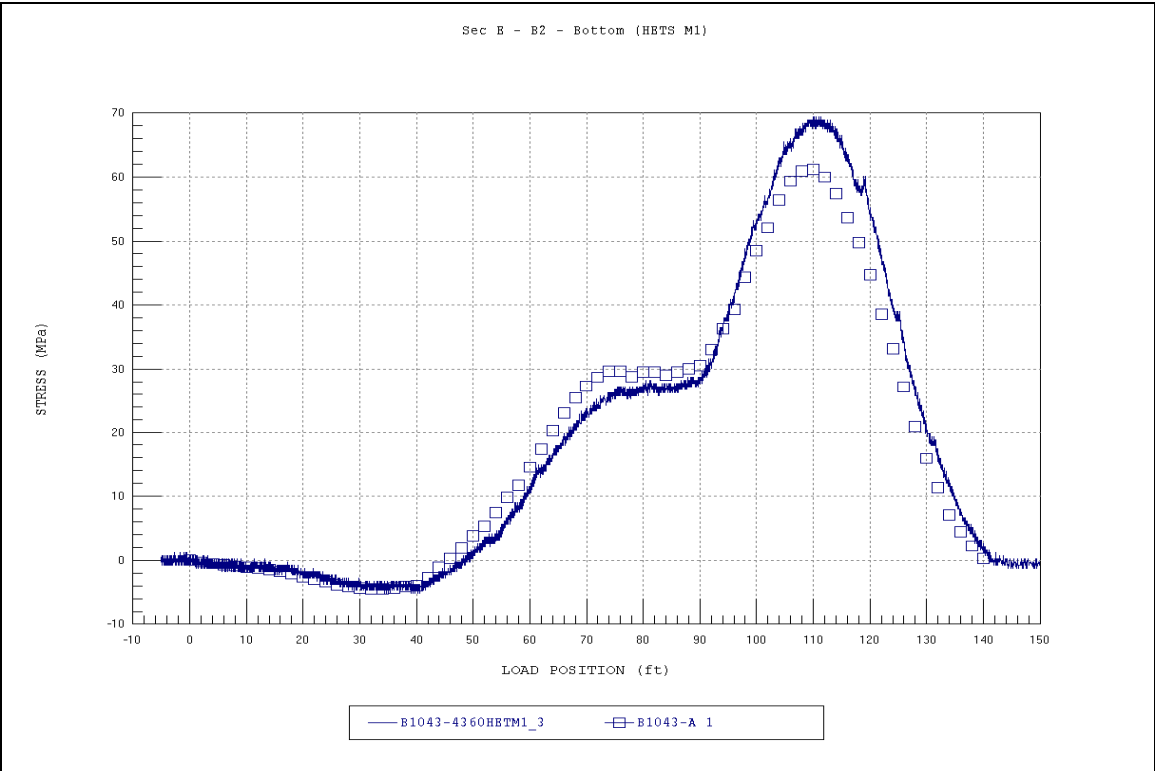


Figure A57. Section E – B2 – Bottom.
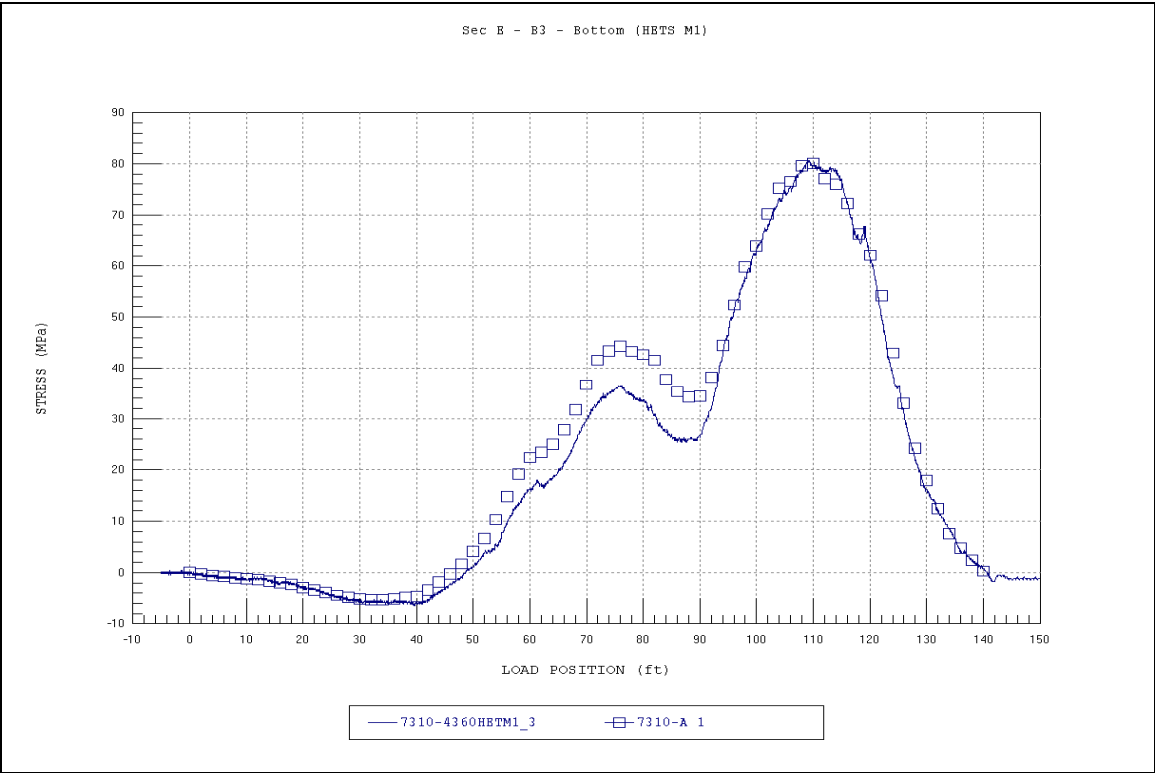
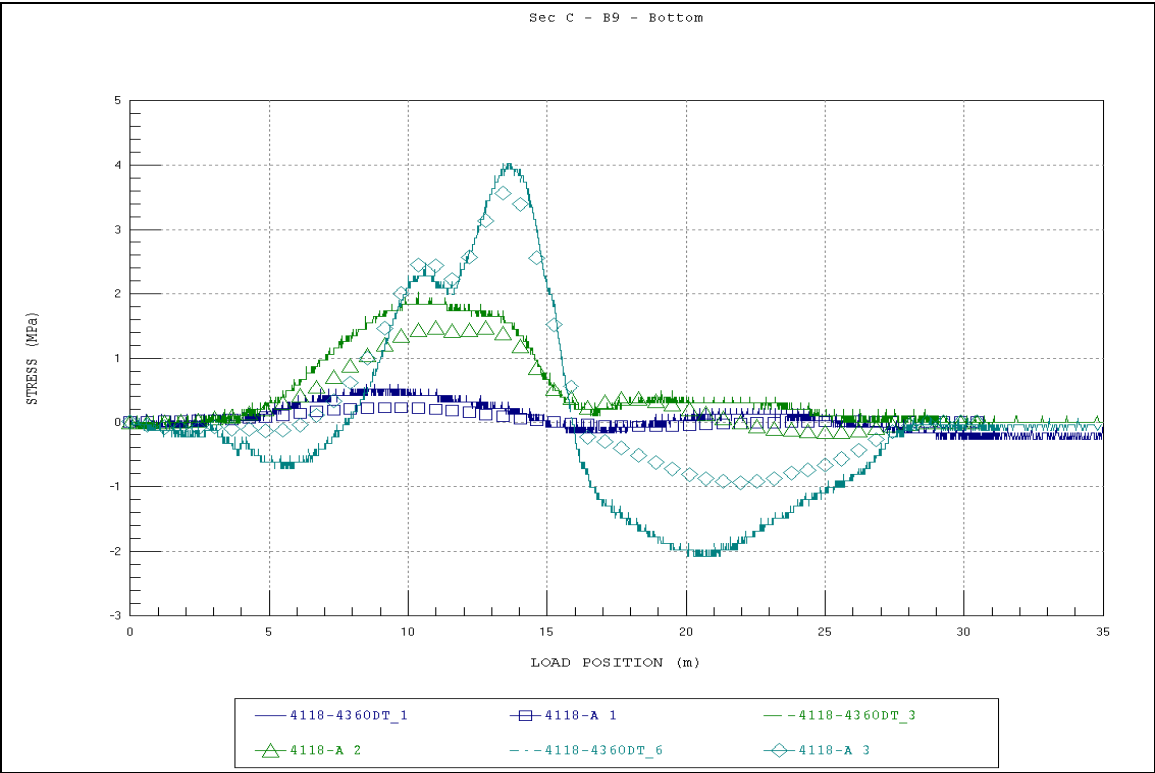Figure A58. Section E – B3 – Bottom.
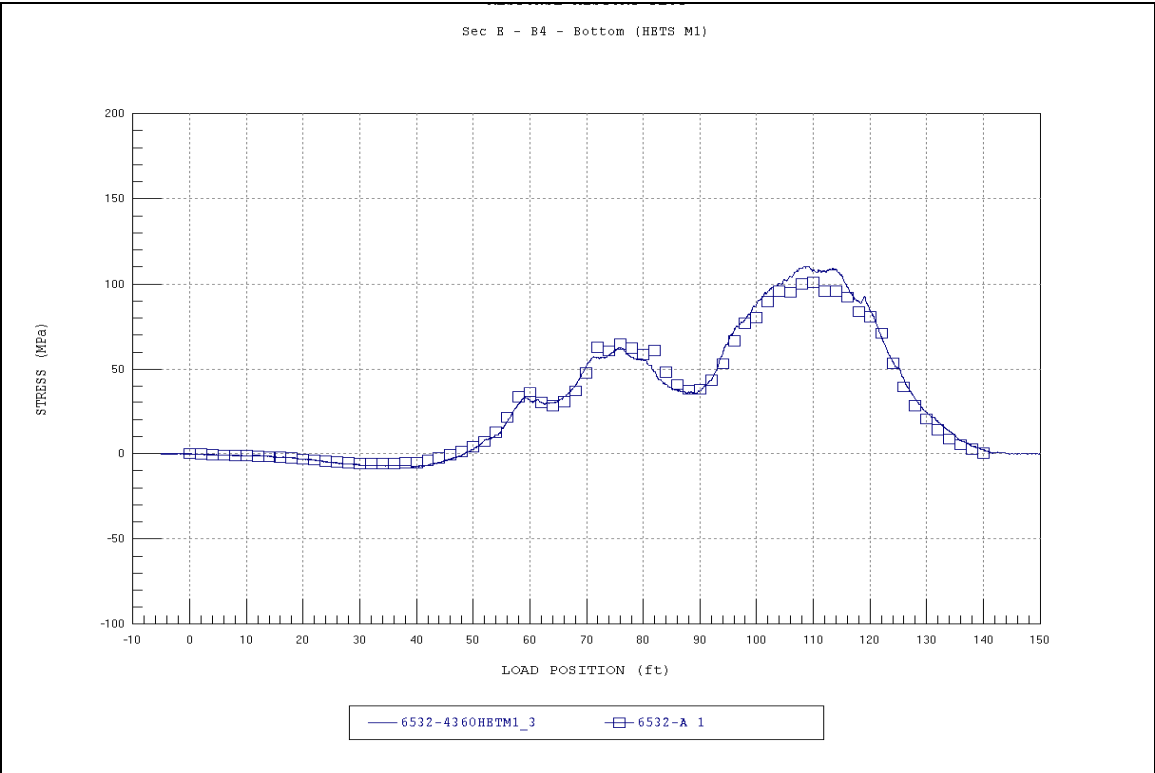


Figure A59. Section E – B4 – Bottom.
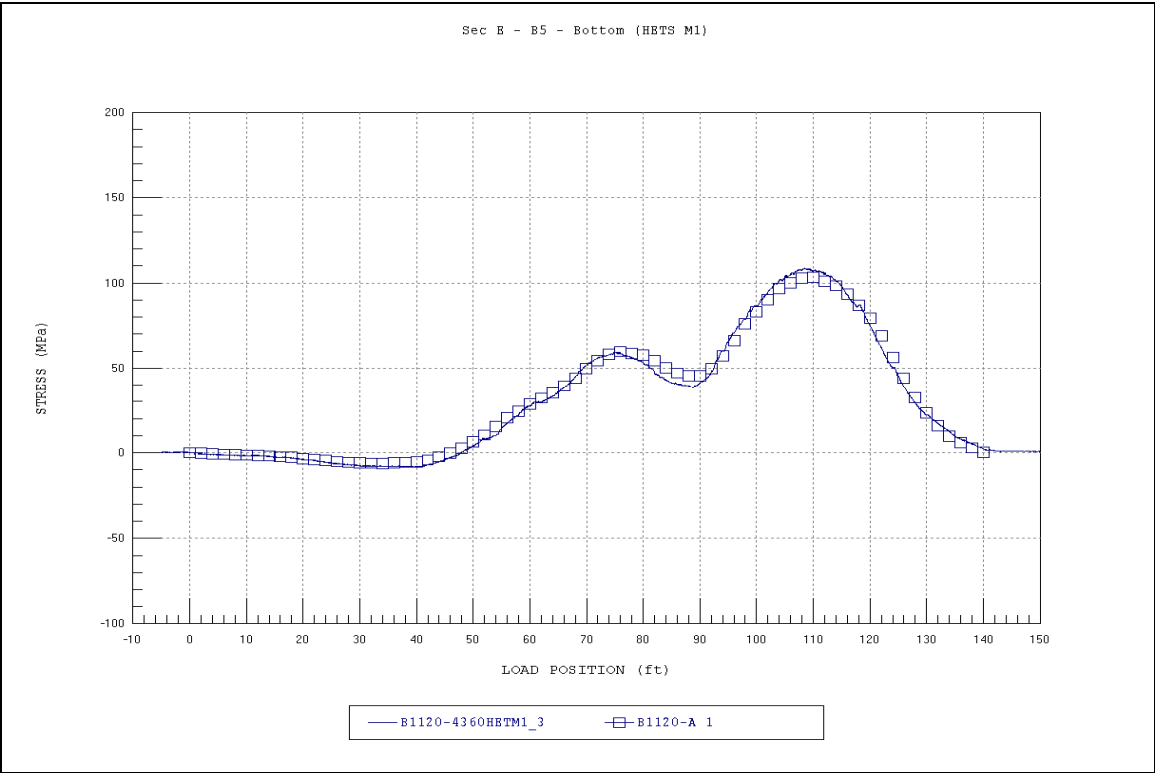
Figure A60. Section E – B5 – Bottom.
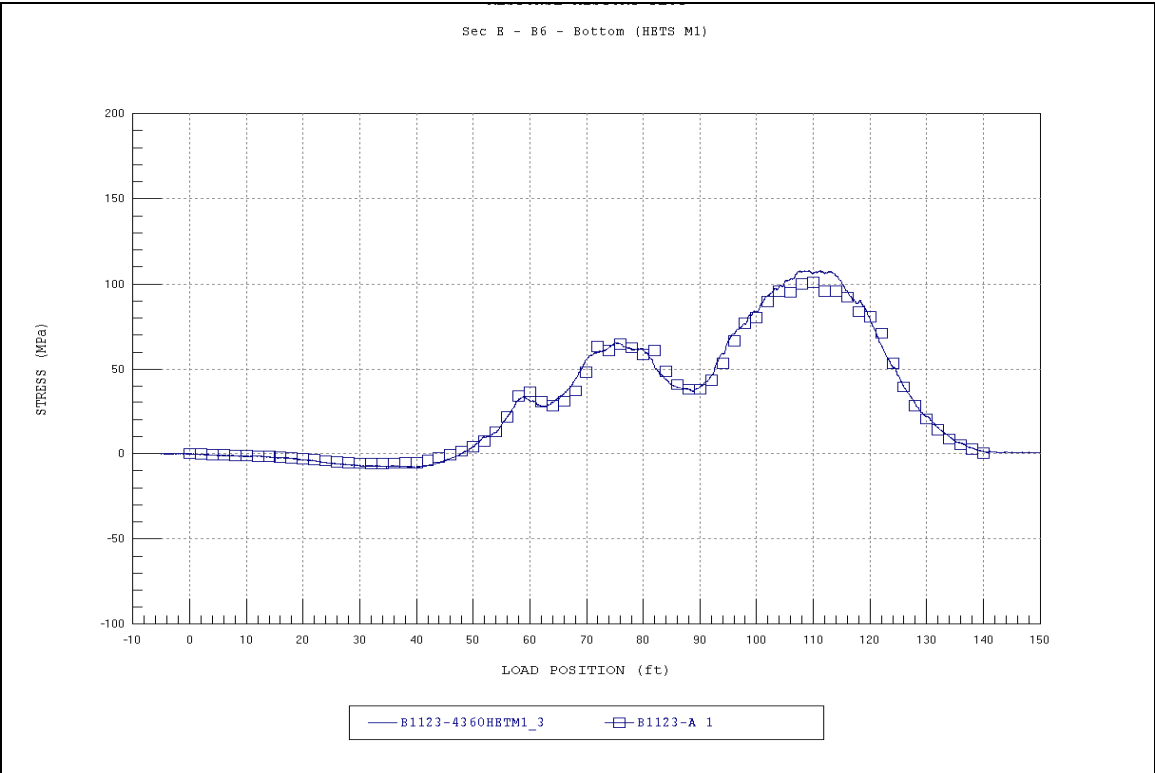


Figure A61. Section E – B6 – Bottom.
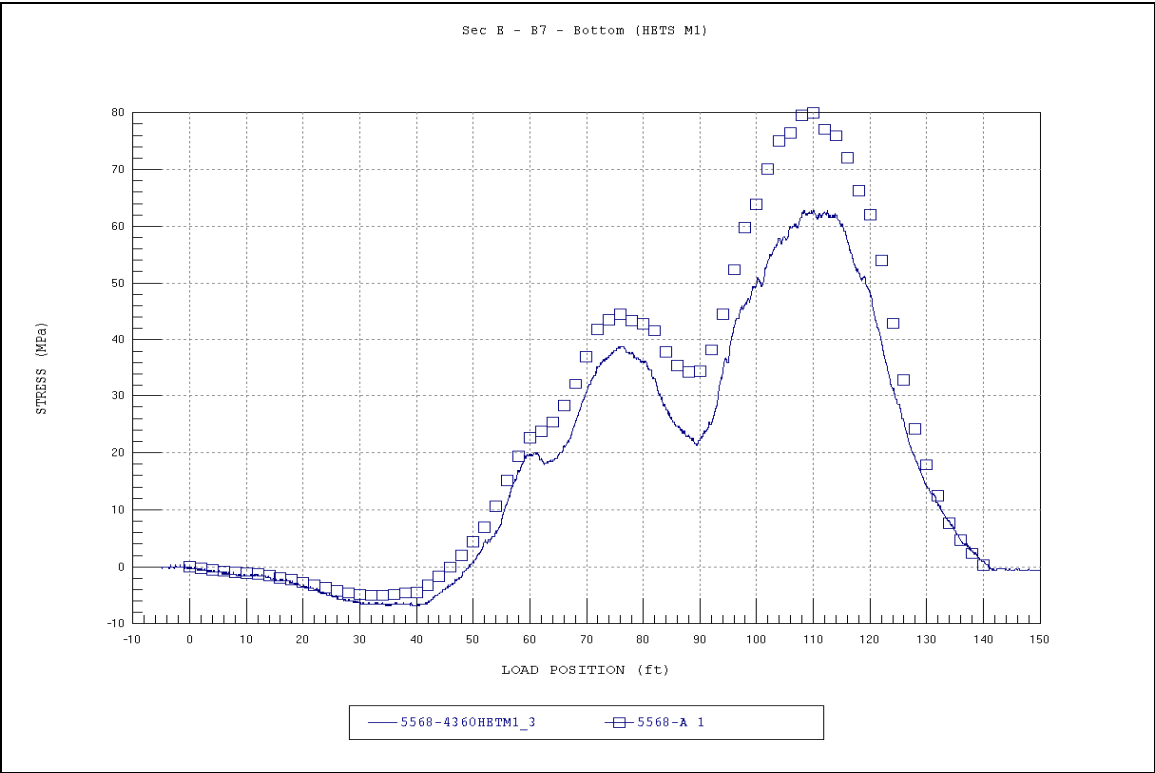
Figure A62. Section E – B7 – Bottom.
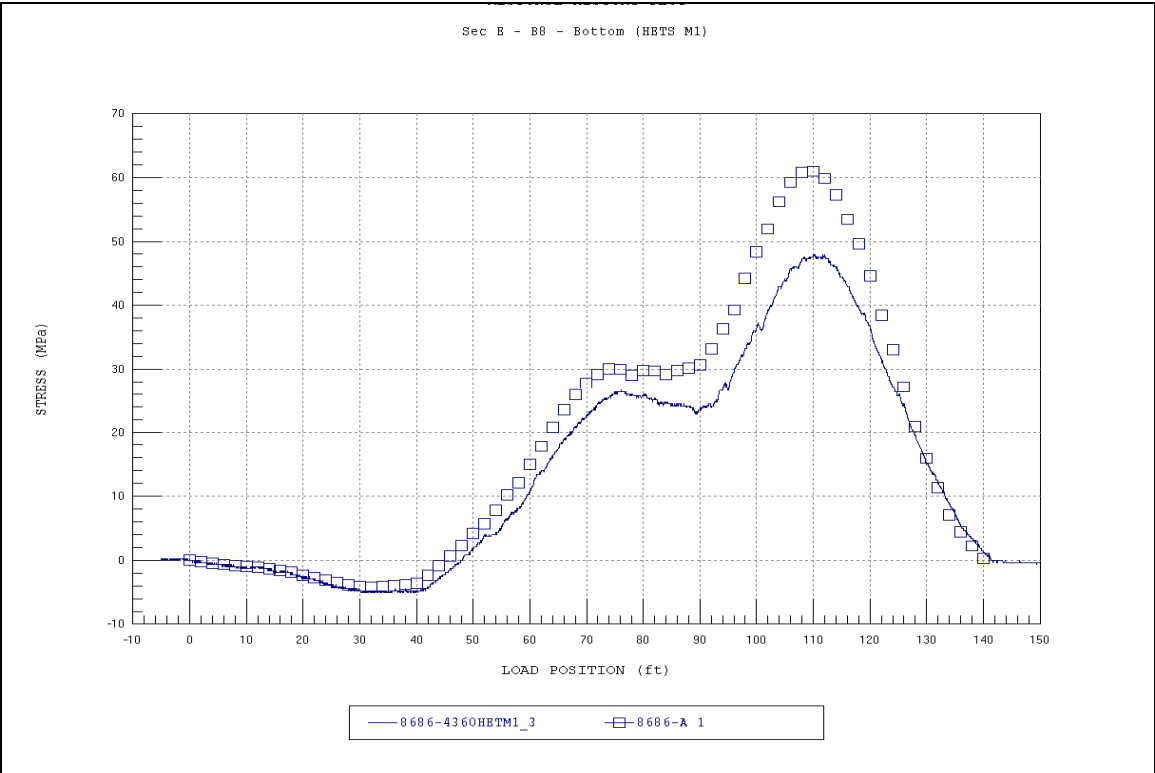


Figure A63. Section E – B8 – Bottom.
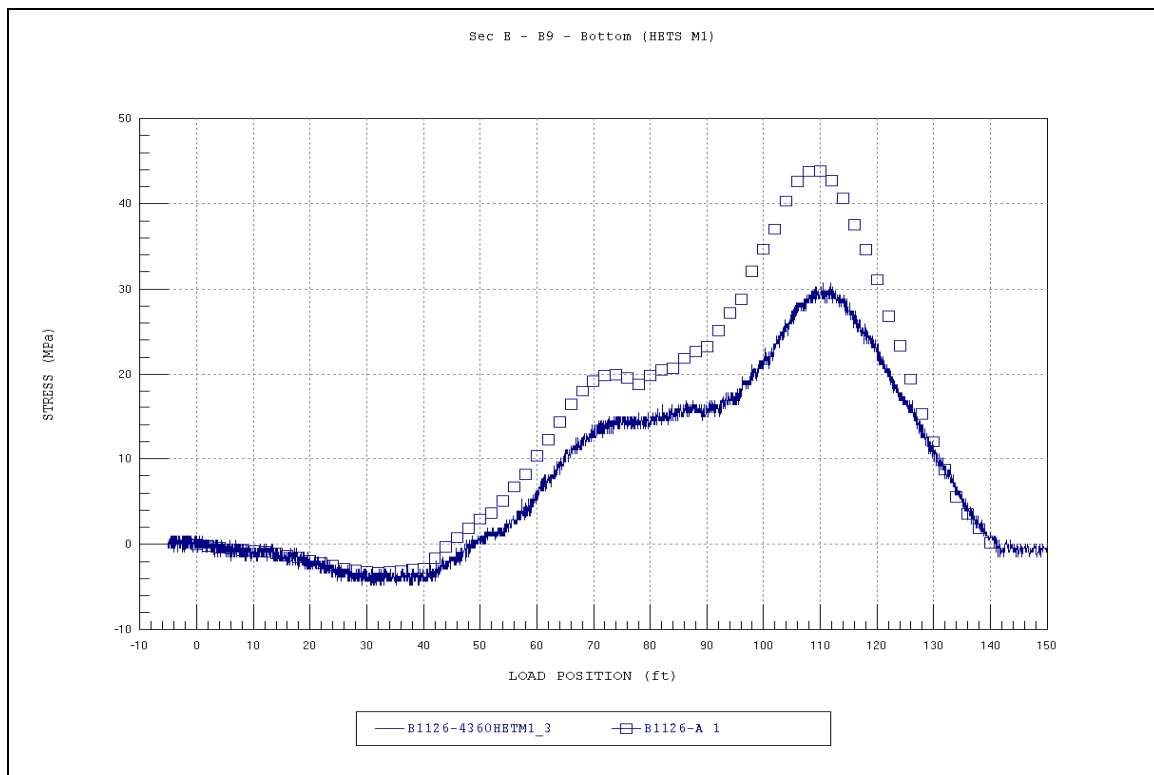
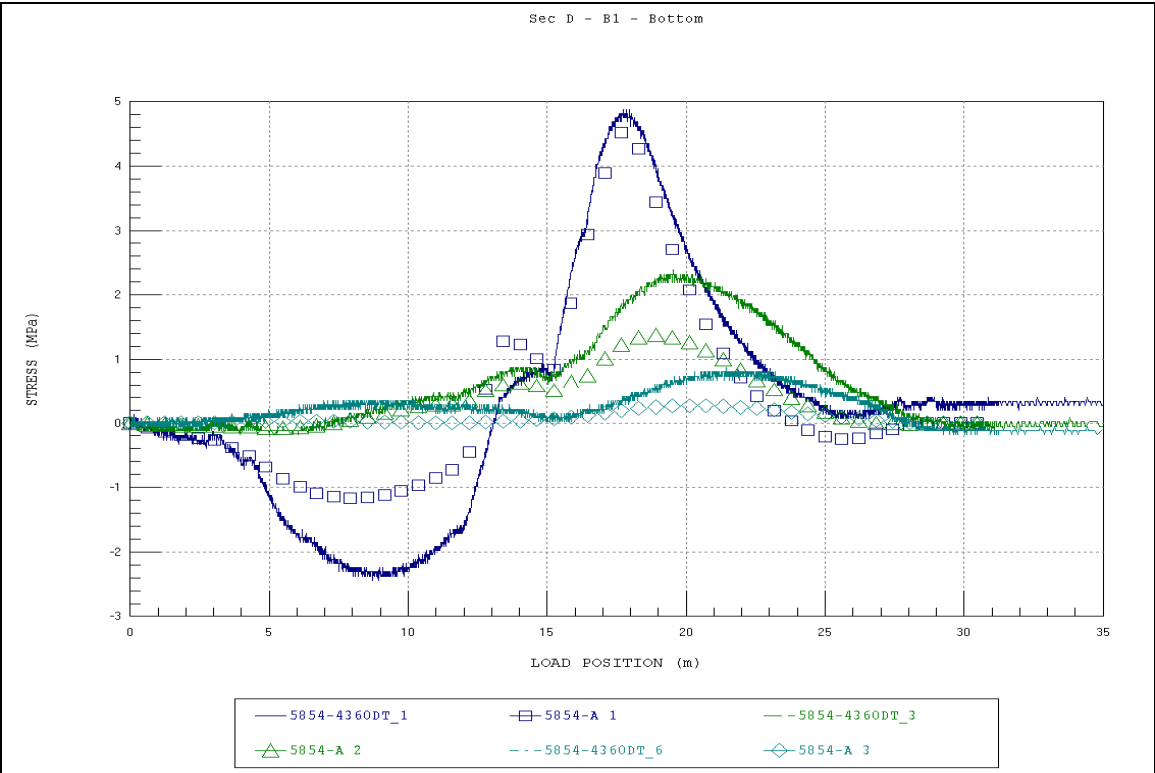Figure A64. Section E – B9 – Bottom.

## M1 Tank
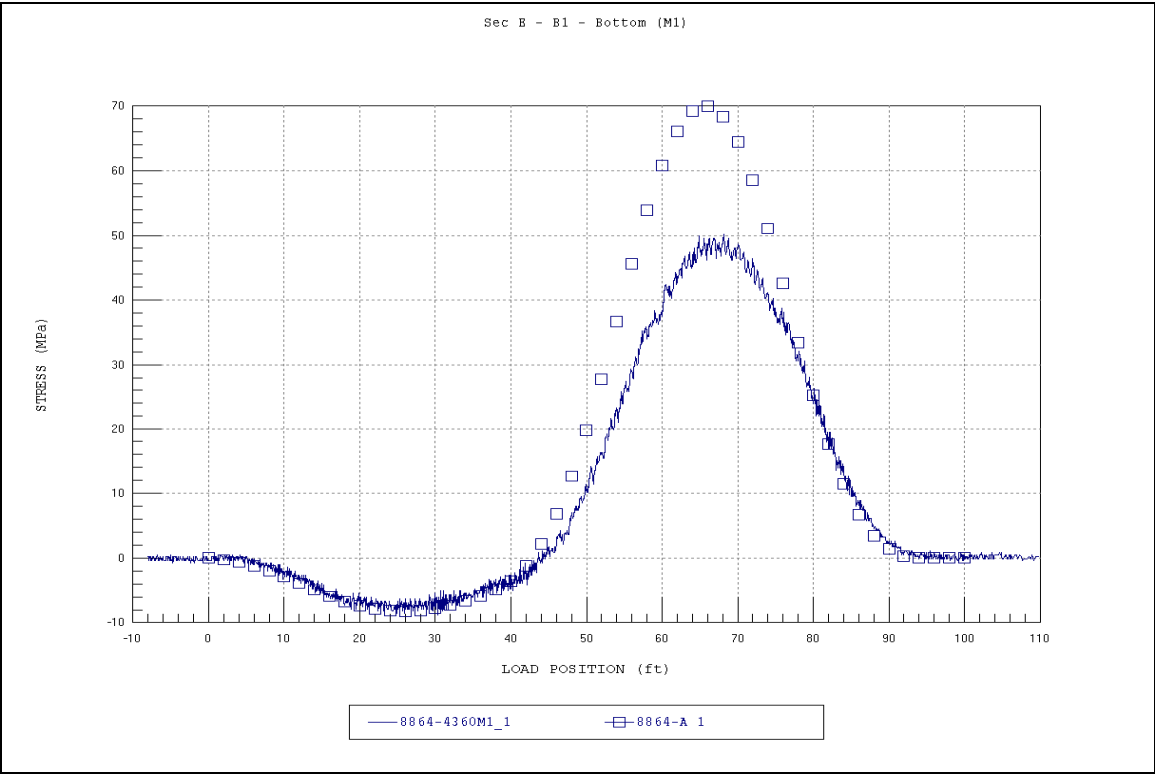


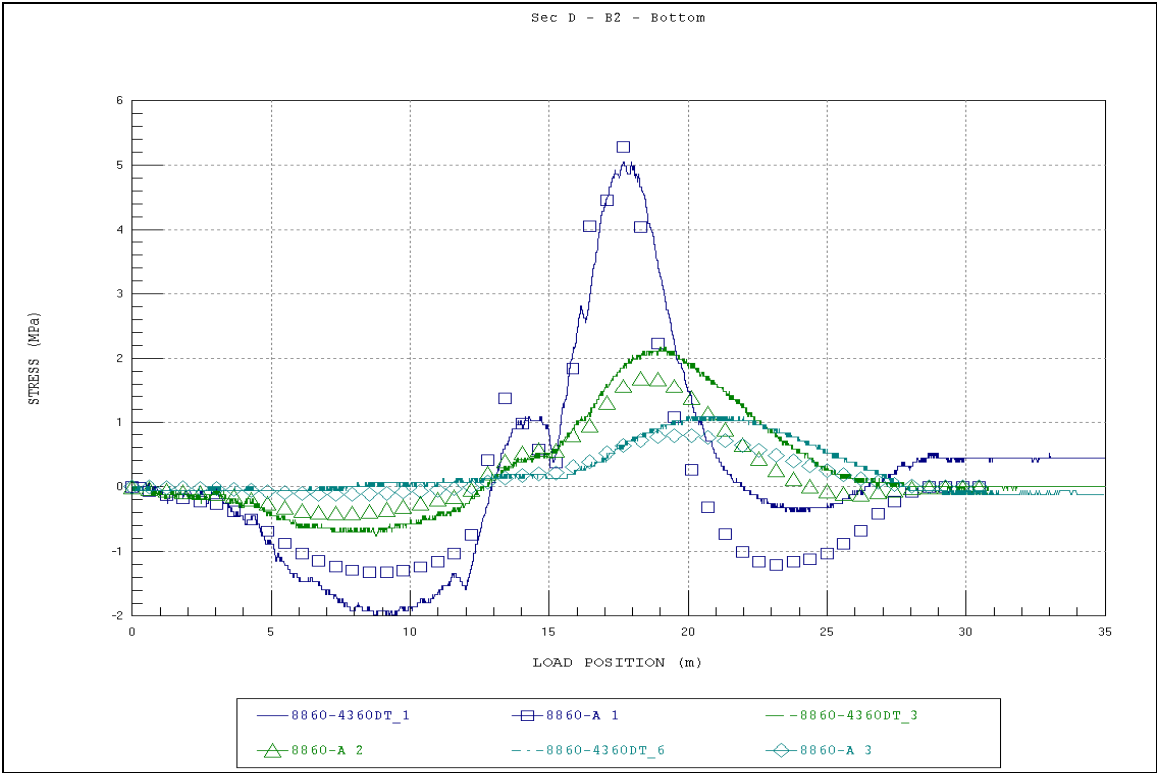Figure A65. Section E – B1 – Bottom.
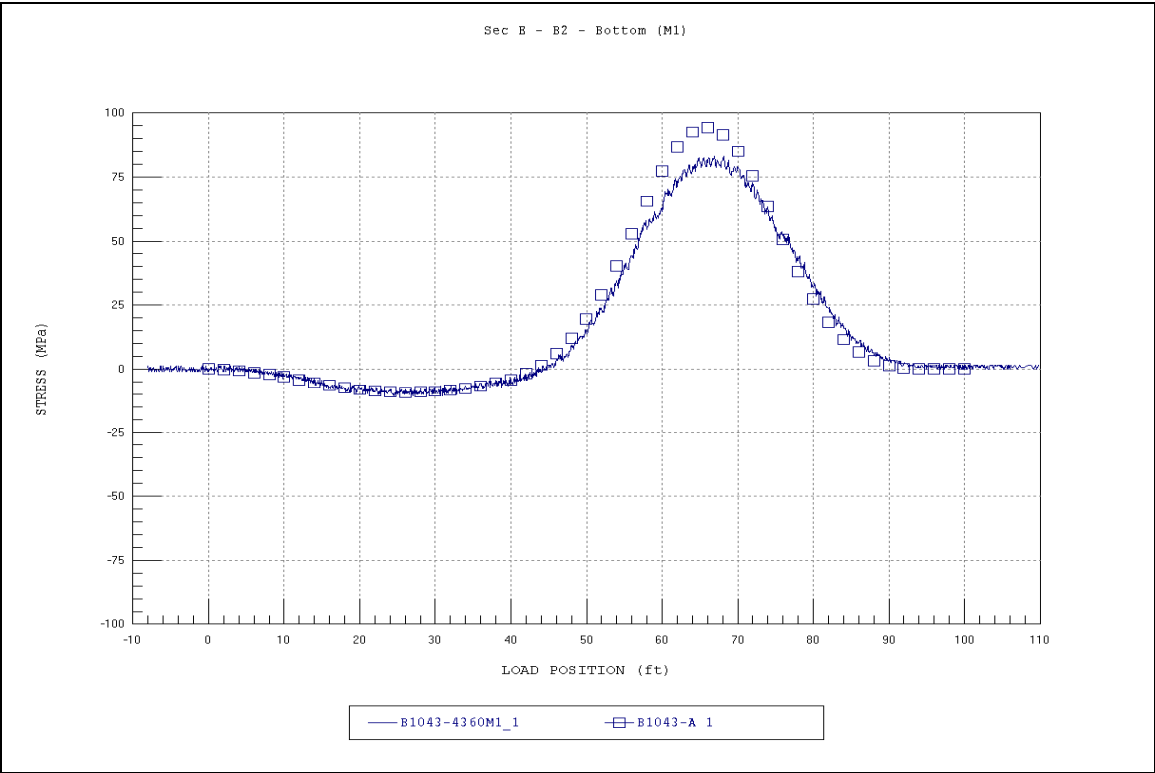


Figure A66. Section E – B2 – Bottom.
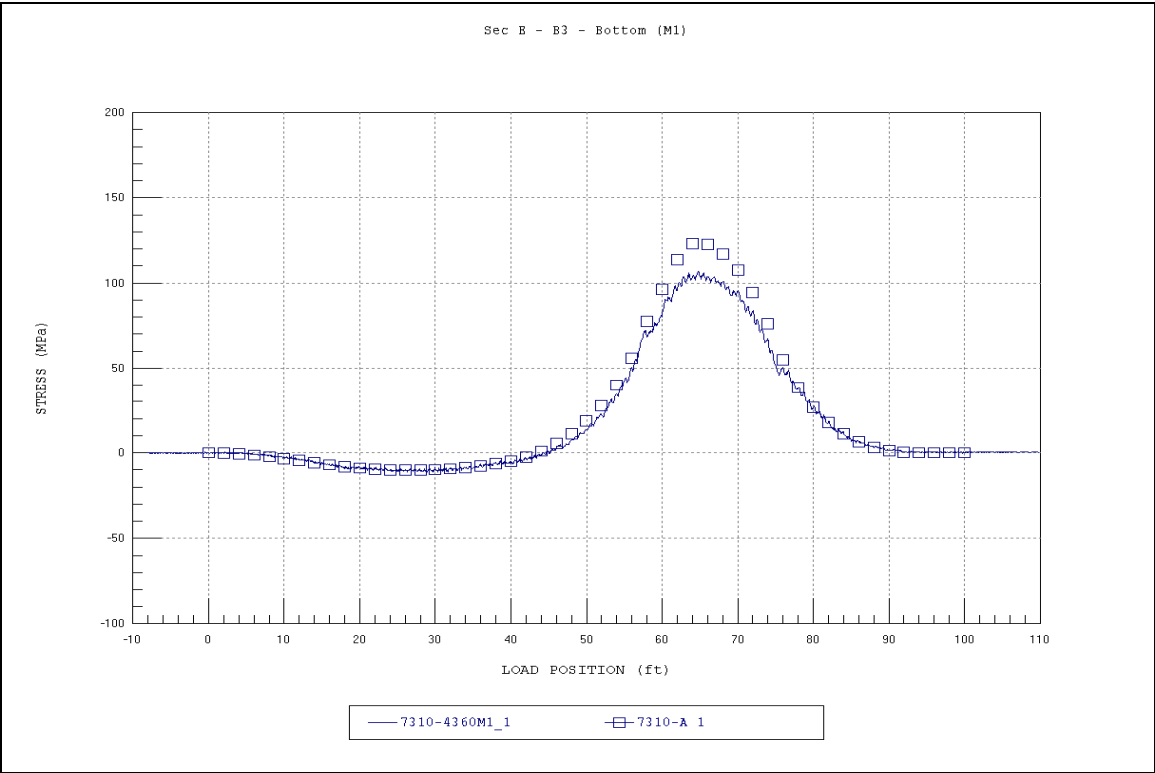
Figure A67. Section E – B3 – Bottom.
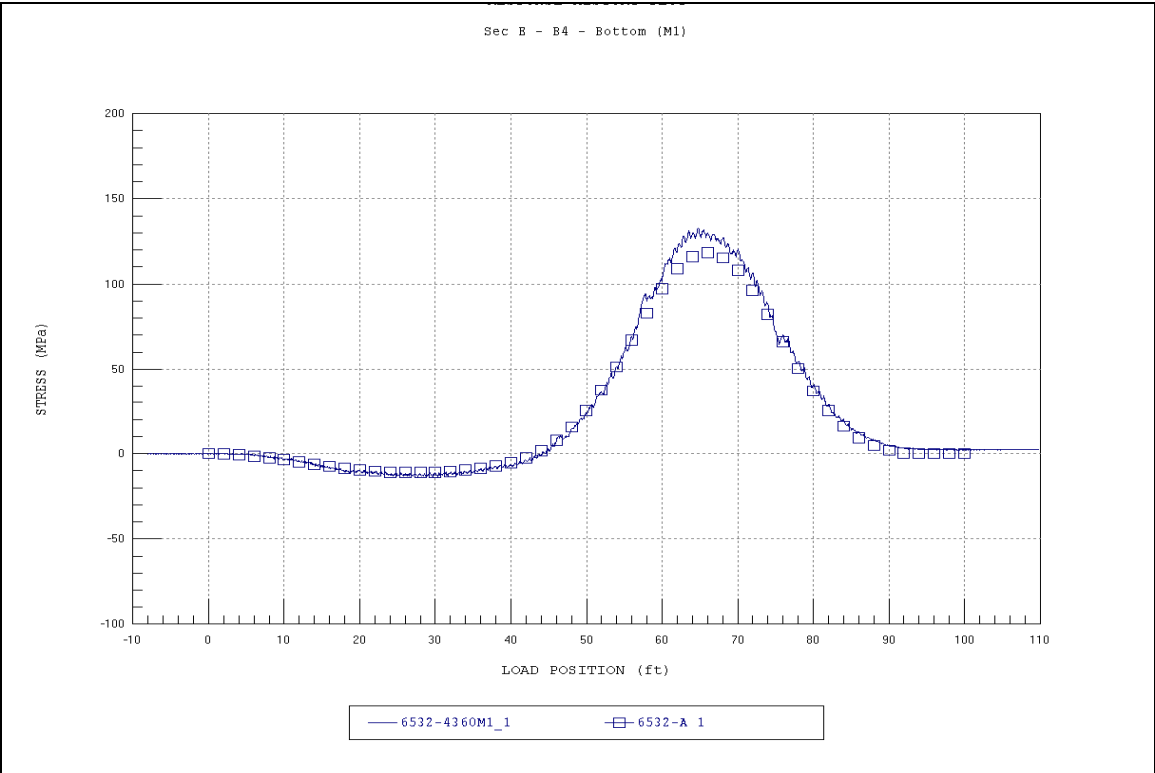


Figure A68. Section E – B4 – Bottom.
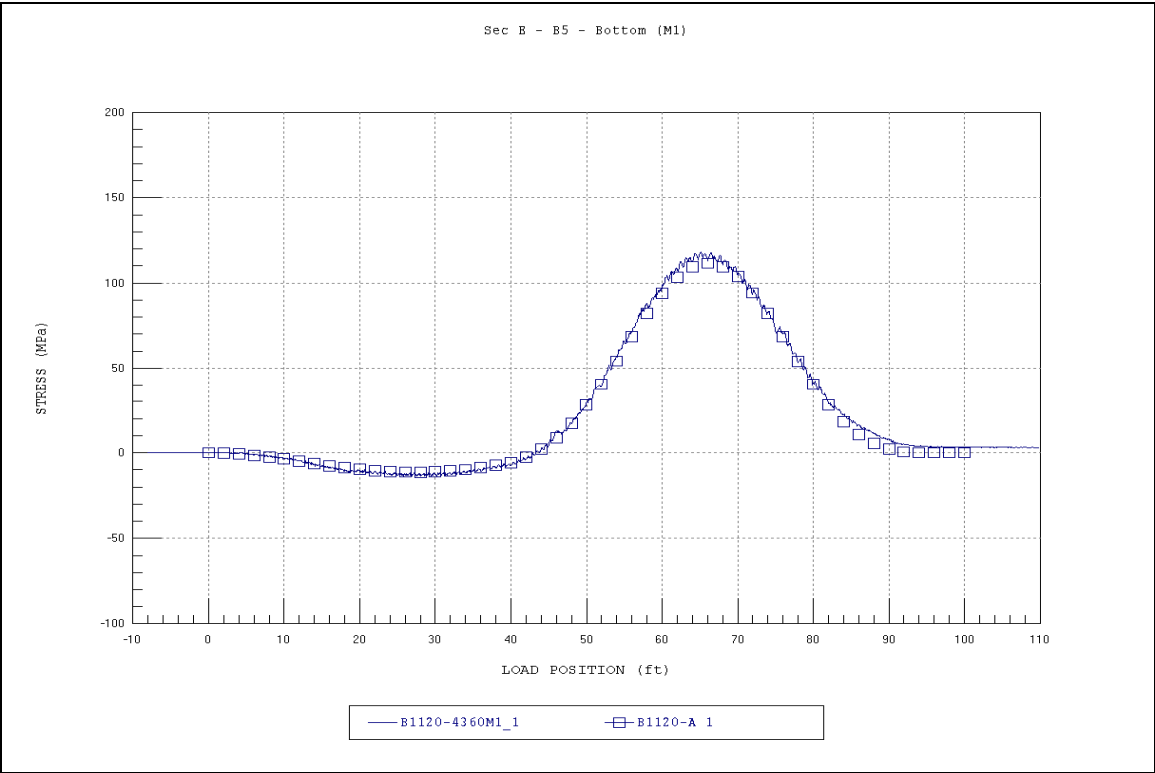
Figure A69. Section E – B5 – Bottom.



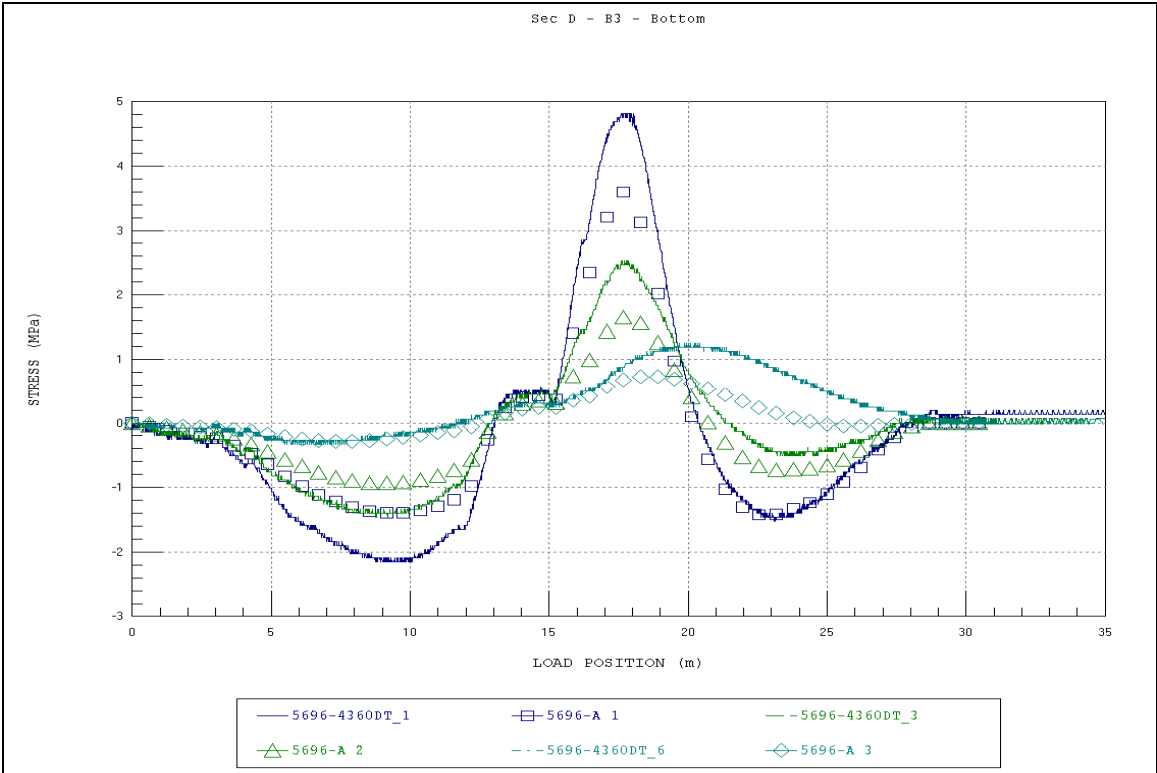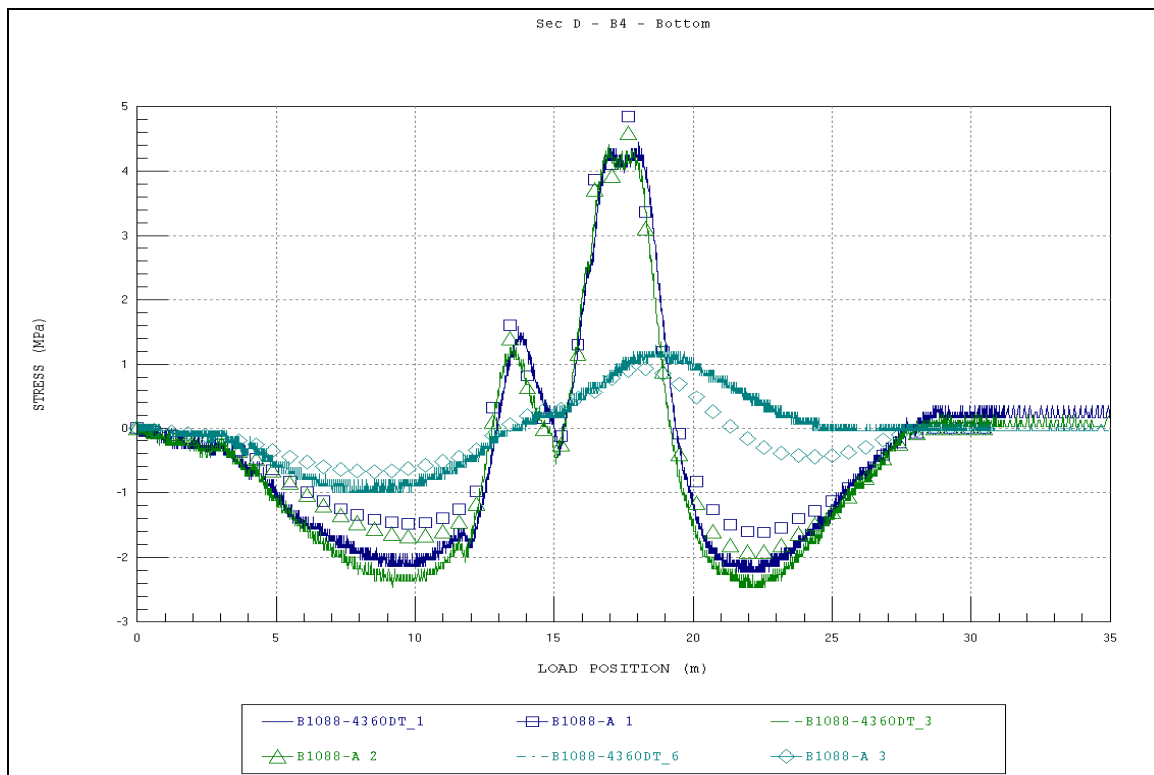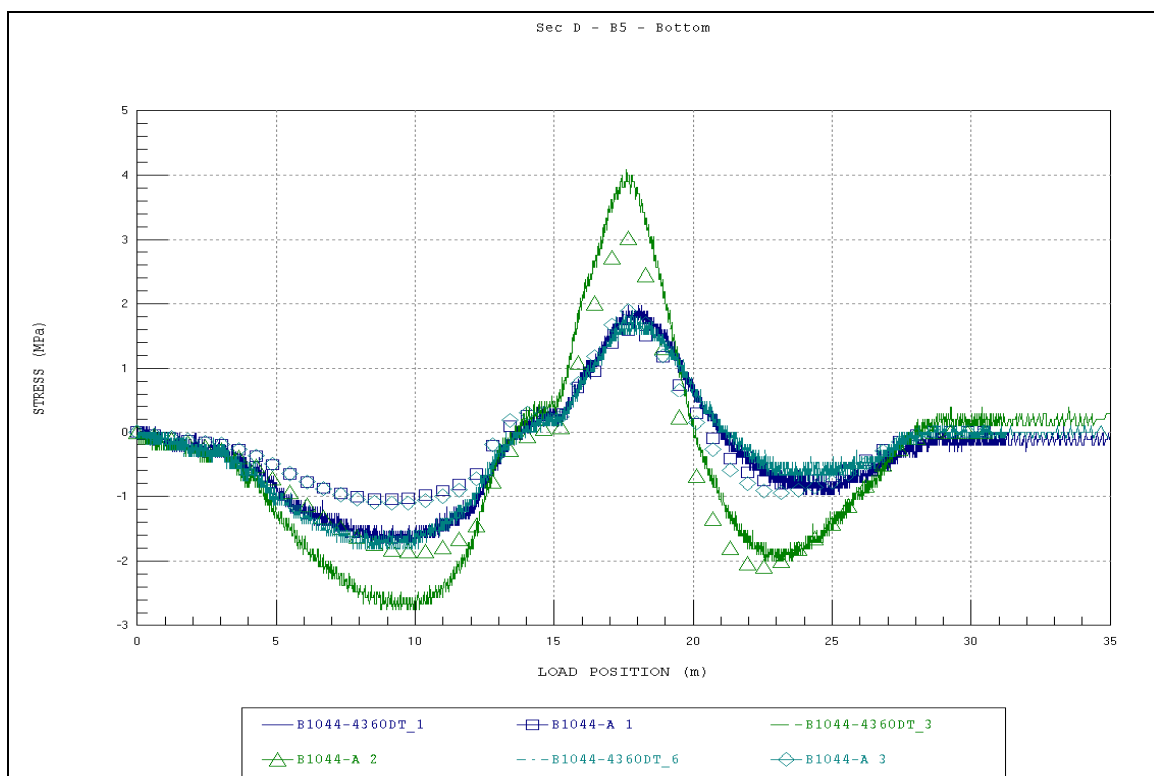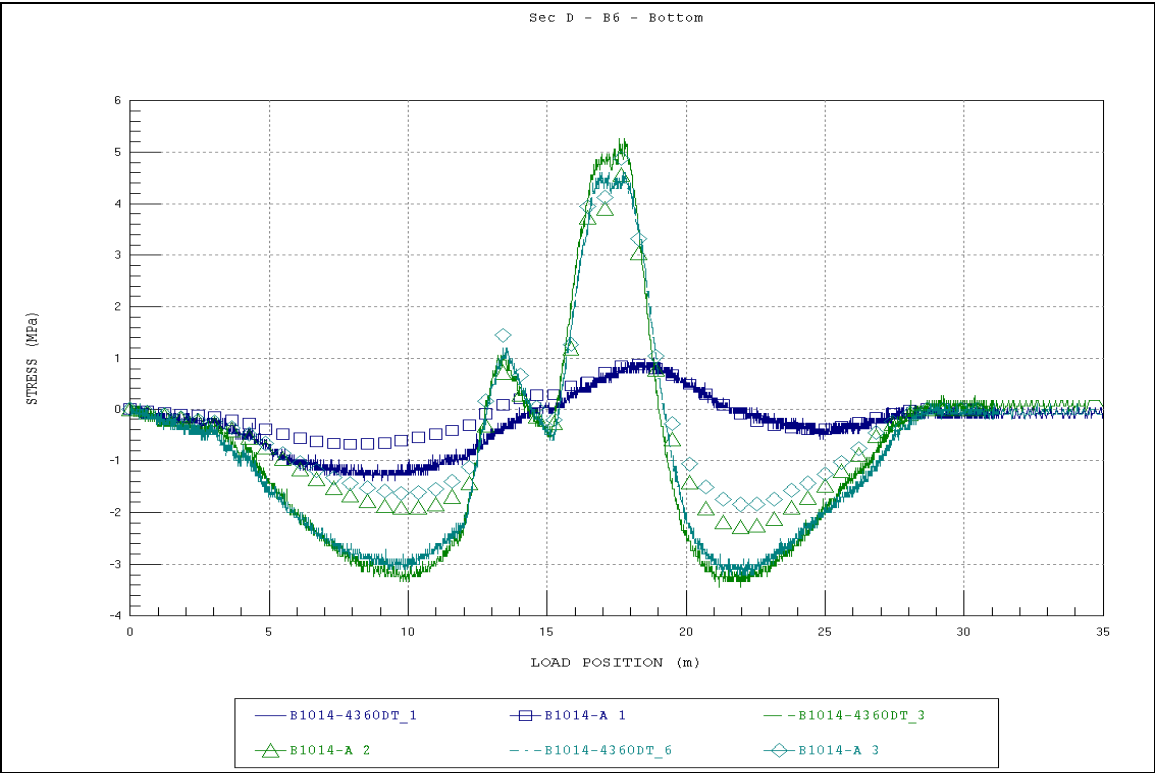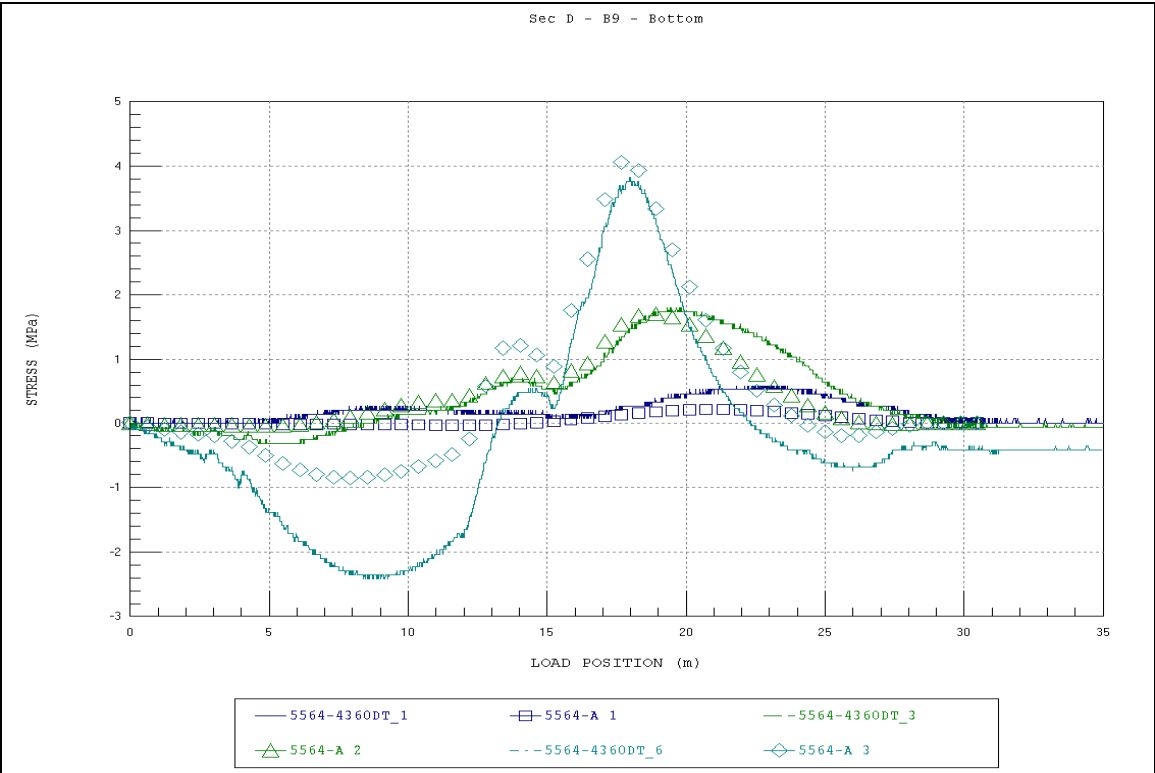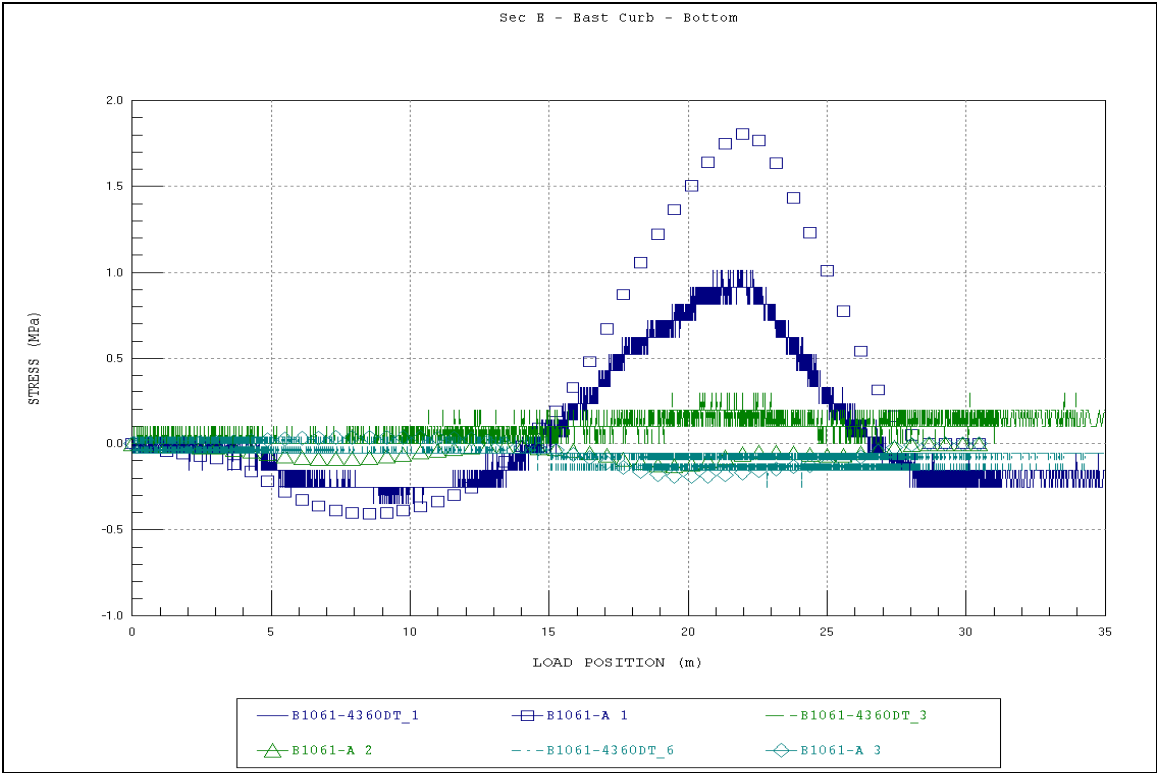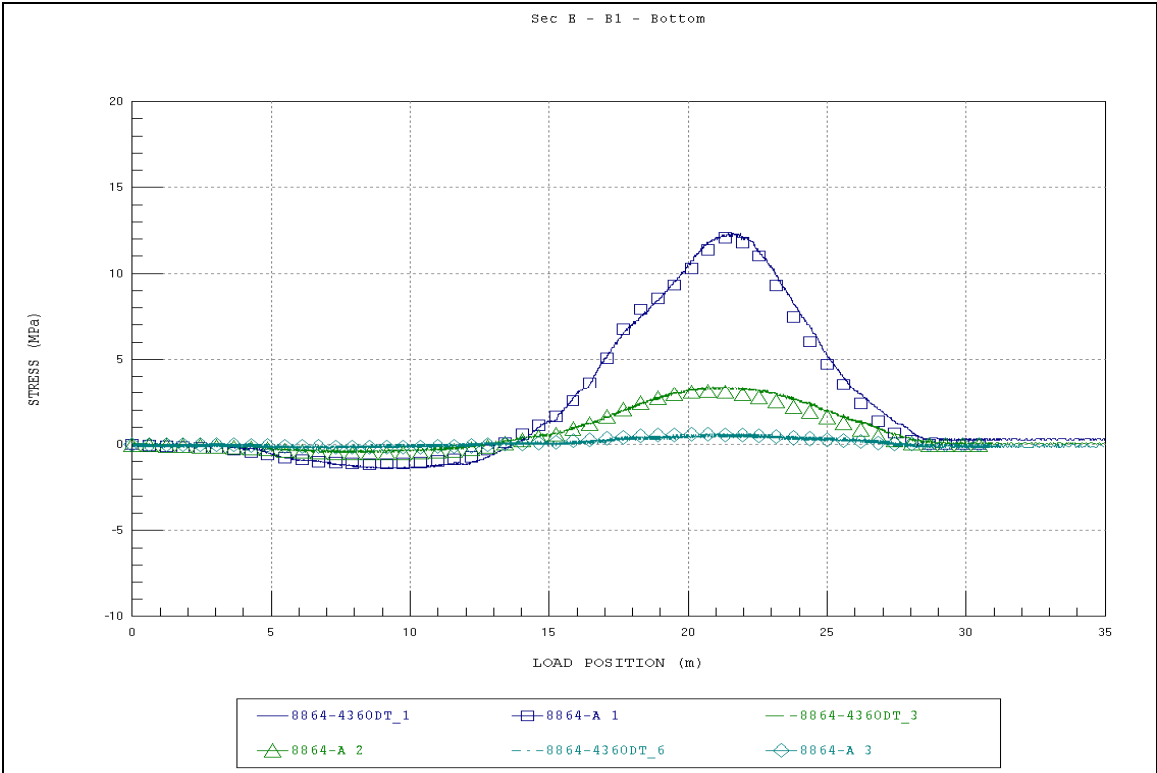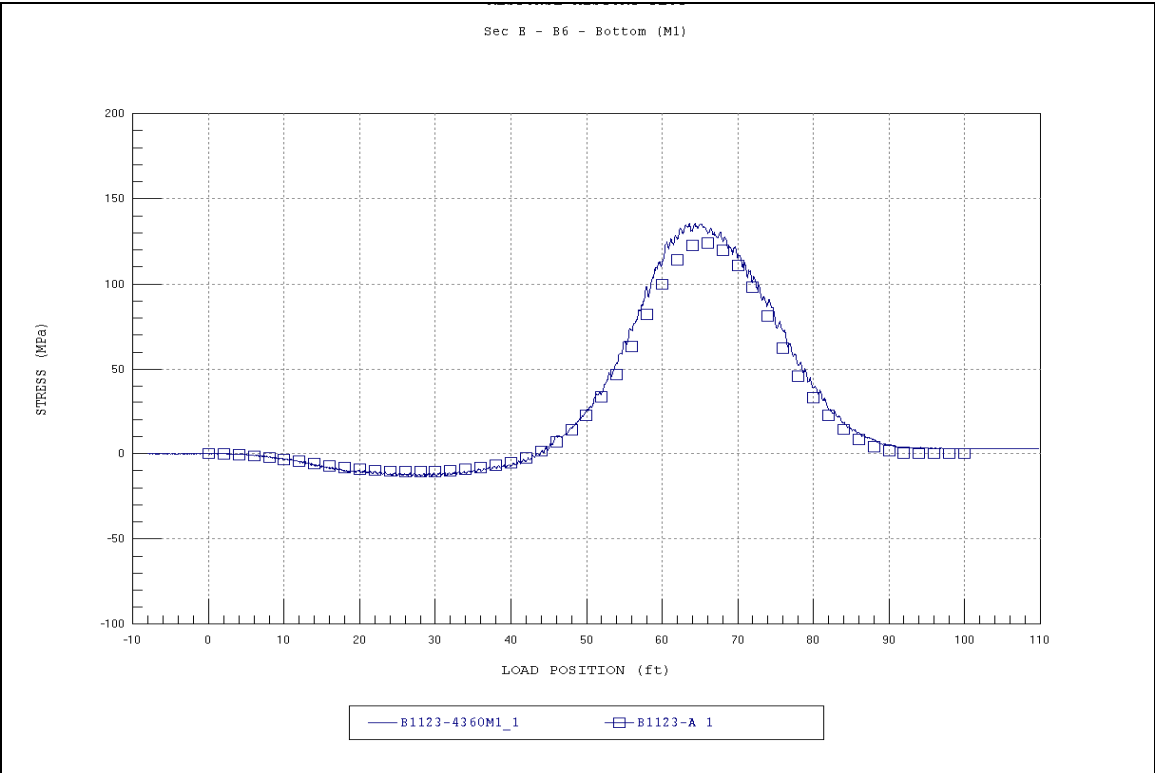Figure A70. Section E – B6 – Bottom.
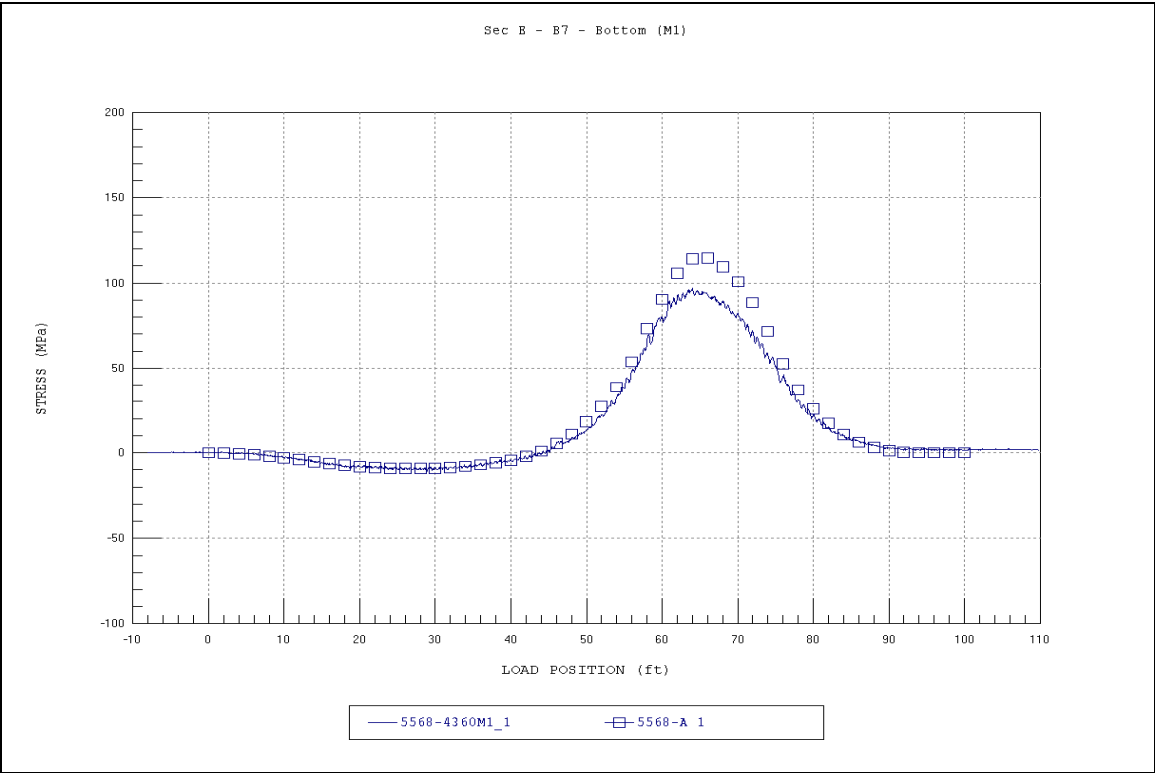
Figure A71. Section E – B7 – Bottom.
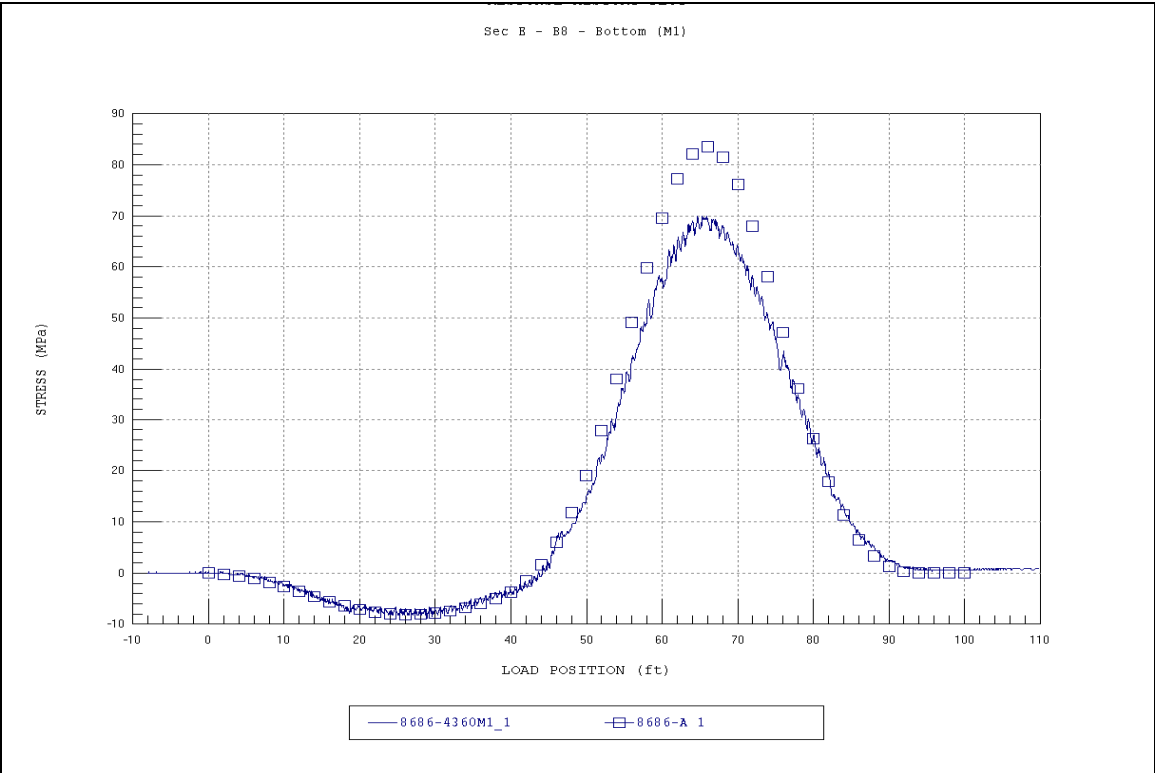


Figure A72. Section E – B8 – Bottom.
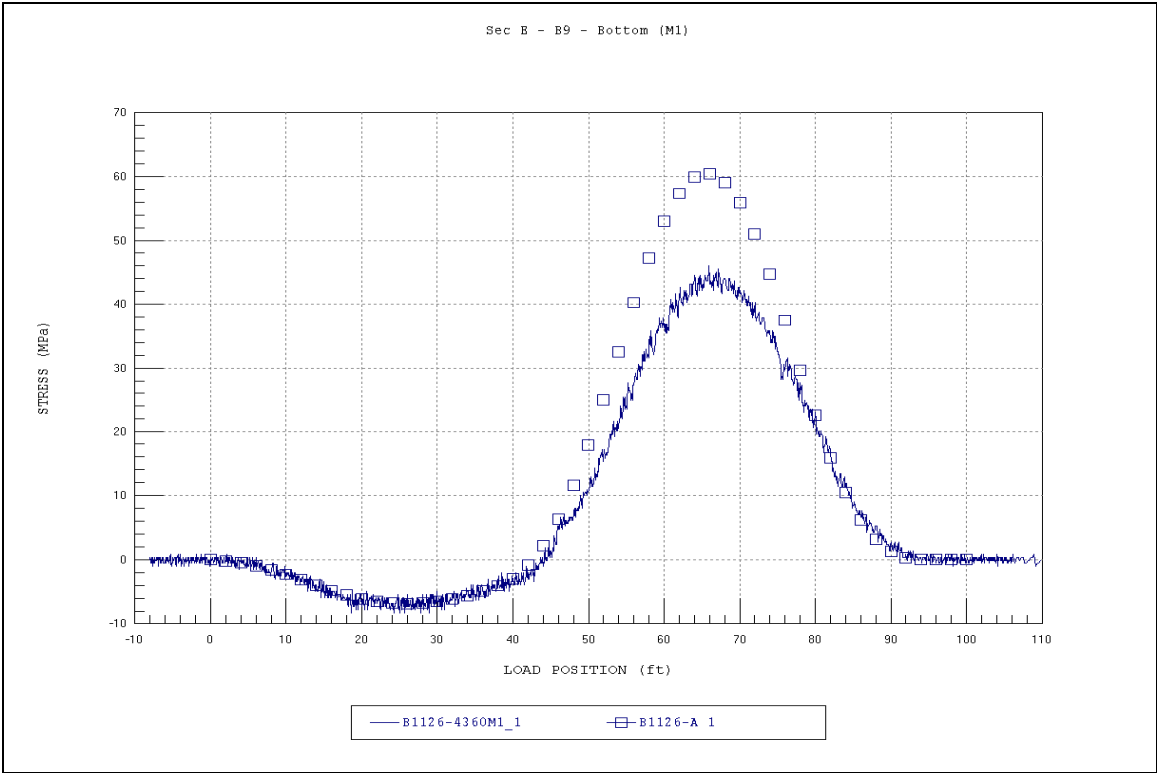
Figure A73. Section E – B9 – Bottom.

# Appendix B: Field Notes (Scanned)

PROJ. # 060701-103

## FIELD NOTES & TESTING CHECKLIST
### (TYPICAL BEAM-SLAB BRIDGES)

PROJECT NAME OR #:  4360   Camp Hovey

FIELD NOTE TAKER:  JLG                                DATE:  June 12th, 2007

STRUCTURE NAME OR ID:  #4360

3 CAD DRAWINGS:  1-Gage ID,   1-Gage Dimensions,   1-General Dimensions.

### MEASUREMENTS AND GAGE INSTALLATION PROCEDURES (BELOW)

SPAN LENGTH(S):  ~ 40'

SKEW:   YES   (NO)                ANGLE:  —

BEAM SIZE:  2 sizes (see plans        BEAM SPACING:

DIAPHRAGM SPACING:  6' - 10"                SIZE:  $\bigsqcup$  $d = 12"$  $t_f = \frac{1}{4}"$
                                                              $b_f = 2\frac{7}{8}"$  $t_w = \frac{1}{4}"$

BENT INFO:  SIZE:  checked  see gage x-sections    # OF PILES:  —   PILE SPACING:  —

GAGE INSTALLATION: 1. Measure gage location & write it on the beam.
                   2. Install gage and take picture(s) w/ a reference point.
                   3. Write gage ID and dimensions on CAD notes.
                   4. Repeat for every gage location!!!
                   5. Take multiple pics from different angles.

SUPPORT CONDITIONS:  steel bearing pads, no neoprene.

ABUTMENT DETAILS: (Draw elevation detail)

DECK THICKNESS:  ?                COMPOSITE:  ~~YES~~ ? ~~NO~~

GENERAL OBSERVATIONS:

1

## MEASUREMENTS AND TESTING PROCEDURES (ABOVE)

BEGINNING OF WORLD (BOW)     VERIFY NORTH ON PLANS:   YES   NO
(X=0, Y=0, location)

South East corner of Sidewalk

BOW PHOTOS: ☑                ROAD MARKINGS PHOTOS: ☑

                                        Different Bm sizes

ROADWAY WIDTH (CURB-TO-CURB):  24'     SYMMETRIC:   YES   NO

STRUCTURE WIDTH (Out-to-Out):  32'

WEARING SURFACE:  Concrete ← Deck only   THICKNESS:  N/A

STARTING TEST POSITION:  −10' + ½ wheel Rev  DIRECTION:  North / North West

VEHICLE ROLL OUT (5 REVS!):  see notes       A/C LOCATION:
*****MAKE SURE YOU PUT THE A/C ON THE SAME WHEEL AS WAS USED TO MEASURE THE ROLL OUT*****

VEHICLE MEASUREMENTS:
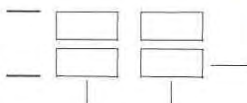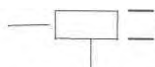
See vehicle Plans.

AXLE WEIGHTS:

   FRONT: ✕       REAR: ✕       GROSS: ✕

VEHICLE PROVIDED BY:  ACE / CASEY

TRAFFIC CONTROL PROVIDED BY:  ACE / CASEY

ACCESS PROVIDED BY:  ACE / CASEY

2

<u>LATERAL TESTING POSITIONS:</u> (REFERENCED FROM BOW)

Y1:  2' Pass          Y2:  15.5   Driver

Y3:  21.8' Driver     Y4:  16.6   Driver

Y5:                   Y6:

LATERAL POSITIONS CHECKED BY:   SA

## TESTING OPERATIONS (WINSTS)

VERIFY GAGE ID & # OF CHANNELS WITH WINSTS:   ☑

RUN WINSTS TO VERIFY RESPONSES:   GOOD

WEATHER CONDITIONS &   ~ 80-85 °F
AMBIENT TEMPERATURE:               Hazy

<u>RUNNING THE FIELD TESTS</u>
STS OPERATOR:   JLG          TRUCK OPERATOR:   SA

<u>CONTROLLED SEMI-STATIC TESTS</u>
    **SAMPLE RATE:**  40 Hz
    **GAIN:**  1000

| FILE NAME | LATERAL POSITION | COMMENTS |
|---|---|---|
| 4360 DT_1.dat | Y1 | Dump Truck - GOOD |
| - 2.dat | Y1 | - GOOD |
| - 3.dat | Y2 | GOOD |
| - 4.dat | Y2 | GOOD (starting position |
| - 5.dat | Y3 | GOOD (may be ~ + 1 ft) |
| - 6.dat | Y3 | GOOD |
|  |  |  |
| 4360 HET_1.dat | Y2 | Het unloaded - too fast - bad clicks, |
| - 2.dat | Y2 | No clicks ! |
| - 3.dat | Y2 | GOOD |
| - 4.dat | Y2 | GOOD (start = ~5') |
|  |  |  |

Dump Truck

3

<u>High-Speed Test(s) or Additional Tests</u>
**Sample Rate:** 40Hz

| File Name | Lateral Position | Speed | Comments |
|---|---|---|---|
| 4360HETM1-1.dat | Y2 | HET +M1 | - missed 1ˢᵗ Click. |
|  | Y2 | " | - missed a click in the middle |
|  | Y2 | " | GOOD |
|  |  |  |  |
| 4360M1 - 1.dat | Y4 | M1 only | GOOD |
| -2.dat | Y4 | " | GOOD |
|  |  |  |  |
|  |  |  |  |
|  |  |  |  |

**Backup Data Files:**  2 Flash: ☑  2 PC's: ☐  Email: ☐

**Take Pictures of Notes:** ☑  **Backup Pics:** ☐

**All Notes Checked By:** SA

**Any Additional Testing Comments:**

4360HET_#.dat : Test started @ -10 Exact. Manual clicking was used.

4360HETM1_#.dat : Loaded HET (M1 tank) used AC.
　　- Starting Position = -10' + ½ wheel Rev.
4360M1_#.dat : - M1 Tank only.
　　- used AC
　　- Start position = -10' + ½ wheel Rev.

4

SECTION A-A

1122
1118  1116  4050  5859  5563  5833  7901

B1  B2  B3  B4  B5  B6  B7  B8  B9

SECTION B-B

B1127
6"
3"

1.5"  B1119      1191  1100  1133  6327  6150

B1129  B1046  B1032  1095  1094  1128  8665  1097  1125

B1  B2  B3  B4  B5  B6  B7  B8  B9

SECTION C-C

5864
5560  9065  7906  8687  5698  8688  4118

B1  B2  B3  B4  B5  B6  B7  B8  B9

SECTION D-D

8267    4123

5854  8860  5696  B1088  B1044  B1014  8863  9020  5564

B1  B2  B3  B4  B5  B6  B7  B8  B9

SECTION E-E

1060

B1061    81045  81132  8984  4029  B1087  B1139  5565  8861  1190  B1124

8864  1643  7310  6531  B1120  B1123  5568  8686  1126

B1  B2  B3  B4  B5  B6  B7  B8  B9

SECTION

①  ①  ②  ①  ②  ①  ②  ①  ①

B1  B2  B3  B4  B5  B6  B7  B8  B9

① FLANGE THICKNESS = 5/8"
FLANGE WIDTH = 9"
BEAM DEPTH = 24 1/8"

② FLANGE THICKNESS = 7/8"
FLANGE WIDTH = 12"
BEAM DEPTH = 23 1/2"

Abutment $ BOW Reference          4360



Pier

# Appendix C: Field Testing Procedures

## Background

The motivation for developing a relatively easy-to-implement field-testing system was to allow short- and medium-span bridges to be tested on a routine basis. Original development of the hardware began in 1988 at the University of Colorado under a contract with the Pennsylvania Department of Transportation. Subsequent to that project, the Integrated Technique was refined on another study funded by the Federal Highway Administration, in which 35 bridges located on the Interstate system throughout the country were tested and evaluated. Further refinement has been implemented over the years through testing and evaluating hundreds of bridges, lock gates, and other structures.

## Structural testing hardware

The real key to being able to complete the field testing quickly is the use of strain transducers (rather than standard foil strain gages) that can be attached to the structural members in only a few minutes. These sensors were originally developed for monitoring dynamic strains on foundation piles during the driving process. They have been adapted for use in structural testing through special modifications, have very high accuracy, and are periodically re-calibrated to National Institute of Standards and Technology standards. (Refer to Appendix D for specifications on the BDI Strain Transducers.)

In addition to the strain sensors, the data acquisition hardware has been designed specifically for structural live-load testing, which means it is extremely easy to use in the field. (Appendix E presents specifications of the BDI Structural Testing System.) Briefly, some of the features include military-style connections for quick assembly and self-identifying sensors that dramatically reduce bookkeeping efforts. The WinSTS testing software has been written to allow easy hardware configuration and data recording operation. Other enhancements include the BDI AutoClicker, which is an automatic load position indicator that is mounted directly on the vehicle. As the test truck crosses the structure along the preset path, a communication radio sends a signal to the STS, which receives it and puts

a mark in the data. This allows the field strains to be compared to analytical strains as a function of vehicle position, not only as a function of time. (Refer to Appendix F for the AutoClicker specifications.) The end result of using all of the above-described components is a system that can be used by people other than computer experts or electrical engineers. Typical testing times with the STS range from 20 to 60 channel tests being completed in 1 day, depending on access and other field conditions.

The following general directions describe how to run a typical diagnostic load test on a short- to medium-span highway bridge up to about 61 m in length. With only minor modifications, these directions can be applied to railroad bridges (use a locomotive rather than a truck for the load vehicle), lock gates (monitor the water level in the lock chamber), amusement park rides (track the position of the ride vehicle), and other structures in which the live load can be applied easily. The basic scenario is to instrument the structure with the required number of sensors, run a series of tests, and then remove all the sensors. These procedures can often be completed within 1 workday, depending on field conditions such as access and traffic.

## Instrumentation of structure

This outline is intended to describe the general procedures used for completing a successful field test on a highway bridge using the BDI-STS. For a detailed explanation of the instrumentation and testing procedures, please contact Bridge Diagnostics, Inc., and request a copy of the Structural Testing System Operation Manual.

## Attaching strain transducers

Once a tentative instrumentation plan has been developed for the structure in question, the strain transducers must be attached and the STS prepared for running the test. There are several methods for attaching the strain transducers to the structural members, depending on whether they are steel, concrete, timber, fiber-reinforced polymer (FRP), or other. For steel structures, quite often the transducers can be clamped directly to the steel flanges of rolled sections or plate girders. If significant lateral bending is assumed to be present, then one transducer may be clamped to each edge of the flange. In general, the transducers can be clamped directly to painted surfaces. The alternative to clamping is the tab attachment method that involves cleaning the mounting area and then using a fast-setting cyanoacrylate adhesive to temporarily install the transducers.

Small steel "tabs" are used with this technique, and these are removed when testing is completed; touch-up paint can be applied to the exposed steel surfaces.

Installation of transducers on pre-stressed concrete (PS/C) and FRP members is usually accomplished with the tab technique outlined above, while readily available wood screws and a battery-operated hand drill are used for timber members. Installing transducers on reinforced concrete (R/C) is more complex in that gage extensions are used and must be mounted with concrete studs.

If the above steps are followed, it should be possible to mount each transducer in approximately 5 to 10 min. The following figures illustrate transducers mounted on both steel (Figure C1) and R/C (Figure C2) members.
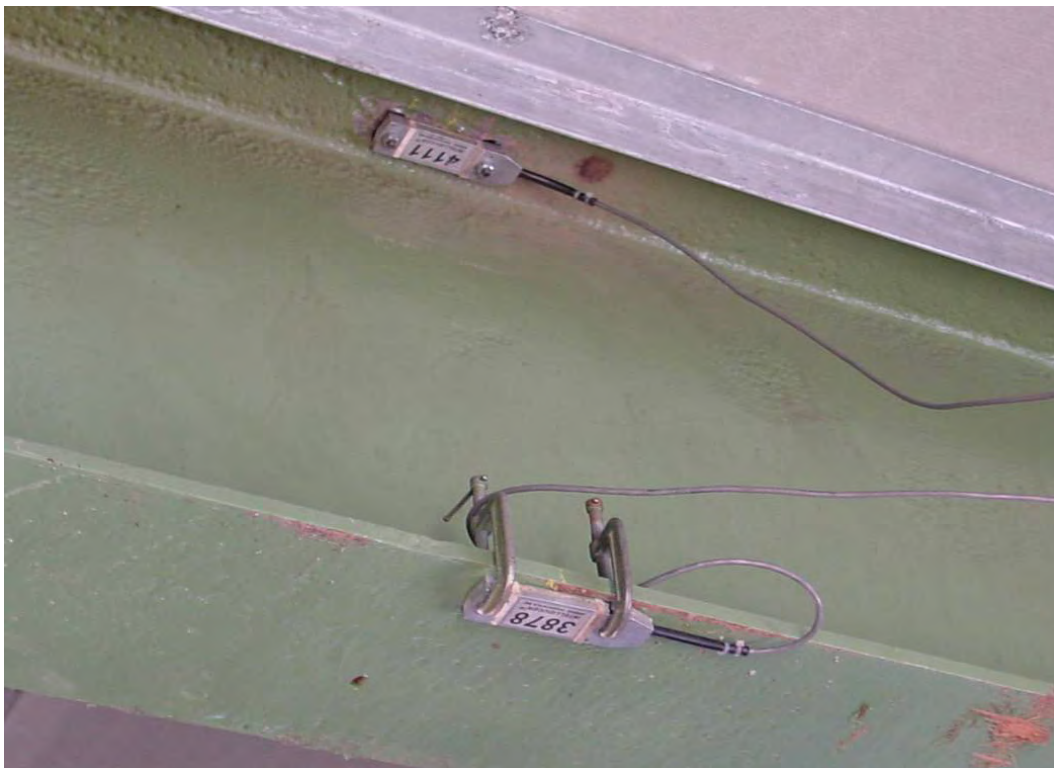


Figure C1. Strain transducers mounted on a steel girder.
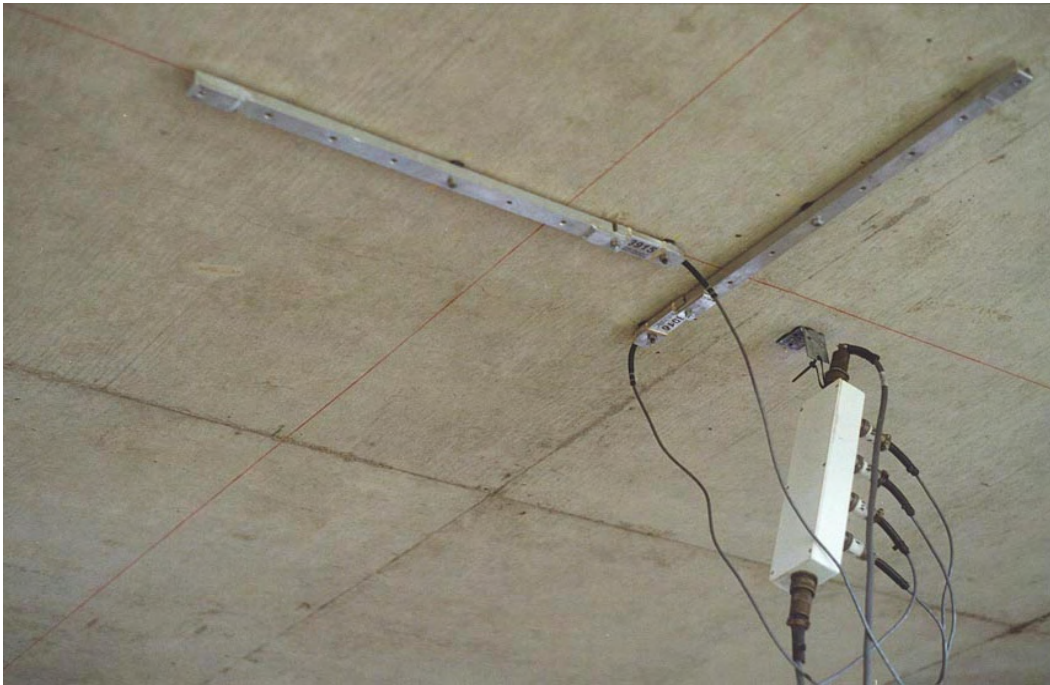
Figure C2. Transducer with gage extensions mounted on R/C slab.

## Assembly of system

Once the transducers have been mounted, they are connected to the four-channel STS units that are also located on the bridge. The STS units can be easily clamped to the bridge girders, or if the structure is concrete and no flanges are available on which to set the STS units, transducer tabs glued to the structure and plastic zip-ties or small wire can be used to mount them. Since the transducers will identify themselves to the system, there is no special order in which they must be plugged into the system. The only information that must be recorded is the transducer serial number and its location on the structure. Signal cables are then used to connect STS units, either in series or in a "tree" structure through the use of cable splitters. If several gages are in close proximity to each other, the STS units can be plugged directly to each other without the use of a cable.

Once all of the STS units have been connected, only one cable must be run and connected to the STS Power Supply located near the PC. Once power and communication cables are connected, the system is ready to acquire data. One last step entails installing the AutoClicker on the test vehicle, as shown in Figure C3.

Figure C3. AutoClicker mounted on test vehicle.

## Establishing load vehicle positions

Once the structure is instrumented and the loading vehicle prepared, some reference points must be established on the deck in order to determine where the vehicle will cross. This process is important so that future analysis comparisons can be made with the loading vehicle in the same locations as it was in the field. Therefore, a "zero" or initial reference point is selected and usually corresponds to the point on the deck directly above the abutment bearing and the center line of one of the fascia beams. All other measurements on the deck will then be related to this zero reference point. For concrete T-beams, box beams, and slabs, this can correspond to where the edge of the slab or the beam web meets the face of the abutment. If the bridge is skewed, the first point encountered from the direction of travel is used. In any case, it should be a point that is easily located on the drawings of the structure.

Once the zero reference location is known, the lateral load paths for the vehicle are determined. Often, the painted roadway lines are used for the driver to follow if they are in convenient locations. For example, for a two-lane bridge, a northbound shoulder line will correspond to Y1 (passenger-side wheel), the center dashed line to Y2 (center of truck), and the south-bound shoulder line to Y3 (driver's side wheel). Often, the structure will be symmetrical with respect to its longitudinal center line. If so, it is good practice is to take advantage of this symmetry by selecting three Y locations that are also symmetric. This will allow for a data quality check since the response should be very similar, say, on the middle beam if the truck is on the left side of the bridge or the right side of the bridge. In general, it is best to have the truck travel in each lane (at least on the lane line) and also as close to each shoulder or sidewalk as possible. When the deck layout is completed, the loading vehicle's axle weights and dimensions are recorded.

## Running the load tests

After the structure has been instrumented and the reference system laid out on the bridge deck, the actual testing procedures are completed. The WinSTS software is initialized and configured. When all personnel are ready to commence the test, traffic control is initiated and the Run Test option is selected, which places the system in an activated state. When the truck passes over the first deck mark, the AutoClicker is tripped and data are being collected at the specified sample rate. An effort is made to get the truck across with no other traffic on the bridge. When the rear axle of the vehicle completely crosses over the structure, the data collection is stopped and several strain histories evaluated for data quality. Usually, at least two passes are made at each "Y" position to ensure data reproducibility and then, if conditions permit, high-speed or dynamic tests are completed.

The use of a moving load as opposed to placing the truck at discrete locations has two major benefits. First, the testing can be completed much quicker, meaning there is less impact on traffic. Second, and more importantly, much more information can be obtained (both quantitative and qualitative). Discontinuities or unusual responses in the strain histories, which are often signs of distress, can be easily detected. Since the load position is monitored, as well, it is easy to determine what loading conditions cause the observed effects. If readings are recorded only at discrete truck locations, the risk of losing information between the points is great.

The advantages of continuous readings have been proven over and over again.

When the testing procedures are complete, the instrumentation is removed and any touch-up work is completed.

# Appendix D: Specifications – BDI Strain Transducers



Figure D1. BDI strain transducer.

Table D1. Strain transducer specifications.

| | |
|---|---|
| Effective Gage Length | 3.0 in. (76.2 mm); extensions available for use on R/C structures |
| Overall Size | 4.4 x 1.2 x 0.5 in. (110 x 33 x 12 mm) |
| Cable Length | 10 ft (3 m) standard, any length available |
| Material | Aluminum |
| Circuit | Full Wheatstone bridge with four active 350Ω foil gages, 4-wire hookup |
| Accuracy | ±2%, individually calibrated to NIST standards (National Institute of Standards and Technology) |
| Strain Range | Approximately ±4000 $\mu\varepsilon$ |
| Force req'd for 1000 $\mu\varepsilon$ | Approximately 9 lb (40 N) |
| Sensitivity | Approximately 500 $\mu\varepsilon$/mV/V |
| Weight | Approximately 3 oz. (88 g) |
| Environmental | Built-in protective cover, also water-resistant |
| Temperature Range | -60°F to 250°F (-50°C to 120°C ) operation range |
| Cable | BDI RC-187: 22 gage, two individually shielded pairs w/drain |
| Options | Fully waterproofed, heavy-duty cable, special quick-lock connector |
| Attachment Methods | C-clamps or threaded mounting tabs and quick-setting adhesive |

# Appendix E: Specifications – BDI Structural Testing System



Figure E1. BDI structural testing system.

Table E1. Structural testing system specifications.

| Channels | 4 to 128, expandable in multiples of four |
|---|---|
| Hardware Accuracy | ±0.2% (2% for strain transducers) |
| Sample Rates | 0.01 to 1,000 Hz sample rate;<br>Internal over-sampling rate is 15 KHz |
| Max Test Lengths | 20 min at 100 Hz;<br>128K samples per channel maximum test length |
| Gain Levels | 1, 250, 500, 1000 |
| Digital Filter | Fixed by selected sample rate |
| Analog Filter | 200 Hz, -3db, 3rd-order Bessel |
| Max. Input Voltage | ±10V |
| Power | 85 - 264 VAC, 47-440 Hz;<br>-25 to 55 °C |
| 12VDC Power | External inverter included |
| Excitation Voltages:<br>    Standard:<br>    LVDT: | <br>5V DC @ 200 mA;<br>±15V DC @ 200 mA |
| A/D Resolution | 2.44 uV/bit (14-bit ADC) |
| PC Requirements | Windows 2000, XP |

| PC Interface | USB 1.1 Port (compatible with USB 2.0) |
|---|---|
| Self-Balancing Range | ±20 mV @ input with 350Ω Wheatstone bridge |
| Enclosures | Aluminum, splash-resistant |
| Cable Connections | All aluminum military grade, circular bayonet "snap" lock |
| Vehicle Tracking: | See "AutoClicker" specifications |
| Sensors | See "BDI Strain Transducer" specifications;<br>Also supports LVDTs, foil strain gages, accelerometers, various DC output sensors;<br>Single RS232 serially interfaced sensor |
| Weights:<br>    Power Unit:<br>    STS Unit | <br>6.2 lb (2.8 kg)<br>1.6 lb (0.7 kg) |
| Dimensions:<br>    Power Unit:<br>    STS Unit: | <br>13.5 x 9.5 x 2.4 in. (343 x 242 x 61 mm)<br>11.8 x 3.4 x 1.7 in. (300 x 87 x 44 mm) |

# Appendix F: Specifications – BDI AutoClicker



Figure F1. AutoClicker mounted on test truck.

Table F1. AutoClicker specifications.

| 3 Handheld Radios | Motorola P1225 2-channel (or equal) modified for both *Rx* and *Tx* |
|---|---|
| Power | 9V battery |
| Mounting | Universal front fender mounting system |
| Target | Retroreflective tape mounted on universal wheel clamp |
| Bands/Power | VHF/1 watt or UHF/2 watt |
| Frequencies | User-specified |
| Data Acquisition System Requirements | TTL/CMOS input (pull-up resistor to 5V) |
| Output | Isolated contact closure (200V 0.5A max switch current) |

# Appendix G: Modeling and Analysis – The Integrated Approach

## Introduction

In order for load testing to be a practical means of evaluating short- to medium-span bridges, it is apparent that testing procedures must be economic to implement in the field and the test results translatable into a load rating. A well-defined set of procedures must exist for the field applications as well as for the interpretation of results. An evaluation approach based on these requirements was first developed at the University of Colorado during a research project sponsored by the Pennsylvania Department of Transportation. Over several years, the techniques originating from this project have been refined and expanded into a complete bridge rating system.

The ultimate goal of the Integrated Approach is to obtain realistic rating values for highway bridges in a cost-effective manner. This is accomplished by measuring the response behavior of the bridge due to a known load and determining the structural parameters that produce the measured responses. With the availability of field measurements, many structural parameters in the analytical model can be evaluated that are otherwise conservatively estimated or ignored entirely. Items that can be quantified through this procedure include the effects of structural geometry, effective beam stiffness, realistic support conditions, effects of parapets and other nonstructural components, lateral load transfer capabilities of the deck and transverse members, and the effects of damage or deterioration. Often, bridges are rated poorly because of inaccurate representations of the structural geometry or because the material and/or cross-sectional properties of main structural elements are not well defined. A realistic rating can be obtained, however, when all of the relevant structural parameters are defined and implemented in the analysis process.

One of the most important phases of this approach is a qualitative evaluation of the raw field data. Much is learned during this step to aid in the rapid development of a representative model.

## Initial data evaluation

The first step in structural evaluation consists of a visual inspection of the data in the form of graphic response histories. Graphic software was developed to display the raw strain data in various forms. Strain histories can be viewed in terms of time or truck position. Since strain transducers are typically placed in pairs, neutral axis (NA) measurements, curvature responses, and strain averages can also be viewed. Linearity between the responses and load magnitude can be observed by the continuity in the strain histories. Consistency in the NA measurements from beam to beam and as a function of load position provides great insight into the nature of the bridge condition. The direction and relative magnitudes of flexural responses along a beam-line are useful in determining if end-restraints play a significant role in the response behavior. In general, the initial data inspection provides the engineer with information concerning modeling requirements and can help locate damaged areas.

Having strain measurements at two depths on each beam cross section, the flexural curvature and the location of the neutral axis can be computed directly from the field data. Figure G1 illustrates how curvature and neutral axis values are computed from the strain measurements.



$$\overline{y} = \frac{\varepsilon_B d}{\varepsilon_T - \varepsilon_B}$$

$$\phi = \frac{\varepsilon_T - \varepsilon_B}{d}$$
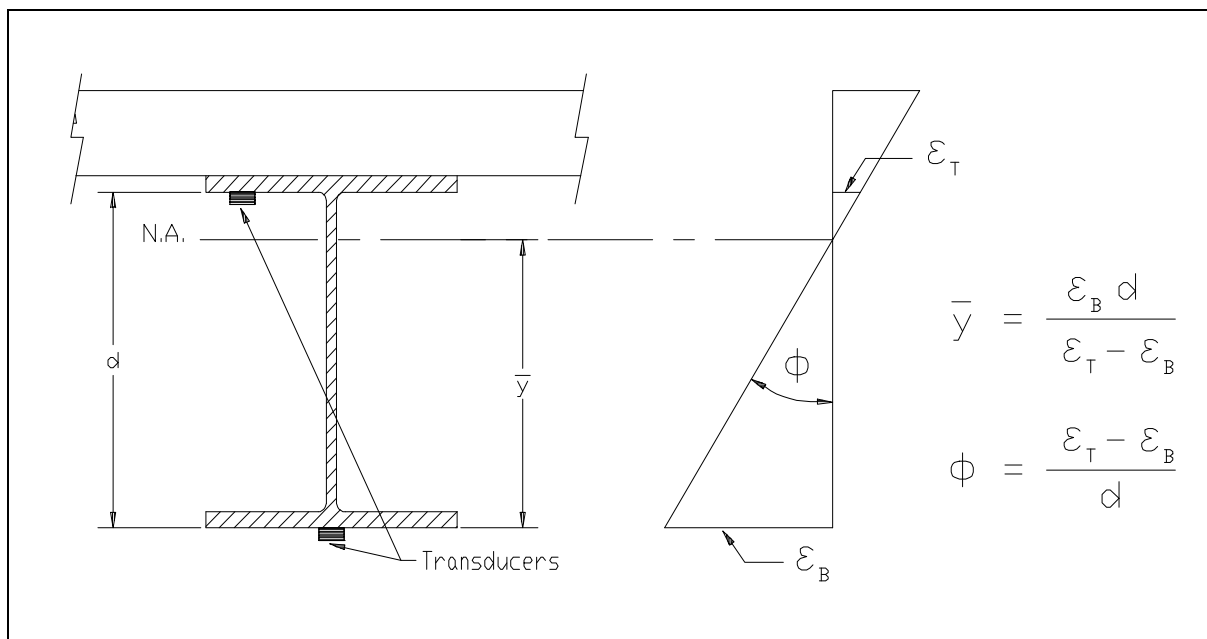
Figure G1. Illustration of neutral axis and curvature calculations.

The consistency in the NA values between beams indicates the degree of consistency in beam stiffness. Also, the consistency of the NA measurement on a single beam as a function of truck position provides a good quality check for that beam. If for some reason a beam's stiffness changes with respect to the applied moment (i.e., loss of composite action or loss of effective flange width due to a deteriorated deck), it will be observed by a shift in the NA history.

Since strain values are translated from a function of time into a function of vehicle position on the structure and the data acquisition channel and the truck position tracked, a considerable amount of bookkeeping is required to perform the strain comparisons. In the past, this required manipulation of result files and spreadsheets, which was tedious and a major source of error. This process in now performed automatically by the software, and all of the information can be verified visually.

## Finite element modeling and analysis

The primary function of the load test data is to aid in the development of an accurate finite element model of the bridge. Finite element analysis is used because it provides the most general tool for evaluating various types of structures. Since a comparison of measured and computed responses is performed, it is necessary that the analysis be able to represent the actual response behavior. This requires that actual geometry and boundary conditions be realistically represented. In maintaining reasonable modeling efforts and computer run-times, a certain amount of simplicity is also required. Thus, a planar grid model is generated for most structures, and linear-elastic responses are assumed. A grid of frame elements is assembled in the same geometry as the actual structure. Frame elements represent the longitudinal and transverse members of the bridge. The load transfer characteristics of the deck are provided by attaching plate elements to the grid. When end-restraints are determined to be present, elastic spring elements having both translational and rotational stiffness terms are inserted at the support locations.

Loads are applied in a manner similar to the actual load test. A model of the test truck, defined by a two-dimensional group of point loads, is placed on the structure model at discrete locations along the same path that the test truck followed during the load test. Gage locations identical to those in the field are also defined on the structure model so that strains can be computed at the same locations under the same loading conditions.

## Evaluation of rotational end-restraint

A common requirement in structural identification is the need to determine effective spring stiffnesses that best represent in situ support conditions. Whereas it is generally simple to evaluate a spring constant in terms of moment per rotation, the value generally has little meaning to the engineer. A more conceptual approach is to evaluate the spring stiffness as a percentage of a fully restrained condition—for example, 0% being a pinned condition and 100% being fixed. This is best accomplished by examining the ratio of the beam or slab stiffness to the rotational stiffness of the support.

As an illustration, a point load is applied to a simple beam with elastic supports (see Figure G2). By examining the moment diagram, it is apparent that the ratio of the end moment to the midspan moment ($M_e/M_m$) equals 0.0 if the rotational stiffness ($K_r$) of the springs is equal to 0.0. Conversely, if the value of $K_r$ is set to infinity (rigid), the moment ratio will equal 1.0. If a fixity term is defined as the ratio ($M_e/M_m$), which ranges from 0 to 100%, a more conceptual measure of end-restraint can be obtained.
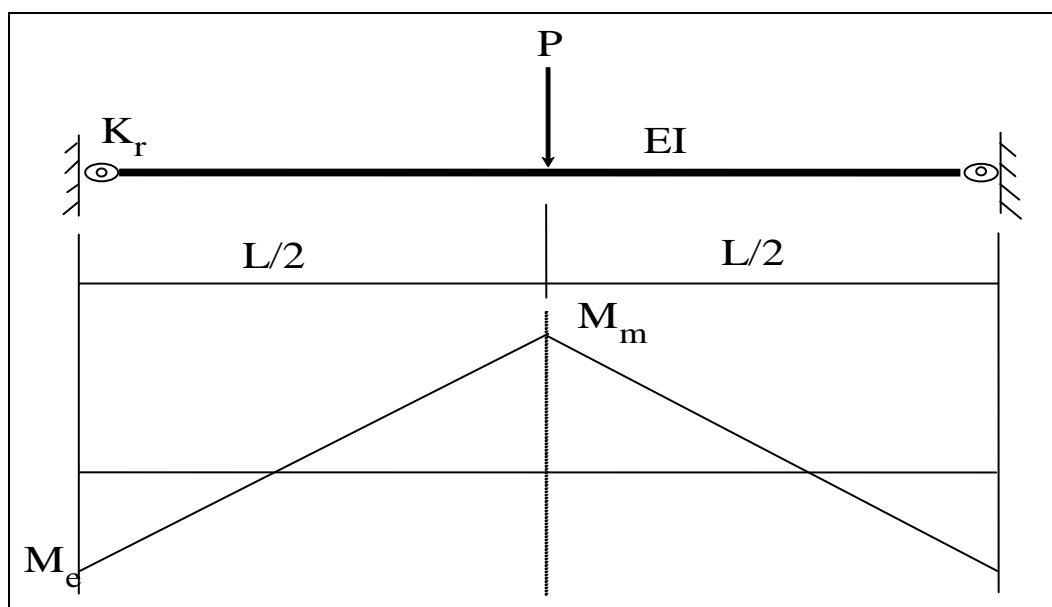


Figure G2. Moment diagram of beam with rotational end-restraint.

The next step is to relate the fixity term to the actual spring stiffness ($K_r$). The degree to which the $K_r$ affects the fixity term depends on the beam or slab stiffness to which the spring is attached. Therefore, the fixity term

must be related to the ratio of the beam/spring stiffness. Figure G3 contains a graphical representation of the end-restraint effect on a simple beam. Using the graph, a conceptual measure of end-restraint can be defined after the beam and spring constants are evaluated through structural identification techniques.
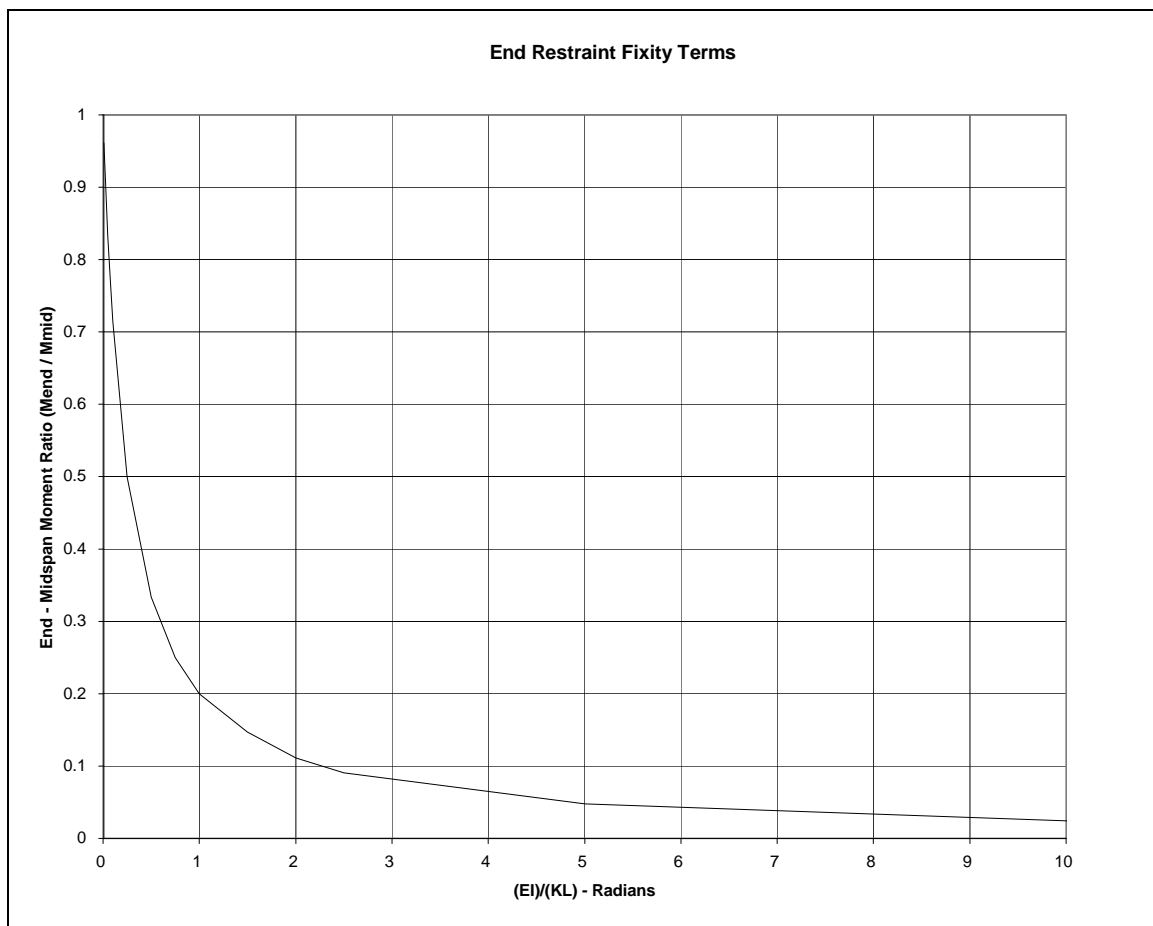


Figure G3. Relationship between spring stiffness and fixity ratio.

## Model correlation and parameter modification

The accuracy of the model is determined numerically by the analysis using several statistical relationships and through visual comparison of the strain histories. The numeric accuracy values are useful in evaluating the effect of any changes to the model, whereas the graphical representations provide the engineer with the best perception for why the model is responding differently than the measurements indicate. Member properties that cannot be accurately defined by conventional methods or directly from the field data are evaluated by comparing the computed strains with the measured strains. These properties are defined as variables and are

evaluated such that the best correlation is obtained between the two sets of data. It is the engineer's responsibility to determine which parameters need to be refined and to assign realistic upper and lower limits to each parameter. The evaluation of the member property is accomplished with the aid of a parameter identification process (optimizer) built into the analysis. In short, the process consists of an iterative process of analysis, data comparison, and parameter modification. It is important to note that the optimization process is merely a tool to help evaluate various modeling parameters. The process works best when the number of parameters is minimized and reasonable initial values are used.

During the optimization process, various error values are computed by the analysis program, which provides a quantitative measure of the model accuracy and improvement. The error is quantified in four ways, each providing a different perspective of the model's ability to represent the actual structure: an absolute error, a percent error, a scale error, and a correlation coefficient.

The **absolute error** is computed from the absolute sum of the strain differences. Algebraic differences between the measured and theoretical strains are computed at each gage location for each truck position used in the analysis; therefore, several hundred strain comparisons are generally used in this calculation. This quantity is typically used to determine the relative accuracy from one model to the next and to evaluate the effect of various structural parameters. It is used by the optimization algorithm as the objective function to minimize. Because the absolute error is in terms of micro-strain (m$\varepsilon$), the value can vary significantly depending on the magnitude of the strains, the number of gages, and number of different loading scenarios. For this reason, it has little conceptual value except for determining the relative improvement of a particular model.

A **percent error** is calculated to provide a better qualitative measure of accuracy. It is computed as the sum of the strain differences squared divided by the sum of the measured strains squared. The terms are squared so that error values of different sign will not cancel each other out, and to put more emphasis on the areas with higher strain magnitudes. A model with acceptable accuracy will usually have a percent error of less than 10%.

The **scale error** is similar to the percent error except that it is based on the maximum error from each gage divided by the maximum strain value from each gage. This number is useful because it is based only on strain measurements recorded when the loading vehicle is in the vicinity of each gage. Depending on the geometry of the structure, the number of truck positions, and various other factors, many of the strain readings are essentially negligible. This error function uses only the most relevant measurement from each gage.

Another useful quantity is the **correlation coefficient,** which is a measure of the linearity between the measured and computed data. This value determines how well the shapes of the computed response histories match the measured responses. The correlation coefficient can have a value between 1.0 (indicating a perfect linear relationship) and -1.0 (exact opposite linear relationship). A good model will generally have a correlation coefficient greater than 0.90. A poor correlation coefficient is usually an indication that a major error in the modeling process has occurred. This generally results from poor representations of the boundary conditions or from the loads being applied incorrectly (i.e., truck traveling in wrong direction).

Table G1 presents the equations used to compute each of the statistical error values.

Table G1. Error functions.

| Error Function | Equation |
|---|---|
| Absolute Error | $\sum \lvert \varepsilon_m - \varepsilon_c \rvert$ |
| Percent Error | $\sum (\varepsilon_m - \varepsilon_c)^2 / \sum (\varepsilon_m)^2$ |
| Scale Error | $\dfrac{\sum \mathbf{max} \lvert \varepsilon_m - \varepsilon_c \rvert_{gage}}{\sum \mathbf{max} \lvert \varepsilon_m \rvert_{gage}}$ |
| Correlation Coefficient | $\dfrac{\sum (\varepsilon_m - \overline{\varepsilon_m})(\varepsilon_c - \overline{\varepsilon_c})}{\sum \sqrt{(\varepsilon_m - \overline{\varepsilon_m})^2 (\varepsilon_c - \overline{\varepsilon_c})^2}}$ |

In addition to the numerical comparisons made by the program, periodic visual comparisons of the response histories are made to obtain a conceptual measure of accuracy. Again, engineering judgment is essential in

determining which parameters should be adjusted so as to obtain the most accurate model. The selection of adjustable parameters is performed by determining what properties have a significant effect on the strain comparison and determining which values cannot be accurately estimated through conventional engineering procedures. Experience in examining the data comparisons is helpful; however, two general rules apply concerning model refinement. When the shapes of the computed response histories are similar to the measured strain records but the magnitudes are incorrect, this implies that member stiffness must be adjusted. When the shapes of the computed and measured response histories are not very similar, then the boundary conditions or the structural geometry is not well represented and must be refined.

In some cases, an accurate model cannot be obtained, particularly when the responses are observed to be nonlinear with load position. Even then, a great deal can be learned about the structure, and intelligent evaluation decisions can be made.

# Appendix H: Load Rating Procedures

A load rating factor is a numeric value indicating a structure's ability to carry a specific load. Load rating factors were computed by applying standard design loads along with the structure's self-weight and asphalt overlay. Rating factors are computed for various structural components and are equal to the ratio of the component's live-load capacity and the live load applied to that component, including all appropriate load factors. A load rating factor greater than 1.0 indicates a member's capacity exceeds the applied loads with the desired factors of safety. A rating factor less than 1.0 indicates a member is deficient such that a specific vehicle cannot cross the bridge with the desired factor of safety. A number near 0.0 indicates the structure cannot carry its own dead weight and maintain the desired safety factor. The lowest component rating factor generally controls the load rating of the entire structure. Additional factors are applied to account for variability in material, load application, and dynamic effects. Two levels of load rating are performed for the bridge. An Inventory Level rating corresponds to the design stress levels and/or factors of safety and represents the loads that can be applied on a daily basis. The Operating Rating levels correspond to the maximum load limits above which the structure may experience damage or failure.

For borderline bridges (those for which calculations indicate a posting is required), the primary drawback to conventional bridge rating is an over-simplified procedure for estimating the load applied to a given beam (i.e., wheel load distribution factors) and a poor representation of the beam itself. Because of a lack of information and the need for conservatism, material and cross-section properties are generally underestimated, and beam end supports are assumed to be simple when, in fact, even relatively simple beam bearings have a substantial effect on the midspan moments. Inaccuracies associated with conservative assumptions are compounded with complex framing geometries. From an analysis standpoint, the goal here is to generate a model of the structure that is capable of reproducing the measured strains. Decisions concerning load rating are then based on the performance of the model once it is proven to be accurate.

The main purpose for obtaining an accurate model is to evaluate how the bridge will respond when standard design loads, rating vehicles, or permit

loads are applied to the structure. Since load testing is generally not performed with all of the vehicles of interest, an analysis must be performed to determine load rating factors for each truck type. Load rating is accomplished by applying the desired rating loads to the model and computing the stresses on the primary members. Rating factors are computed using the equation specified in the AASHTO (2003) Manual [see Equation H1 below].

It is important to understand that diagnostic load testing and the integrated approach are most applicable to obtaining Inventory (service load) rating values. This is because it is assumed that all of the measured and computed responses are linear with respect to load. The integrated approach is an excellent method for estimating service load stress values, but it generally provides little additional information regarding the ultimate strength of particular structural members. Therefore, operating rating values must be computed using conventional assumptions regarding member capacity. This limitation of the integrated approach is not viewed as a serious concern, however, because load responses should never be permitted to reach the inelastic range.

Operating and/or Load Factor rating values must also be computed to ensure a factor of safety between the ultimate strength and the maximum allowed service loads. The safety to the public is of vital importance; however, as long as load limits are imposed such that the structure is not damaged, then safety is no longer an issue.

The following outline describes how field data are used to develop a load rating for the superstructure. These procedures will only complement the rating process, and must be used with due consideration to the substructure and inspection reports.

1.  **Preliminary investigation.** Verify linear and elastic behavior through continuity of strain histories, locate neutral axis of flexural members, detect moment resistance at beam supports, and qualitatively evaluate behavior.
2.  **Develop representative model.** Use graphic pre-processors to represent the actual geometry of the structure, including span lengths, girder spacing, skew, transverse members, and deck. Identify gage locations on model identical to those applied in the field.

3. **Simulate load test on computer model.** Generate two-dimensional model of test vehicle and apply to structure model at discrete positions along same paths defined during field tests. Perform analysis and compute strains at gage location for each truck position.

4. **Compare measured and initial computed strain values.** Various global and local error values at each gage location are computed, and visual comparisons made with post-processor.

5. **Evaluate modeling parameters.** Improve model based on data comparisons. Engineering judgment and experience is required to determine which variables are to be modified. A combination of direct evaluation techniques and parameter optimization is used to obtain a realistic model. General rules have been defined to simplify this operation.

6. **Model evaluation.** In some cases it is not desirable to rely on secondary stiffening effects, if it is likely they will not be effective at higher load levels. It is beneficial, though, to quantify their effects on the structural response so that a representative computer model can be obtained. The stiffening effects that are deemed unreliable can be eliminated from the model prior to the computation of rating factors. For instance, if a noncomposite bridge is exhibiting composite behavior, then it can conservatively be ignored for rating purposes. However, if it has been in service for 50 years and it is still behaving compositely, chances are that very heavy loads have crossed over it and any bond-breaking would have already occurred. Therefore, probably some level of composite behavior can be relied upon. When unintended composite action is allowed in the rating, additional load limits should be computed based on an allowable shear stress between the steel and concrete and an ultimate load of the noncomposite structure.

7. **Perform load rating.** Apply HS-20 and/or other standard design, rating, and permit loads to the calibrated model. Rating and posting load configurations recommended by AASHTO are shown in Figure H1.

8. **Apply rating equation** specified by the **Manual for the Condition Evaluation of Bridges** (AASHTO 2003):

$$RF = \frac{C - \gamma_{DC}(DC) - \gamma_{DW}(DW) \pm \gamma_P(P)}{\gamma_{LL}(LL + IM)} \qquad \text{(H1)}$$
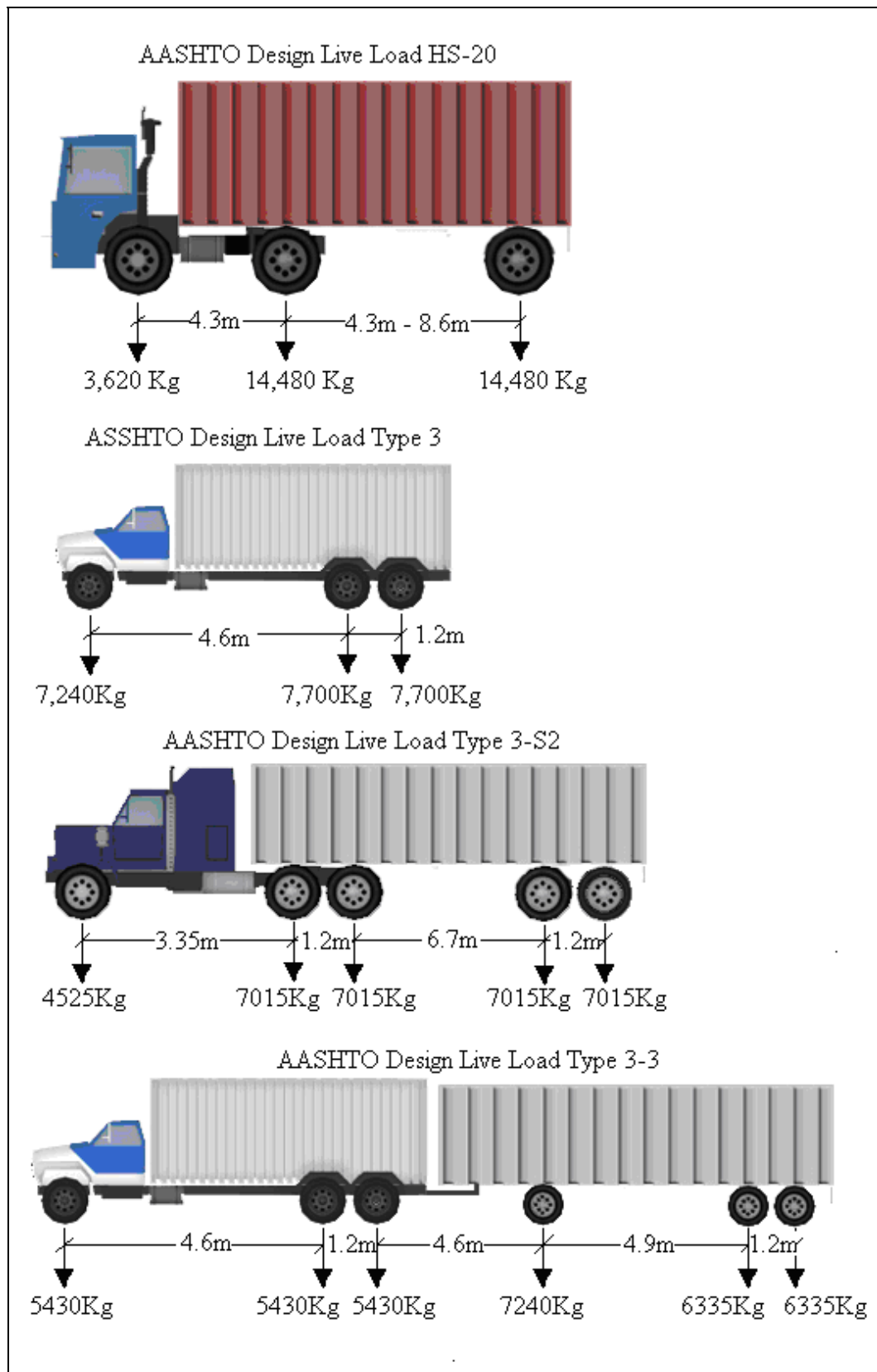
Figure H1. AASHTO rating and posting load configurations (SI).

where:

$RF$ = Rating Factor for individual member
$C$ = member capacity
$\gamma_{DC}$ = LRFD load factor for structural components and attachments
$DC$ = dead-load effect due to structural components
$\gamma_{DW}$ = LRFD load factor for wearing surfaces and utilities
$DW$ = dead-load effect due to wearing surface and utilities
$\gamma_P$ = LRFD load factor for permanent loads other than dead loads = 1.0
$P$ = permanent loads other than dead loads
$\gamma_{LL}$ = LRFD load factor for live load
$LL$ = live-load effect
$IM$ = impact effect, either AASHTO or measured

The only difference between this rating technique and standard beam rating programs is that a more realistic model is used to determine the dead-load and live-load effects. Two-dimensional loading techniques are applied because wheel load distribution factors are not applicable to a planar model. Stress envelopes are generated for several truck paths; envelopes for paths separated by normal lane widths are combined to determine multiple-lane loading effects.

9. **Consider other factors**: Other factors such as the condition of the deck and/or substructure, traffic volume, and other information in the inspection report should be taken into consideration and the rating factors adjusted accordingly (Tables H1 and H2).

Table H1. LRFR load and resistance factors.

| Dead Load | DC (dead-load effects due to structural components and attachments) | 1.25 |
|---|---|---|
| | DW (dead-load effect due to wearing surface and utilities) | 1.50 |
| Live Load | Inventory | 1.75 |
| | Operating | 1.35 |
| Condition Factor, $\varphi_c$ | Good or Satisfactory | 1.00 |
| | Fair | 0.95 |
| | Poor | 0.85 |
| System Factor, $\varphi_s$ | Welded members in two-girder/truss/arch bridges | 0.85 |
| | Riveted members in two-girder/truss/arch bridges | 0.90 |
| | Multiple eyebar members in truss bridges | 0.90 |
| | Three-girder bridges with girder spacing ≤1.8 m | 0.85 |
| | Four-girder bridges with girder spacing ≤1.2 m | 0.95 |
| | All other girder bridges and slab bridges | 1.00 |
| | Floor beams with spacing >3.6 m and noncontinuous stringers | 0.85 |
| | Redundant stringer subsystems between floor beams | 1.00 |

Table H2. LRFD resistance factors.

| Capacity | Steel Resistance Factor | R/C Resistance Factor | PS/C Resistance Factor |
|---|---|---|---|
| Flexure, $\Phi_b$ | 1.00 | 0.90 | 1.00 |
| Shear, $\Phi_v$ | 1.00 | 0.90 | 0.90 |

**The configuration and layout of all the vehicles used in the load rating and the axle spacings for each vehicle are shown in Figures H2–H4 and Tables H3–H7.**
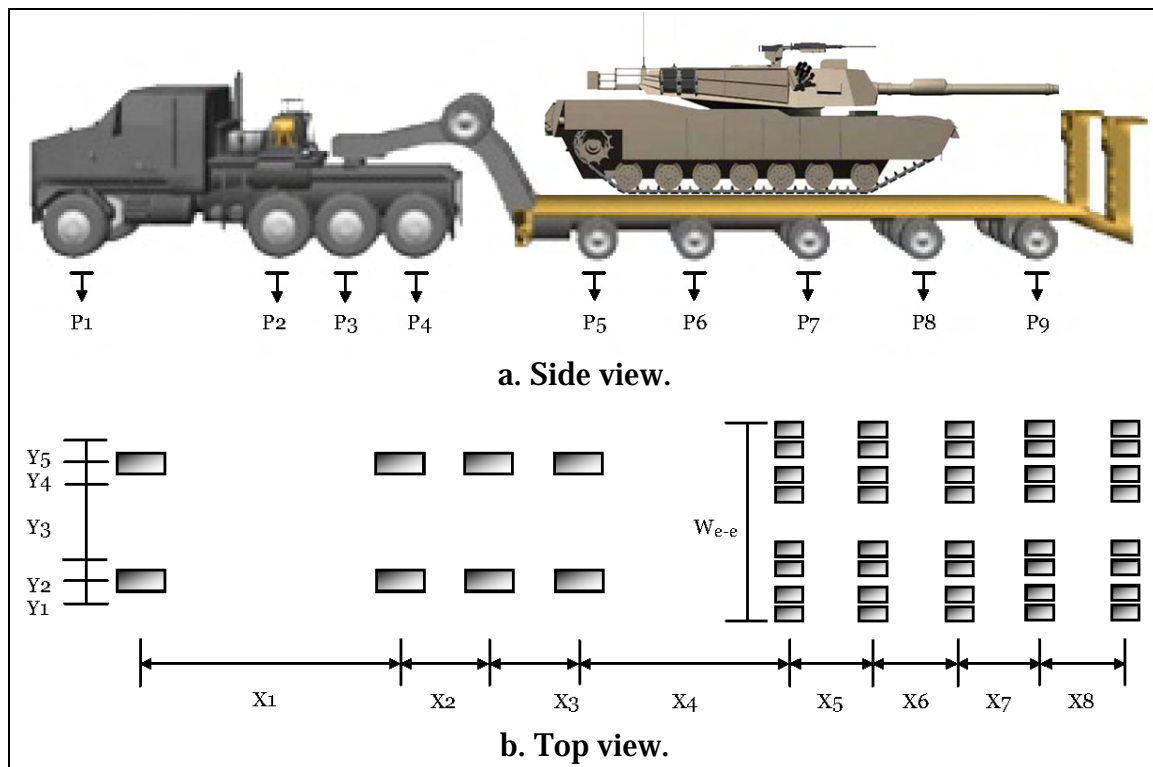
Figure H2. Configuration of HETS vehicle load distribution.

Table H3. Loading data and dimensions of HETS with M1A1.

| Loading Data | | | | | | | | | |
|---|---|---|---|---|---|---|---|---|---|
| Axle Loads (kg) | P1 | P2 | P3 | P4 | P5 | P6 | P7 | P8 | P9 |
| | 9820 | 10090 | 9820 | 9005 | 12217 | 13440 | 12670 | 12670 | 14210 |
| Dimensions | | | | | | | | | |
| Transverse Spacing (m) | We-e | Y1 | Y2 | Y3 | Y4 | Y5 | | | |
| | 3.66 | 0.51 | 0.34 | 1.48 | 0.34 | 0.51 | | | |
| Longitudinal Spacing (m) | X1 | X2 | X3 | X4 | X5 | X6 | X7 | X8 | |
| | 3.94 | 1.52 | 1.52 | 4.86 | 1.81 | 1.81 | 1.81 | 1.81 | |

Table H4. Loading data and dimensions of empty HET.

| Loading Data | | | | | | | | | |
|---|---|---|---|---|---|---|---|---|---|
| Axle Loads (kg) | P1 | P2 | P3 | P4 | P5 | P6 | P7 | P8 | P9 |
| | 8890 | 5020 | 5050 | 4890 | 3780 | 3620 | 3760 | 5520 | 5590 |
| Dimensions | | | | | | | | | |
| Transverse Spacing (m) | We-e | Y1 | Y2 | Y3 | Y4 | Y5 | | | |
| | 3.66 | 0.509 | 0.341 | 1.48 | 0.341 | 0.509 | | | |
| Longitudinal Spacing (m) | X1 | X2 | X3 | X4 | X5 | X6 | X7 | X8 | |
| | 3.94 | 1.52 | 1.52 | 4.86 | 1.81 | 1.81 | 1.81 | 1.81 | |
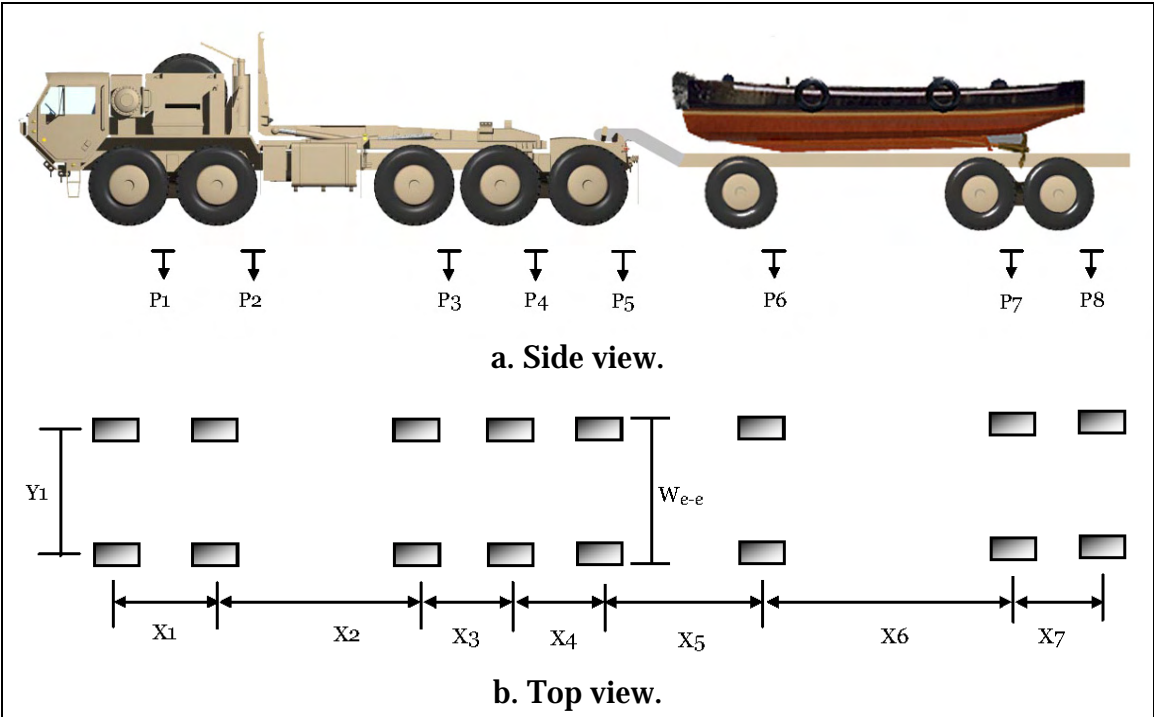
**Figure H3. Configuration of PLS vehicle load distribution.**

Table H5. Loading data and dimensions of PLS.

| Loading Data | | | | | | | | |
|---|---|---|---|---|---|---|---|---|
| Axle Loads (kg) | P1 | P2 | P3 | P4 | P5 | P6 | P7 | P8 |
| | 5158 | 5158 | 9593 | 9593 | 9593 | 4434 | 9321 | 9321 |
| Dimensions | | | | | | | | |
| Transverse Spacing (m) | $W_{e-e}$ | Y1 | | | | | | |
| | 2.44 | 2.03 | | | | | | |
| Longitudinal Spacing (m) | X1 | X2 | X3 | X4 | X5 | X6 | X7 | |
| | 1.52 | 3.41 | 1.52 | 1.52 | 2.59 | 3.05 | 1.40 | |

Table H6. MLC loading data and dimensions.

| MLC | Tracked | Wheeled |
|---|---|---|
| 60 |  |  |
| 70 |  |  |

a. Side view.

b. Top view.
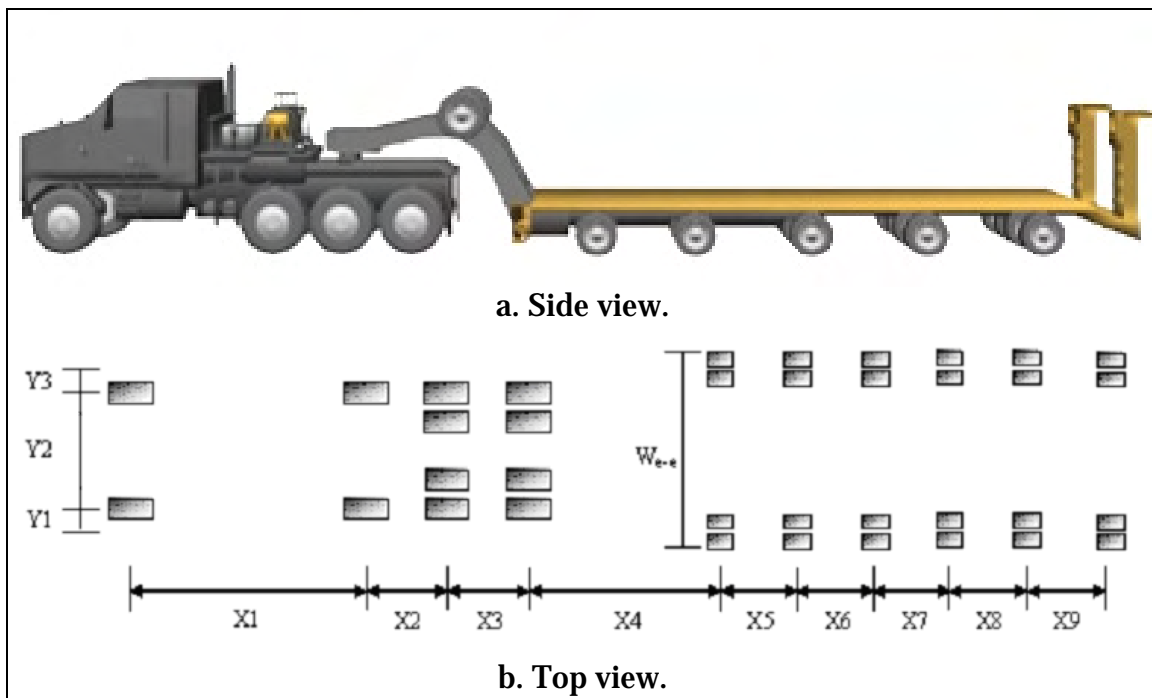
Figure H4. Configuration of Korean MHET vehicle load distribution.

Table H7. Loading data and dimensions of Korean MHET.

| Loading Data | | | | | | | | | |
|---|---|---|---|---|---|---|---|---|---|
| Axle Loads (kg) | P1 | P2 | P3 | P4 | P5 | P6 | P7 | P8 | P9 | P10 |
| | 7560 | 9980 | 12000 | 11300 | 9320 | 9590 | 9460 | 9860 | 9710 | 9520 |
| Dimensions | | | | | | | | | |
| Transverse Spacing (m) | We-e | Y1 | Y2 | Y3 | | | | | |
| | 3.25 | 0.357 | 2.03 | 0.357 | | | | | |
| Longitudinal Spacing (m) | X1 | X2 | X3 | X4 | X5 | X6 | X7 | X8 | X9 |
| | 1.70 | 3.20 | 1.35 | 5.92 | 1.30 | 1.30 | 1.30 | 1.30 | 1.30 |

# REPORT DOCUMENTATION PAGE

Public reporting burden for this collection of information is estimated to average 1 hour per response, including the time for reviewing instructions, searching existing data sources, gathering and maintaining the data needed, and completing and reviewing this collection of information. Send comments regarding this burden estimate or any other aspect of this collection of information, including suggestions for reducing this burden to Department of Defense, Washington Headquarters Services, Directorate for Information Operations and Reports (0704-0188), 1215 Jefferson Davis Highway, Suite 1204, Arlington, VA 22202-4302. Respondents should be aware that notwithstanding any other provision of law, no person shall be subject to any penalty for failing to comply with a collection of information if it does not display a currently valid OMB control number. **PLEASE DO NOT RETURN YOUR FORM TO THE ABOVE ADDRESS.**

| 1. REPORT DATE (DD-MM-YYYY) July 2008 | 2. REPORT TYPE Final report | 3. DATES COVERED (From - To) |
|---|---|---|

| 4. TITLE AND SUBTITLE | 5a. CONTRACT NUMBER |
|---|---|
| Field Testing and Load Rating Report, Bridge S-4360, Camp Hovey, South Korea | 5b. GRANT NUMBER |
| | 5c. PROGRAM ELEMENT NUMBER |
| 6. AUTHOR(S) | 5d. PROJECT NUMBER |
| Brett Commander, Jesse Grimson, Wilmel Varela-Ortiz, Terry R. Stanton, Carmen Y. Lugo, and Gerald M. Hansler | 5e. TASK NUMBER |
| | 5f. WORK UNIT NUMBER |

| 7. PERFORMING ORGANIZATION NAME(S) AND ADDRESS(ES) | 8. PERFORMING ORGANIZATION REPORT NUMBER |
|---|---|
| Bridge Diagnostics, Inc., 1965 57th Court North, Suite 106, Boulder, CO 80301-2826; U.S. Army Engineer Research and Development Center Geotechnical and Structures Laboratory 3909 Halls Ferry Road, Vicksburg, MS 39180-6199; Eighth U.S. Army, Seoul, South Korea | ERDC/GSL TR-08-18 |

| 9. SPONSORING / MONITORING AGENCY NAME(S) AND ADDRESS(ES) | 10. SPONSOR/MONITOR'S ACRONYM(S) |
|---|---|
| Headquarters, Installation Management Command (IMCOM) Arlington, VA 22202 | 11. SPONSOR/MONITOR'S REPORT NUMBER(S) |

**12. DISTRIBUTION / AVAILABILITY STATEMENT**
Approved for public release; distribution is unlimited.

**13. SUPPLEMENTARY NOTES**

**14. ABSTRACT**

In June 2007, Bridge Diagnostics, Inc. (BDI), was contracted by the U.S. Army Corps of Engineers to perform live-load testing and load rating on Bridge S-4360 at Camp Hovey, South Korea, in conjunction with two other structures, S-1801 and S-1090 at Camp Casey. A primary goal of the live-load testing was to determine the relative effects of different military load configurations. Of particular interest was determining the benefit of using the Heavy Equipment Transporter System (HETS) to transport heavy equipment such as an M1A1 tank. Another goal was to use the measured load responses to verify and calibrate a finite element model of the structure.

The model resulting from the structural identification procedure was then used to generate accurate load ratings for specific AASHTO (American Association of State Highway and Transportation Officials) and military load configurations. Both the direct load test and subsequent load rating results indicated that the MIA1 tank generated greater flexural stresses than did the HETS carrying the M1A1 tank.

The bridge appeared to be in good condition and was apparently designed to carry heavy military loads. Load rating calculations determined that all vehicles considered could cross the bridge within Inventory (normal design) stress limits.

| 15. SUBJECT TERMS |  |  |
|---|---|---|
| Distribution factor | Load rating | Military vehicles |
| Finite element analyses | Load test | Steel beam bridge |

| 16. SECURITY CLASSIFICATION OF: | | | 17. LIMITATION OF ABSTRACT | 18. NUMBER OF PAGES | 19a. NAME OF RESPONSIBLE PERSON |
|---|---|---|---|---|---|
| a. REPORT UNCLASSIFIED | b. ABSTRACT UNCLASSIFIED | c. THIS PAGE UNCLASSIFIED | | 125 | 19b. TELEPHONE NUMBER (include area code) |